EVAPOTRANSPIRATION MEASUREMENTS OF NATIVE VEGETATION, OWENS VALLEY, CALIFORNIA, JUNE 1986

Edited by David H. Wilson, Robert J. Reginato, *and* Kenneth J. Hollett

---

U.S. GEOLOGICAL SURVEY

Water-Resources Investigations Report 91-4159

Contributions from:

City of Los Angeles, Department of Water and Power
Inyo County Water Department
University of Arizona
University of California
U.S. Geological Survey
U.S. Water Conservation Laboratory

7221-22

Sacramento, California
1992

U.S. DEPARTMENT OF THE INTERIOR
MANUEL LUJAN, JR., *Secretary*

U.S. GEOLOGICAL SURVEY
Dallas L. Peck, *Director*

For sale by the Books and
Open-File Reports Section,
U.S. Geological Survey
Federal Center, Box 25425
Denver, CO 80225

For additional information write to:
District Chief
U.S. Geological Survey
Federal Building, Room W-2233
2800 Cottage Way
Sacramento, CA 95825

CONTENTS

FIGURES

TABLES

Conversion Factors and Vertical Datum

Multiply	By	To obtain
centimeter (cm)	0.3937	inch
degree Celsius (°C)	1.8 °C+32	degree Fahrenheit
gram (g)	0.0022	pound
gram per square meter (g/m^2)	0.1076	gram per square foot
gram per cubic meter (g/m^3)	35.31	gram per cubic foot
	6.24×10^{-5}	pound mass per cubic foot
joule (J)	9.4787×10^{-4}	British thermal unit
	0.2388	calorie
joules per gram (J/g) per pound mass	0.4303	British thermal units
kelvin (K)	(1.8K)-459.67	degree Fahrenheit
kilometer (km)	0.6214	mile
meter (m)	3.281	foot
	1.094	yard
meter per second (m/s)	3.281	foot per second
micrometer (μm)	0.3937×10^{-4}	inch
millimeter (mm)	0.03937	inch
square centimeter (cm^2)	0.155	square inch
square meter (m^2)	10.76	square foot
square meter per second (m^2/s)	10.76	square foot per second
millibar (mbar)	0.10	kilopascal
megajoule per square meter (MJ/m^2)	88.05	British thermal unit per square foot
ohm (Ω)	1.000	EMU of resistance
Watt (W)	3.412	British thermal units per hour
	1.340×10^{-3}	horsepower
	0.2388	calories per second
Watt per square meter (W/m^2)	5.2895×10^{-3}	British thermal units per square foot

Sea level: In this report "sea level" refers to the National Geodetic Vertical Datum of 1929 (NGVD of 1929)--a geodetic datum derived from a general adjustment of the first-order level nets of both the United States and Canada, formerly called Sea Level Datum of 1929.

Symbols Used in Text

Az_u	Wind direction
B^{-1}	Resistance to the transfer of heat above that for momentum
b	Day of year on which maximum leaf area was likely to occur
C_b	Fraction of vegetative cover
C_p	Heat capacity of air
c	Coefficient
DN_b	Digital number (DN) brightness of an image pixel for each band, b
d	Displacement height
d	Maximum leaf area
E	Quantity of water evapotranspired
E_{eb}	Energy-balance-residual estimate of ET by the eddy-correlation method
EM_{nb}'	nth image endmember for each band, b, in DN units
ET	Evapotranspiration
ET_{br}	Evapotranspiration by the Bowen-ratio method
ET_{eb}	Evapotranspiration by the eddy-correlation energy-balance-residual method
ET_{ec}	Evapotranspiration, direct eddy-correlation method
e	Vapor pressure
Δe	Difference in vapor pressure at two heights (Z_2-Z_1)
f_n	Fraction of endmember, n
G	Soil-heat flux
g	Gravitational acceleration
H	Sensible-heat flux
H_{br}	Sensible-heat flux, Bowen-ratio method
H_{ec}	Sensible-heat flux, eddy-correlation method
h	Plant height
i	Subscript refers to the ith plant species or instantaneous data
J	Day of year
j	Subscript refers to the jth site
$K\downarrow$	Solar radiation
K_h	Eddy-diffusion coefficient for heat transport
K_v	Eddy-diffusion coefficient for vapor transport
k	Von Karman's constant
L	Solar (longwave) radiation
$LAIPs$	Leaf-area indexes
N	Daylength (in hours)
ND	Normalized difference of near-infrared wavebands
P	Atmospheric pressure at site
P_0	Atmospheric pressure at sea level
Q	Net radiation
q	Water-vapor density
Δq	Difference in vapor-density at two heights (Z_2-Z_1)
Ri	Richardson number
$R_L\uparrow$	Outgoing longwave radiation
$R_L\downarrow$	Incoming longwave radiation
$R_S\downarrow$	Incoming shortwave radiation
$R_S\uparrow$	Outgoing shortwave radiation
r^2	Coefficient of determination
r_a	Stability-corrected aerodynamic resistance
r_h	Resistance to heat transport
r_v	Resistance to vapor transport
S	Solar (shortwave) radiation
T	Air temperature
ΔT	Difference in air temperature at two heights (Z_2-Z_1)
T_s	Soil-surface temperature
$\hat{T}$	Transpiration
t	Time of day
U	Horizontal windspeed
U_*	Friction velocity
w	Vertical windspeed
Z_o	Roughness length for momentum
Z	Height of measurement for windspeed, temperature, and vapor pressure
ΔZ	Difference in vertical distance at two heights (Z_2-Z_1)
α	Coefficient
β	Bowen ratio
β_0,β_1,β_2	Regression coefficients
Γ	Dry adiabatic lapse rate
γ	Psychrometer constant
λ	Latent heat of vaporization
λE	Latent-heat flux
λE_{br}	Latent-heat flux, Bowen-ratio method
λE_d	Daily total latent-heat flux
λE_{ec}	Latent-heat flux, direct eddy-correlation method
λE_{eb}	Latent-heat flux, energy-balance-residual eddy-correlation method
λE_i	Instantaneous latent-heat flux
φ	Expression of windspeed and temperature difference
ρC_p	Volumetric heat capacity of air
ρw	Water density
σ	Stefan-Boltzmann constant
$\Delta\Theta$	Difference in potential temperature at two heights (Z_2-Z_1)
υ	Kinematic viscosity of air
ε_a	Longwave emissivity of the atmosphere
ε_s	Longwave emissivity of the surface
$'$	Instantaneous deviation from the mean
$\overline{\quad}$	Mean for indicated period

EVAPOTRANSPIRATION MEASUREMENTS OF NATIVE VEGETATION, OWENS VALLEY, CALIFORNIA, JUNE 1986

Edited by David H. Wilson,[1] Robert J. Reginato[2], *and* Kenneth J. Hollett[1]

Abstract

Evapotranspiration (*ET*) is a major component of a hydrologic budget, but one of the least understood. Measurements of *ET* at the land surface are usually point measurements because of local effects caused by the immediate surroundings. These point measurements can be made by using the Bowen-ratio or eddy-correlation methods. It is useful to know how far these measurements can be extrapolated over a large area, such as a basin. Remote sensing of reflected and emitted radiation offer methods to estimate *ET* spatially and temporally. Measurements were made at three study sites in Owens Valley, California, in June 1986, to compare the results of ground-based Bowen-ratio and eddy-correlation systems with airborne radiometric methods and satellite Thematic-Mapper data. The results of the comparison indicate that all the methods used gave approximate values of *ET* at each of the study sites. The daily *ET* derived from all methods was similar, indicating that each adequately described water loss from each of the sites.

INTRODUCTION

A cooperative study was conducted during the first week of June 1986 to investigate the spatial and temporal variability of evapotranspiration (*ET*) in Owens Valley, California (fig. 1). Both remotely sensed and ground-based measurements were taken to evaluate *ET* from three sites which have different plant communities and depths to ground water.

Measurements of *ET* on the ground by use of Bowen-ratio or eddy-correlation methods are usually considered point measurements because they are influenced by the immediate surroundings. It is of interest to know how far these measurements can be reliably extrapolated, even over similar terrain and vegetative types. This can be important where the water table is at varying depths. Remotely sensed observations of reflected and emitted radiation offer the opportunity to evaluate *ET* both in space and time. This report discusses the results of the experiment.

---

[1]U.S. Geological Survey, Sacramento, California

[2]U.S. Department of Agriculture, Agricultural Research Service, Albany, California; formerly with the U.S. Water Conservation Laboratory, Phoenix, Arizona

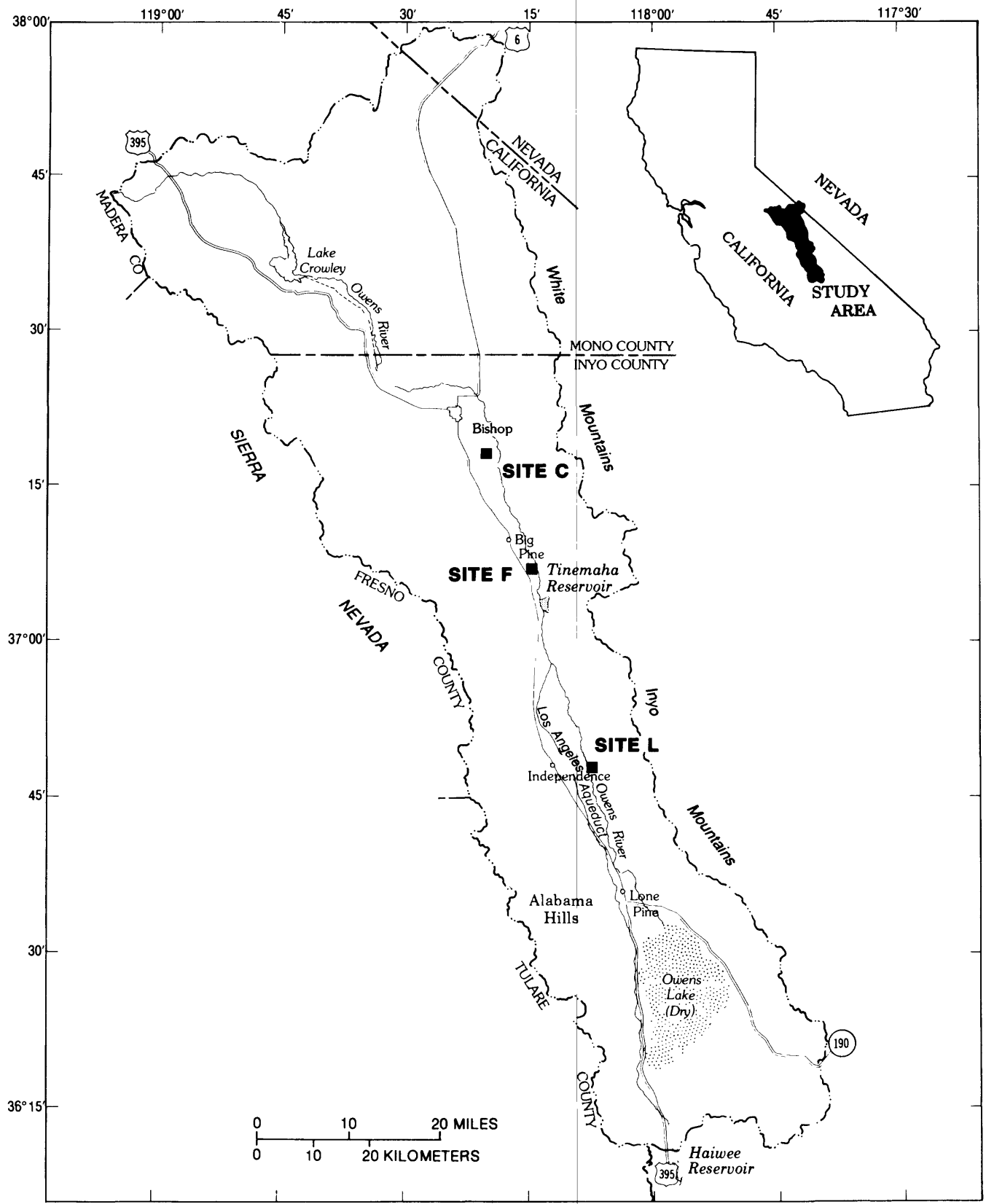

Figure 1. Location of Owens Valley and vicinity, and evapotranspiration measurement sites.

Measurements were made at three locations during the first week in June 1986. Bowen-ratio and eddy-correlation systems were operated, hand-held radiometric measurements were made, and airborne radiometric data were collected at the three sites. Additionally, plant, soil-water, and climatic data were collected when possible. Data were collected intensively for the period June 2-5, 1986.

Bowen-ratio and eddy-correlation measurements were made continuously and were averaged over periods ranging from 5 to 10 minutes. Observations using a hand-held radiometer were made about the time of Landsat 5 flyover (1052 hours Pacific daylight time, P.d.t.), solar noon (approximately 1251 hours P.d.t.), and about 2 hours past solar noon. Airborne observations, from an altitude of 150 m, were made at the same time the hand-held radiometer was in use. The ground-based sensors, including pyranometers, net radiometers, and soil-heat-flux plates, were calibrated prior to the experiment.

In addition to these intensive measurements, soil-water content was measured with a neutron probe before and during the study. Water levels were measured in observation wells at each of the three sites, and data from the California Irrigation Management Information System (CIMIS) weather station in Bishop, California, were also collected. The weather was clear and warm during the study except for one slightly cloudy day, June 4, 1986.

This report includes eight chapters, each written by individuals responsible for a particular method. Each chapter is intended to stand alone; the concluding chapter compares the individual *ET* measurement techniques. A list of the measurements made at each site and the agencies involved follows.

SITE C	
Bowen ratio	University of Arizona, U.S. Geological Survey
Eddy correlation	U.S. Geological Survey
Hand-held radiometer	U.S. Water Conservation Laboratory
Plant photosynthesis	University of California, Davis
Leaf-diffusion resistance	Inyo County Water Department
Plant model	Inyo County Water Department
SITE F	
Bowen ratio	U.S. Geological Survey
Eddy correlation	U.S. Geological Survey
Hand-held radiometer	U.S. Water Conservation Laboratory
Plant model	Inyo County Water Department
SITE L	
Bowen ratio	University of Arizona
Eddy correlation	U.S. Geological Survey
Hand-held radiometer	U.S. Water Conservation Laboratory
Plant model	Inyo County Water Department
Airborne	
Radiometers and video system all three sites	University of Arizona and U.S. Water Conservation Laboratory
Satellite Thematic Mapper and Airborne Imaging Spectrometer and Thematic Mapper simulator all three sites	University of California, Davis

Melvin L. Blevins
Department of Water and Power
City of Los Angeles
P.O. Box 111, Room 1466
Los Angeles, CA 90051
(213) 481-5339

Wesley R. Danskin
U.S. Geological Survey
5735 Kearny Villa Road, Suite O
San Diego, CA 92123
(619) 557-6700

Lowell F.W. Duell, Jr.
U.S. Geological Survey
5735 Kearny Villa Road, Suite O
San Diego, CA 92123
(619) 557-6700

Lloyd W. Gay
School of Renewable Natural Resources
University of Arizona
Tucson, AZ 85721
(602) 621-7268

David P. Groeneveld
Inyo County Water Department
163 May Street
Bishop, CA 93514
(619) 872-1168

Kenneth J. Hollett
U.S. Geological Survey
Office of the Regional Hydrologist
12201 Sunrise Valley Dr., MS 433
Reston, VA 22092
(703) 648-5805

Ray D. Jackson
U.S. Water Conservation Laboratory
4331 East Broadway Road
Phoenix, AZ 85040
(602) 379-4356

M. Susan Moran
U.S. Water Conservation Laboratory
4331 East Broadway Road
Phoenix, AZ 85040
(602) 379-4356

Russel H. Rawson
Department of Water and Power
City of Los Angeles
873 North Main Street
Bishop, CA 93514
(619) 872-1104

Robert J. Reginato
U.S. Department of Agriculture
Agricultural Research Service
800 Buchanan
Albany, CA 94710
(510) 559-6060

David I. Stannard
U.S. Geological Survey
Box 25046, MS 413
Denver Federal Center
Lakewood, CO 80225
(303) 236-4983

Susan L. Ustin
Department of Land, Air, and Water Resources
University of California
Davis, CA 95616
(916) 752-0621

Daniel C. Warren
Department of Natural and
Renewable Resources
University of Arizona
Tucson, AZ 85721

Harold L. Weaver
(formerly U.S. Geological Survey)
HCR 88, Box 160
Baker City, OR 97814
(503) 893-6467

CHAPTER A.--BOWEN-RATIO MEASUREMENTS AT SITES C AND L

By Lloyd W. Gay (University of Arizona, Tucson)

INTRODUCTION

Owens Valley is an arid basin located just east of the Sierra Nevada in central California. Despite the low annual precipitation (about 100 to 150 mm), the basin contains large quantities of ground water derived from the nearby mountains. Owens Valley is an important source of water for the city of Los Angeles.

Owens Valley has been the focus of an intensive cooperative study of the relation between vegetation and ground water, conducted by the Los Angeles Department of Water and Power, the U.S. Geological Survey, and the Inyo County Water Department. Previous results from this cooperative study have been reported by Dileanis and others (1985), Duell and Nork (1985), and Groeneveld and others (1985). As part of this study, a number of investigators measured evapotranspiration simultaneously at several locations in Owens Valley, California, in early June 1986, by using several different methods in an evaluation of areal evapotranspiration. Chapter A describes the Bowen-ratio method and specialized instrumentation used by the University of Arizona, and presents the results collected at a dry site (site C) and at a meadow site (site L) for the period June 2-5, 1986. Site C is near Bishop, California, and site L is near Independence, California (fig. 1).

BOWEN-RATIO METHOD

The Bowen-ratio method combines measurements of certain atmospheric variables (gradients of temperature and vapor concentration) and available energy (net radiation and changes in stored thermal energy) to determine estimates of evapotranspiration (*ET*). Units of *ET* are the depth of water evaporated per unit of time, or millimeter per day in this study. The method is commonly used and described in many studies. The method and field applications are described by Tanner (1960) and Spittlehouse and Black (1980). The model and units of measurement used by the University of Arizona, Tucson, in this chapter are described below.

The method is based on an energy-budget analysis of the gains and losses of thermal energy at the evaporating surface of soil and vegetation. Four major energy flows at the surface are: (1) net exchange of all wave thermal radiation (net radiation, Q); (2) rate of energy storage in the soil and vegetation (soil-heat flux, G); (3) convection, or sensible heat exchange between the surface and the atmosphere (sensible-heat flux, H); and (4) latent energy associated with the water vapor that flows between the surface and the atmosphere (latent-heat flux, λE). These energy flows are flux densities, or energy per unit time per unit area, and are measured as joules per second per square meter [$(J/s)/m^2$], or watts per square meter (W/m^2) as 1 J/s equals 1 W.

The latent energy term differs from the others in that it represents a mass flux density of water vapor between the surface and the atmosphere (E, $[(kg/s)/m^2]$) and the latent heat of vaporization (λ equal to about 2,450 J/g at 20 °C). Note that there is complete equivalence between the λE and the depth of

evaporated water that contains an equivalent amount of latent heat of vaporization. *ET* can be computed from λE as $ET = \lambda E/\rho w\lambda$, where ρw is the density of water. In practice, the latent energy-flux density is integrated over a 24-hour period to yield the daily energy total (in megajoules per square meter per day), and divided by the coefficient 2.45 to yield daily *ET* (in millimeters).

The surface energy-balance equation used in this chapter is:

$$Q + G + H + \lambda E = 0, \tag{A1}$$

where

Q is net radiation, in watts per square meter;
G is soil-heat flux, in watts per square meter;
H is sensible-heat flux, in watts per square meter; and
λE is latent-heat flux, in watts per square meter.

The sum of the four energy-flux densities must always equal zero for the period of evaluation, regardless of whether this period extends over seconds, minutes, hours, or days. Each flux density term in equation A1 can represent either a gain or a loss of energy to the surface, depending on environmental conditions. The polarities of the energy flows in this chapter are defined as positive when directed to the surface, and negative when directed away. The polarity can be visualized for Q, H, and λE, but is less apparent for G. Flux density G will be negative whenever thermal energy flows into the soil and vegetation substrate in a direction away from the interface with the atmosphere; it will be positive whenever energy flows out of the substrate into the atmosphere.

The Q and G terms in equation A1 can be evaluated by direct measurement, using net radiometers and soil-heat-flux plates, respectively. The H and λE terms are estimated in this chapter by the Bowen-ratio method (Bowen, 1926)

$$\lambda E_{br} = -(Q + G)/(1 + \beta), \tag{A2}$$

where

λE_{br} is latent-heat flux by the Bowen-ratio method, in watts per square meter; and
β is the Bowen ratio, the ratio $H_{br} / \lambda E_{br}$, dimensionless, where
H_{br} is the sensible-heat flux by the Bowen-ratio method, in watts per square meter.

β is measured as defined below. The method is well known and described in many articles and texts (Tanner, 1960; Spittlehouse and Black, 1980).

β is a function of measured gradients of temperature and vapor concentration in the atmosphere just above the evaporating surface. The exact formulation depends primarily upon the units chosen to represent vapor concentration in the atmosphere (Spittlehouse and Black, 1980). The formulation used in this chapter is

$$\beta = H_{br} / \lambda E_{br} = \gamma(\Delta\Theta/\Delta e), \tag{A3}$$

where

γ is the psychrometer constant, in millibars per degree Celsius;
$\Delta\Theta$ is the difference in potential temperature in the atmosphere between upper level, Z_2, and lower level, Z_1, just above the evaporating surface, in degree Celsius; and
Δe is the difference in vapor pressure between the same two levels, in millibars.

The psychrometric constant is taken here as $\gamma = 0.66$ mbar/°C at sea level. The sea level constant must be multiplied by P/P_0 to correct for altitude, where P is the atmospheric pressure at the experimental site, and P_0 is atmospheric pressure at sea level. The ratio P/P_0 was approximated from the International Standard Atmosphere (List, 1984) as 0.864 for site C (altitude, 1,220 m) and 0.867 for site L (altitude, 1,190 m), yielding psychrometric constants of 0.57 mbar/°C at sites C and L.

Potential air-temperature differences take into account the adiabatic lapse rate over the vertical distance ΔZ (in meters) between the upper (Z_2) and the lower (Z_1) levels of measurement, and are thus slightly larger than measured air-temperature differences. The potential air-temperature difference over $\Delta Z = Z_2 - Z_1$ is approximated from the measured air-temperature difference ($\Delta T = T_2 - T_1$) as $\Delta\Theta = \Delta T - \Gamma\Delta Z$, where Γ, the dry adiabatic lapse rate in the atmosphere, is taken as -0.01 °C/m. In practice, errors in β from use of ΔT in place of $\Delta\Theta$ tend to be small over drier, smoother surfaces which generally have large air-temperature gradients.

Equation A3 incorporated the usual assumption of equality of the transfer coefficients for sensible- and latent-energy transfer (Tanner, 1960). This assumption is well-confirmed experimentally for unstable conditions (as prevailed at site C throughout the daylight hours), where air temperatures decrease with height and sensible-heat flux is directed from the surface into the atmosphere so that $H<0$ (Denmead and McIlroy, 1970). More recent works (Verma and others, 1978; Lang and others, 1983) suggest that the Bowen ratio may be in error as the transfer coefficients deviate from equality under stable conditions, where air temperatures increase with height and the sensible-heat flux is directed downward toward the surface to that $H>0$. No consistent relations yet have been proposed for correcting the Bowen ratio during stable conditions, as observed during the late afternoons at site L when warm air from the surrounding arid regions moved over the transpiring meadow. However, the magnitude of positive sensible heat occurring at site L during these periods was rather small, and no stability corrections were applied to the Bowen-ratio results at either site.

INSTRUMENTATION

The battery-powered Bowen-ratio recording system used in this study consists of a set of specialized sensors, a data-acquisition recording system, and a microcomputer (Gay, 1988). The field sensors are connected by cables to the data-acquisition and processing instruments, which can operate in an insulated container or in a small trailer. Data collected during this study were sampled with a digital data system (Hewlett Packard 3421A) that transformed, analyzed, and stored data in real time and printed the results. A Bowen-ratio analysis was completed every 12 minutes by the microcomputer and the values were integrated to yield hourly and daily totals of λE_{br}. The λE_{br} totals are converted to an equivalent depth of evaporated water as described earlier.

The key sensors in the University of Arizona *ET* measurement system are psychrometers that include a ceramic wet-bulb element, high output resistance thermometers, and a unique signal circuit which together give precise measurements of temperature and humidity (Hartman and Gay, 1981). The psychrometers are used in pairs, separated vertically by approximately 1 m, to measure the gradients of temperature and vapor concentration in the air layer just above the plant canopy. The performance of the psychrometer is enhanced for gradient measurements by alternating the positions of the two psychrometers between readings to eliminate from the gradients any small biases that may occur between sensors. The psychrometers were interchanged every 6 minutes so that λE_{br} estimates are means for 12-minute periods (Gay, 1988).

MEASUREMENT SITES

Site C in the Owens Valley study was located a few kilometers southeast of Bishop, California, at an altitude of approximately 1,220 m. The site is sparsely vegetated with scattered clumps of plants that range in height from 0.5 to 1 m. The dominant species include Nevada saltbush, rubber rabbitbrush, saltgrass, Russian thistle, greasewood, and alkali sacaton. The deep, well-drained alluvial soil is coarse and loamy. The water table at this site was 4 m below the surface when the soil was described on December 15, 1983, but the depth to water was not known at the time of the study. The water table can be very close to land surface in Owens Valley. The sparse vegetation appeared vigorous during the June 1986 measurements despite the aridity of the site, indicating that the plants were obtaining moisture from the water table.

The data-acquisition instruments at site C were enclosed in a small equipment trailer that was located south of an old observation well. The trailer was parked at the northern edge of the area sampled by airborne instruments (see chapter G, this report). The psychrometer mast was positioned 60 m farther south in this area, and near the climate station operated by the U.S. Water Conservation Laboratory. The lower psychrometer was approximately 1 m above the land surface, and the upper psychrometer was at 1.96 m. The anemometer was placed at 2.45 m above the land surface in order to be 2 m above the zero plane of the vegetation. Three net radiometers were used at this site: one was positioned above bare soil, one was over a bush, and one was above sparse grass. Two sets of paired soil-heat-flux plates were buried at a depth of 1 cm; one set was in an area of bare soil and the second set was set beneath a bush. The Q and G values reported here are equally weighted means of the three net radiometers and the four soil-heat-flux plates.

Site L was about 2 km east of Independence, California, at an altitude of about 1,190 m. The vegetation was low, with scattered clumps growing to a height of about 0.3 m near the psychrometer mast. The dominant species at this site are saltgrass, Baltic rush, and alkali sacaton. The deep, fine loamy soils are poorly drained. The depth to water was not known at the time of the measurements, but it can be close to land surface. The water-table depth at this site was only 1.1 m when the soils were described on August 20, 1983.

The data-acquisition instruments at site L were installed in an insulated field case and connected to the sensors and psychrometer mast by a 15-m-long cable. Instruments were located about 50 m west of the observation well at site L, and northwest of the U.S. Geological Survey eddy-correlation instruments. The lower psychrometer was placed 0.44 m above the land surface, and the upper one was at 1.41 m. The anemometer was 2 m above land surface. The three net radiometers and the pair of soil-heat-flux plates (buried at a depth of 1 cm) were in areas of similar vegetation. The values of Q and G reported here are equally weighted averages of three net radiometers and two soil-heat-flux plates.

RESULTS AND DISCUSSION

TWELVE-MINUTE OBSERVATIONS

The basic Bowen-ratio analysis was for 12-minute periods. The 12-minute microclimate data and energy-budget analyses were internally consistent at both sites throughout the 4 days of measurement. The consistency is evident in the 12-minute energy-budget plots (fig. A1) through one diurnal cycle at both sites on June 5, which was the only completely clear day during the measurement period. The H_{br} and λE_{br} show little short-term fluctuation throughout the day, with H_{br} larger than λE_{br} at site C and much smaller than λE_{br} at site L (fig. A1).

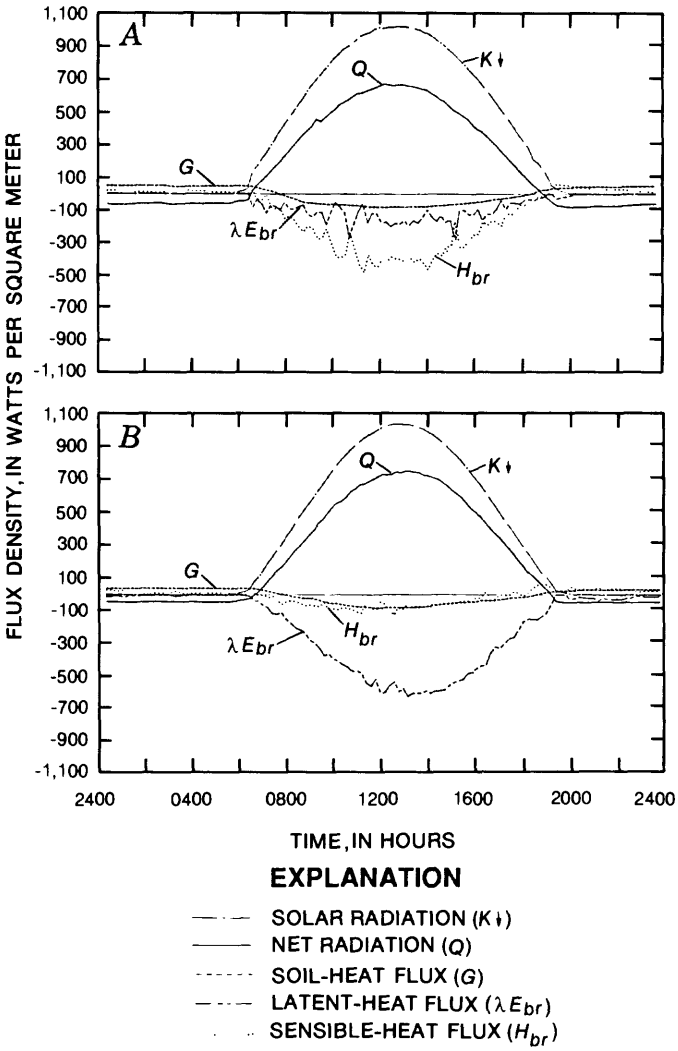

Figure A1. Twelve-minute solar radiation and energy balance at sites C and L, June 5, 1986, using the Bowen-ratio method. *A*, Site C. *B*, Site L.

ONE-HOUR MEANS

The 12-minute data were processed into 1-hour and 24-hour means to facilitate examination and presentation. The 1-hour mean energy budget and microclimate data were tabulated each day in tables A1 (site C) and A2 (site L). Energy-balance means are plotted in figures A2 (site C) and A3 (site L).

DAILY MEANS

The primary purpose of this study was to determine daily means and totals. The daily mean energy-budget components and microclimatic data in tables A1 and A2 are summarized in table A3. The daily mean climatic data confirm that site L (meadow site) was cooler, more humid, and windier than site C (dry site). The daily mean energy-flux densities indicate that (1) net radiation was somewhat greater over the meadow (site L); (2) the soil-heat flux was about the same at both sites; and (3) latent energy was substantially greater at site L. Furthermore, the daily mean Bowen ratio at site L was nearly zero. If β=0, then equation A2 indicates that virtually all the available energy ($Q + G$) at site L went into evaporation of water. In contrast, the daily mean Bowen ratios at site C were nearly 2.0 and the equation $\beta = H_{br} / \lambda E_{br}$ indicates that convection was almost twice as large as latent energy at site C, the drier, more sparsely vegetated site.

The daily mean latent-energy-flux densities in table A3 also are transformed from watts per square meter to *ET*, the equivalent depth of evaporated water, in millimeters. Daily *ET* at site C ranged from -2.27 to -2.45 mm, with a 4-day mean of -2.33 mm/d. In contrast, daily *ET* at site L ranged from -7.38 to -8.32 mm, with a 4-day mean of -7.90 mm/d.

QUALITY OF DATA

The overall quality of the data and analyses in this chapter appear to be satisfactory. However, four points to be considered when assessing the quality of the data measured by the University of Arizona instruments are: (1) interpolation of missing data at site L on June 2, (2) adjustment for wet-bulb bias at site C on June 3, (3) calibration coefficients used for the net radiometers and soil-heat-flux plates at both sites, and (4) placement of the net radiometers and soil-heat-flux plates at site C.

Table A1. Energy budget and microclimate 1-hour means for site C, June 2-5, 1986

[$K\downarrow$, solar radiation, in watts per square meter; Q, net radiation, in watts per square meter; G, soil-heat flux, in watts per square meter; H_{br}, sensible-heat flux, in watts per square meter; λE_{br}, latent-heat flux, in watts per square meter; β, Bowen ratio, dimensionless; T, air temperature, in degree Celsius; ΔT, difference in air temperature at two heights (Z_2-Z_1), in degrees Celsius; e, vapor pressure, in millibars; Δe, difference in vapor pressure at two heights (Z_2-Z_1), in millibars; and U, horizontal windspeed, in meters per second]

Time (hours)	$K\downarrow$	Q	G	H_{br}	λE_{br}	β	T	ΔT	e	Δe	U
					June 2, 1986						
0030	0	-61	36	28	-2	-11	17.7	0.22	10.8	0	1.7
0130	0	-56	36	20	--	68.38	15.6	.21	10.9	0	1.0
0230	0	-54	36	17	--	22.51	14.6	.25	10.8	0	.8
0330	0	-54	34	21	-1	-14	14.6	.22	10.9	0	1.4
0430	0	-53	33	23	-2	-10	14.3	.22	10.5	-.01	1.4
0530	7	-46	33	14	-1	-11	13.0	.22	10.5	-.01	1.1
0630	101	24	24	-11	-37	.30	14.9	.06	10.9	-.06	.4
0730	293	169	4	-96	-77	1.24	18.9	-.23	11.1	-.10	1.4
0830	507	317	-37	-140	-140	1.00	23.1	-.46	11.0	-.27	2.1
0930	703	472	-68	-269	-134	2.00	26.1	-.74	11.4	-.21	1.0
1030	855	588	-74	-321	-193	1.67	28.4	-.79	10.6	-.26	.9
1130	963	659	-81	-447	-131	3.41	30.6	-.98	10.0	-.17	.7
1230	1,021	690	-85	-432	-173	2.50	32.9	-.92	9.3	-.20	1.8
1330	1,015	676	-85	-427	-165	2.59	34.0	-.92	9.4	-.20	1.8
1430	954	616	-79	-378	-159	2.37	34.5	-1.02	8.6	-.24	1.6
1530	842	521	-69	-344	-109	3.15	35.1	-.91	8.4	-.17	1.5
1630	689	395	-52	-210	-124	1.57	35.4	-.62	7.4	-.21	.9
1730	377	162	-15	-69	-78	.89	34.1	-.31	6.5	-.20	1.8
1830	296	100	1	-33	-68	.48	33.5	-.12	7.3	-.22	1.7
1930	73	-41	26	46	-30	-1.50	30.0	.36	8.9	-.16	.2
2030	2	-72	31	44	-4	-11	27.9	.25	8.9	-.15	3.7
2130	0	-67	30	37	--	-9.99	25.9	.20	9.1	-.27	2.4
2230	0	-66	33	41	-9	-4.56	23.8	.28	9.3	-.18	1.8
2330	0	-59	35	41	-17	-2.41	21.6	.31	9.4	-.07	1.0
Mean	. . . 362	198	-10	-118	-69	[1]1.71	25.0		9.7		1.4
					June 3, 1986[2]						
0030	0	-61	33	44	-16	-2.81	21.7	0.40	9.0	--	1.4
0130	0	-59	36	25	-3	-8.83	20.0	.68	9.1	--	.3
0230	0	-51	40	12	-2	-6.44	16.1	1.09	9.1	--	.2
0330	0	-53	37	34	-17	-1.94	15.7	.35	9.2	--	.6
0430	0	-53	37	29	-13	-2.28	14.6	.31	9.3	--	.9
0530	5	-48	35	13	1	9.61	14.2	.21	9.3	--	1.1
0630	107	22	25	-14	-33	.41	16.0	.02	9.7	--	1.5
0730	323	176	-2	-94	-80	1.18	20.9	-.30	10.2	--	1.5
0830	530	333	-45	-187	-101	1.85	25.2	-.52	10.5	--	.8
0930	713	472	-67	-284	-120	2.37	27.6	-.77	11.3	--	.5
1030	865	581	-74	-346	-160	2.17	30.0	-.80	11.0	--	.4
1130	973	657	-83	-404	-170	2.38	31.7	-.94	11.3	--	.4
1230	1,022	688	-87	-406	-194	2.09	33.9	-.83	11.4	--	1.0
1330	1,018	672	-85	-414	-174	2.38	35.1	-.93	10.3	--	1.8

See footnotes at end of table.

Table A1. Energy budget and microclimate 1-hour means for site C, June 2-5, 1986--*Continued*

Time (hours)	$K\downarrow$	Q	G	H_{br}	λE_{br}	β	T	ΔT	e	Δe	U
					June 3, 1986[2]--*Continued*						
1430	970	626	-79	-391	-156	2.50	36.0	-0.93	9.8	--	2.0
1530	822	510	-65	-328	-117	2.81	35.9	-.88	10.1	--	2.8
1630	616	351	-42	-224	-86	2.60	35.6	-.66	10.2	--	3.3
1730	428	207	-21	-132	-54	2.45	35.0	-.52	10.2	--	2.7
1830	281	95	-5	-48	-42	1.14	34.2	-.31	10.5	--	1.6
1930	71	-40	22	23	-4	-5.64	30.5	.23	10.3	--	.5
2030	1	-73	36	37	-2	-19	26.3	.76	9.2	--	.3
2130	0	-71	41	29	-2	-15	23.8	.56	9.3	--	.5
2230	0	-62	43	21	-2	-11	21.2	.98	9.3	--	.2
2330	0	-62	42	17	-2	-8.68	20.9	.68	8.8	--	.7
Mean . . .	364	198	-9	-124	-64	[1]1.93	25.9		9.9		1.1
					June 4, 1986						
0030	0	-58	42	22	-6	-3.42	18.6	1.15	8.7	-0.95	0.2
0130	0	-53	42	19	-8	-2.39	15.6	.59	9.0	-.50	.3
0230	0	-51	43	14	-5	-2.82	14.2	.68	9.0	-.36	.2
0330	0	-49	42	9	-1	-6.31	13.8	.92	8.8	-.24	.4
0430	0	-48	43	7	-3	-2.47	12.0	1.12	8.6	-.24	.2
0530	5	-46	43	3	0	4.95	10.6	.43	8.5	-.35	.3
0630	110	22	31	0	-53	.00	16.2	.08	9.2	-.34	1.0
0730	244	114	17	[3]-65	[3]-66	[3]1.00	23.5	--	9.8	--	1.4
0830	583	359	-46	-190	-124	1.53	24.2	-.59	8.5	-.24	.3
0930	755	487	-66	-240	-181	1.32	28.0	-.61	8.3	-.23	.2
1030	880	594	-76	-388	-131	2.97	29.9	-1.04	9.0	-.20	2.2
1130	987	672	-81	-441	-150	2.94	31.9	-1.00	9.6	-.19	4.0
1230	909	601	-70	-372	-159	2.35	33.2	-.81	7.3	-.19	5.3
1330	782	508	-57	-310	-141	2.19	33.4	-.68	7.2	-.17	5.3
1430	825	538	-57	-333	-148	2.25	34.3	-.73	7.2	-.18	5.6
1530	779	495	-52	-318	-123	2.56	34.4	-.70	7.4	-.15	5.3
1630	666	385	-40	-231	-114	2.02	33.9	-.62	7.5	-.18	5.4
1730	510	270	-23	-171	-76	2.26	33.0	-.44	8.2	-.11	5.3
1830	290	117	-1	-69	-44	1.57	31.8	-.22	8.4	-.09	4.7
1930	91	-27	25	19	-17	-1.11	29.3	.05	7.1	-.07	1.7
2030	3	-84	40	57	-13	-4.36	24.9	.31	6.1	-.03	1.3
2130	0	-85	44	49	-8	-6.48	24.1	.65	6.2	-.04	1.0
2230	0	-82	43	40	-1	-33	20.4	.50	6.7	0	1.4
2330	0	-75	48	27	0	159	16.7	.59	6.4	0	.8
Mean . . .	351	188	-3	-119	-66	[1]1.81	24.5		8.0		2.2
					June 5, 1986						
0030	0	-70	51	19	0	36.23	14.6	0.92	6.3	0.01	0.4
0130	0	-63	51	11	0	18.83	11.4	.93	6.3	.03	.2
0230	0	-63	49	13	0	20.81	11.7	1.08	7.0	.08	.7
0330	0	-65	45	20	0	433	11.4	.60	7.2	.00	.4
0430	0	-62	48	14	0	123	9.2	.67	6.7	.00	.3

See footnotes at end of table.

Table A1. Energy budget and microclimate 1-hour means for site C, June 2-5, 1986--*Continued*

Time (hours)	$K\downarrow$	Q	G	H_{br}	λE_{br}	β	T	ΔT	e	Δe	U
					June 5, 1986--*Continued*						
0530	5	-56	50	6	0	17.67	8.5	1.13	6.6	0.03	0.4
0630	118	15	39	-17	-37	.45	9.4	.09	6.7	-.08	.5
0730	346	171	4	-89	-87	1.02	17.0	-.26	7.0	-.15	.4
0830	556	336	-44	-194	-97	2.00	21.0	-.59	6.2	-.17	.4
0930	749	469	-65	-266	-138	1.93	23.8	-.69	5.4	-.21	.4
1030	901	574	-72	-356	-146	2.45	25.7	-.90	4.9	-.20	.6
1130	1,004	651	-82	-447	-122	3.66	28.0	-1.04	4.9	-.16	.6
1230	1,048	687	-86	-411	-190	2.16	29.9	-.67	5.4	-.17	1.0
1330	1,043	677	-82	-422	-174	2.42	30.6	-.90	5.4	-.21	1.7
1430	981	619	-75	-396	-147	2.69	31.0	-.89	5.3	-.19	1.1
1530	857	511	-62	-291	-158	1.84	31.7	-.69	5.9	-.19	.6
1630	696	388	-46	-211	-131	1.61	31.6	-.65	5.8	-.23	.7
1730	501	241	-24	-148	-69	2.13	31.3	-.57	6.2	-.16	.8
1830	279	82	2	-44	-40	1.11	30.6	-.28	6.7	-.15	.3
1930	72	-48	34	28	-14	-2.04	27.7	.27	8.0	-.22	1.1
2030	2	-83	44	44	-5	-9.52	23.6	.19	7.8	-.00	2.9
2130	0	-77	47	30	0	129	20.4	.31	7.8	.00	1.5
2230	0	-72	47	25	0	-783	18.6	.38	7.6	-.00	.8
2330	0	-64	50	14	0	41.43	15.7	.73	7.7	.00	.2
Mean . . .	382	196	-3	-128	-65	[1]1.98	21.4		6.4		0.7

[1]Mean β calculated as H_{br} / λE_{br}.
[2]H_{br}, λE_{br}, and β values corrected for psychrometer malfunction.
[3]H_{br}, λE_{br}, and β values interpolated for 0730 hours.

Table A2. Energy budget and microclimate 1-hour means for site L, June 2-5, 1986

[$K\downarrow$, solar radiation, in watts per square meter; Q, net radiation, in watts per square meter; G, soil-heat flux, in watts per square meter; H_{br}, sensible-heat flux, in watts per square meter; λE_{br}, latent-heat flux, in watts per square meter; β, Bowen ratio, dimensionless; T, air temperature, in degree Celsius; ΔT, difference in air temperature at two heights (Z_2-Z_1), in degrees Celsius; e, vapor pressure, in millibars; Δe, difference in vapor pressure at two heights (Z_2-Z_1), in millibars; and U, horizontal windspeed, in meters per second]

Time (hours)	$K\downarrow$	Q	G	H_{br}	λE_{br}	β	T	ΔT	e	Δe	U
					June 2, 1986						
0030	0	-45	29	27	-12	2.33	18.7	0.85	10.9	-0.17	2.1
0130	0	-45	28	26	-10	-2.69	17.8	.79	11.0	-.14	1.9
0230	0	-45	29	33	-16	-2.07	16.5	.49	11.3	-.13	2.7
0330	0	-45	29	25	-9	-2.79	16.0	.54	11.1	-.08	2.1
0430	0	-44	29	23	-8	-2.88	14.8	.45	11.1	-.08	2.2
0530	3	-41	28	19	-6	-3.27	14.6	.49	11.1	-.08	1.9

Table A2. Energy budget and microclimate 1-hour means for site L, June 2-5, 1986--*Continued*

Time (hours)	$K\downarrow$	Q	G	H_{br}	λE_{br}	β	T	ΔT	e	Δe	U
					June 2, 1986--*Continued*						
0630[1]	75	13	24	-1	-26	0.03	16.5	--	11.2	--	1.8
0730[1]	260	160	6	-36	-130	.28	20.5	--	11.3	--	1.7
0830[1]	466	320	-17	-59	-244	.24	23.9	--	11.4	--	1.6
0930[1]	668	474	-44	-75	-355	.21	25.4	--	11.5	--	1.6
1030	846	600	-65	-85	-450	.19	26.4	-0.33	11.6	-0.98	1.5
1130	973	705	-81	-78	-546	.14	28.5	-.33	11.4	-1.26	1.1
1230	1,037	765	-86	-50	-629	.08	30.4	-.20	11.5	-1.41	2.2
1330	1,034	779	-68	-36	-674	.05	31.6	-.13	11.5	-1.37	4.1
1430	959	719	-55	-27	-637	.04	32.4	-.10	11.6	-1.28	4.4
1530	827	614	-47	-18	-550	.03	33.1	-.08	11.4	-1.44	3.1
1630	641	455	-41	0	-414	.00	33.2	.00	9.8	-1.47	1.6
1730	438	300	-26	29	-303	-.10	33.1	.26	10.1	-1.55	1.7
1830	219	132	7	91	-229	-.40	31.0	.43	9.8	-.60	5.4
1930	46	-17	22	35	-40	-.88	28.8	.63	9.0	-.40	3.9
2030	1	-52	27	70	-45	-1.56	27.0	.87	7.9	-.35	2.3
2130	0	-44	29	40	-25	-1.60	24.4	2.26	7.6	-.73	1.7
2230	0	-41	31	29	-18	-1.59	19.3	1.23	9.2	-.43	2.0
2330	0	-41	30	27	-16	-1.68	19.3	1.14	9.6	-.34	1.9
Mean . . .	354	232	-8	0	-225	[2]-0.00	24.3		10.6		2.4
					June 3, 1986						
0030	0	-38	30	14	-7	-2.08	18.7	1.61	9.7	-0.40	1.2
0130	0	-35	29	14	-7	-1.90	18.3	1.06	9.9	-.41	1.4
0230	0	-40	29	23	-12	-1.88	17.7	1.15	9.8	-.34	1.6
0330	0	-40	29	28	-17	-1.69	17.6	.89	9.5	-.27	2.0
0430	0	-42	28	27	-14	-1.97	17.4	.90	9.6	-.21	1.9
0530	4	-35	29	9	-3	-3.09	14.8	.89	9.8	-.18	1.6
0630	75	13	24	15	-52	-.29	16.5	.52	10.3	-.40	1.4
0730	260	160	6	11	-177	-.06	21.2	.05	11.0	-.43	2.9
0830	466	320	-17	-23	-280	.08	24.9	-.10	11.6	-.70	2.4
0930	668	474	-44	-34	-396	.09	26.9	-.15	11.2	-.99	2.2
1030	841	608	-66	-46	-496	.09	29.0	-.21	11.5	-1.26	1.5
1130	963	708	-84	-42	-582	.07	30.6	-.20	11.8	-1.50	1.4
1230	1,029	766	-88	-36	-643	.06	31.7	-.17	12.2	-1.68	2.4
1330	1,024	766	-78	-29	-659	.04	32.5	-.14	12.1	-1.00	3.0
1430	953	712	-65	-22	-624	.04	33.0	-.10	12.0	-1.54	3.3
1530	821	615	-46	4	-573	.00	33.2	.02	11.3	-1.43	3.8
1630	636	473	-26	21	-469	-.05	32.9	.08	11.6	-1.02	4.7
1730	415	294	-9	42	-326	-.13	32.2	.20	11.4	-.86	4.2
1830	208	123	5	44	-171	-.25	30.5	.34	11.7	-.72	3.2
1930	44	-9	15	17	-24	-.72	27.7	1.49	11.5	-1.04	2.0
2030	1	-43	23	79	-58	-1.35	27.1	1.38	10.5	-.62	2.0
2130	0	-41	24	50	-33	-1.51	25.7	1.65	10.3	-.68	1.5
2230	0	-40	27	40	-27	-1.44	21.8	1.72	10.4	-.66	1.5
2330	0	-39	30	22	-12	-1.77	20.3	1.76	9.7	-.74	1.1
Mean . . .	350	235	-8	9	-236	[2]-0.04	25.1		10.8		2.3

See footnotes at end of table.

Table A2. Energy budget and microclimate 1-hour means for site L, June 2-5, 1986--*Continued*

Time (hours)	$K\downarrow$	Q	G	H_{br}	λE_{br}	β	T	ΔT	e	Δe	U
					June 4, 1986						
0030	0	-39	31	24	-16	-1.49	16.4	1.95	9.9	-0.74	1.4
0130	0	-39	32	18	-11	-1.72	15.1	1.10	10.5	-.36	1.7
0230	0	-38	31	16	-9	-1.76	14.8	1.17	9.8	-.38	1.6
0330	0	-39	32	14	-7	-2.06	13.3	1.11	10.1	-.29	1.3
0430	0	-39	33	10	-3	-2.96	11.9	1.12	10.1	-.20	1.0
0530	4	-36	33	7	-3	-1.88	10.8	1.11	9.9	-.22	.8
0630	82	12	28	-2	-38	.05	11.7	.29	10.9	-.27	.9
0730	267	152	1	-29	-124	.24	18.2	-.20	12.2	-.47	.7
0830	478	320	-27	-40	-252	.16	22.3	-.23	10.8	-.81	1.3
0930	686	488	-47	-64	-376	.17	25.0	-.31	10.9	-1.00	1.8
1030	863	624	-73	-67	-480	.14	27.6	-.32	10.8	-1.32	1.6
1130	925	679	-76	-35	-568	.06	29.1	-.16	10.8	-1.43	2.5
1230	925	697	-63	-11	-622	.02	30.2	-.04	9.2	-1.31	4.2
1330	870	654	-41	10	-624	-.02	30.5	.04	9.5	-1.01	5.6
1430	785	590	-28	21	-583	-.04	30.4	.06	8.9	-.88	6.4
1530	771	582	-26	5	-560	.00	30.3	.01	10.0	-.78	7.3
1630	514	374	-10	53	-417	-.13	29.7	.16	9.9	-.65	7.0
1730	393	269	-1	68	-336	-.20	29.9	.21	8.7	-.55	7.4
1830	192	98	11	81	-190	-.43	28.6	.35	8.6	-.44	6.0
1930	62	-7	17	30	-39	-.75	27.1	.45	7.9	-.34	5.1
2030	4	-53	24	64	-35	-1.80	24.3	.83	7.1	-.34	2.9
2130	0	-52	30	74	-52	-1.41	22.9	1.59	5.4	-.60	1.6
2230	0	-58	33	78	-53	-1.46	20.6	1.09	5.3	-.39	2.6
2330	0	-49	36	30	-16	-1.84	18.2	2.74	5.5	-.87	1.2
Mean . . .	326	212	0.8	15	-226	[2]-0.06	22.4		9.3		3.1
					June 5, 1986						
0030	0	-48	38	25	-14	-1.74	12.4	1.58	6.3	-0.48	1.5
0130	0	-47	39	15	-7	-2.19	10.0	1.55	6.3	-.40	1.3
0230	0	-45	40	11	-5	-2.05	8.3	1.49	6.5	-.39	1.0
0330	0	-45	40	11	-6	-1.73	6.9	1.37	6.3	-.41	1.3
0430	0	-47	39	10	-2	-4.23	6.4	.65	7.0	-.08	1.7
0530	5	-42	38	7	-3	-2.51	7.0	1.05	7.0	-.14	1.5
0630	80	2	33	0	-34	.03	8.5	.40	8.0	-.29	.8
0730	277	146	7	-33	-119	.28	14.3	-.15	8.5	-.32	.5
0830	491	308	-20	-56	-231	.24	19.5	-.25	8.1	-.58	1.3
0930	693	477	-44	-76	-357	.21	21.7	-.35	7.6	-.92	1.2
1030	870	614	-69	-94	-451	.21	23.4	-.39	7.5	-1.03	1.3
1130	997	712	-82	-79	-550	.14	25.1	-.33	6.7	-1.15	1.4
1230	1,062	759	-83	-94	-581	.16	26.5	-.37	6.5	-1.26	1.1
1330	1,055	766	-80	-73	-613	.12	27.9	-.31	7.6	-1.46	2.2
1430	977	717	-64	-61	-591	.10	28.6	-.25	8.0	-1.36	3.6
1530	837	603	-48	-41	-514	.08	28.9	-.19	7.6	-1.38	2.6
1630	649	455	-36	-15	-404	.04	29.4	-.09	7.0	-1.39	1.8
1730	436	290	-20	6	-276	-.02	29.3	.06	7.7	-1.42	1.7
1830	222	118	-2	36	-152	-.24	27.9	.37	7.6	-1.13	1.8
1930	46	-22	22	34	-34	-.98	24.9	.74	7.5	-.47	2.9
2030	1	-48	30	39	-21	-1.86	20.2	1.62	7.6	-.48	1.7
2130	0	-44	32	38	-26	-1.47	19.2	2.73	7.6	-1.03	1.7
2230	0	-47	33	33	-19	-1.69	17.4	1.28	8.2	-.43	1.5
2330	0	-45	34	22	-11	-2.09	15.4	1.20	8.4	-.32	1.4
Mean . . .	362	229	-5	-14	-209	[2]0.07	19.1		7.4		1.6

[1]All variables interpolated.
[2]Mean β calculated as $H_{br} / \lambda E_{br}$.

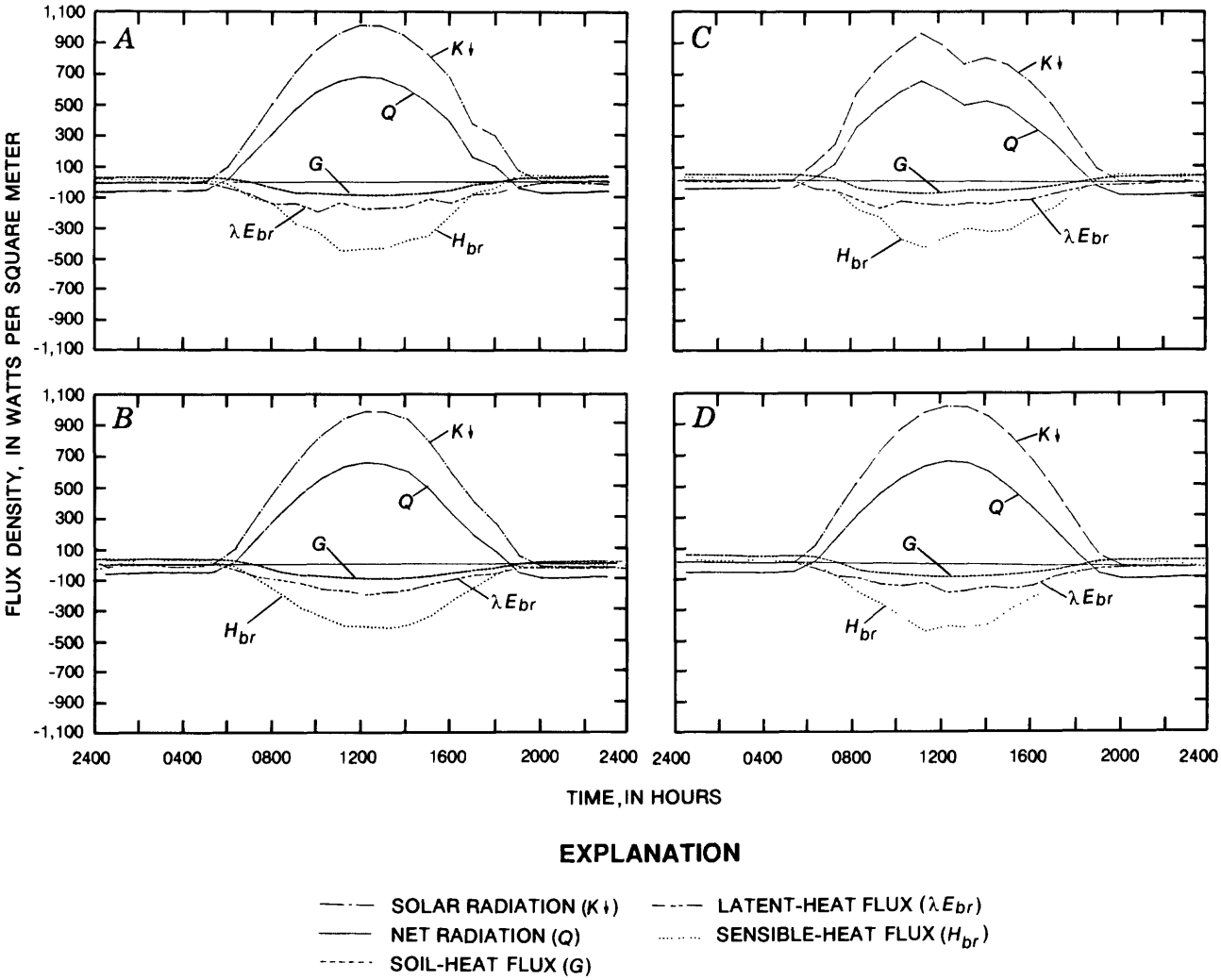

Figure A2. One-hour solar radiation and energy balance at site C, June 2-5, 1986, using the Bowen-ratio method. *A*, June 2. *B*, June 3. *C*, June 4. *D*, June 5.

Data may be missing for short periods during any measurement program for such reasons as instrument maintenance and inadvertent shutdown. However, at site L the microcomputer failed to record data for the 4-hour period, 0630 to 0930 hours, on June 2. The missing energy-budget and microclimate data were interpolated for this period by reference to data collected during the same time period on the preceding and following days with similar conditions. Little uncertainty was introduced into the daily means or total by this procedure because uniform, clear weather conditions prevailed each morning throughout the study.

Because of apparent wet-bulb bias, the λE_{br} values at site C on June 3 were unexpectedly higher than those measured on June 2, despite similar weather conditions. Calibration of the psychrometer early on June 4 indicated a bias in one wet bulb that caused an overestimation of the vapor-pressure gradient with a corresponding overestimation of the evaporation rate. The problem was corrected in the field and the values measured on June 4 and 5 were again similar to those obtained on June 2. The data from these

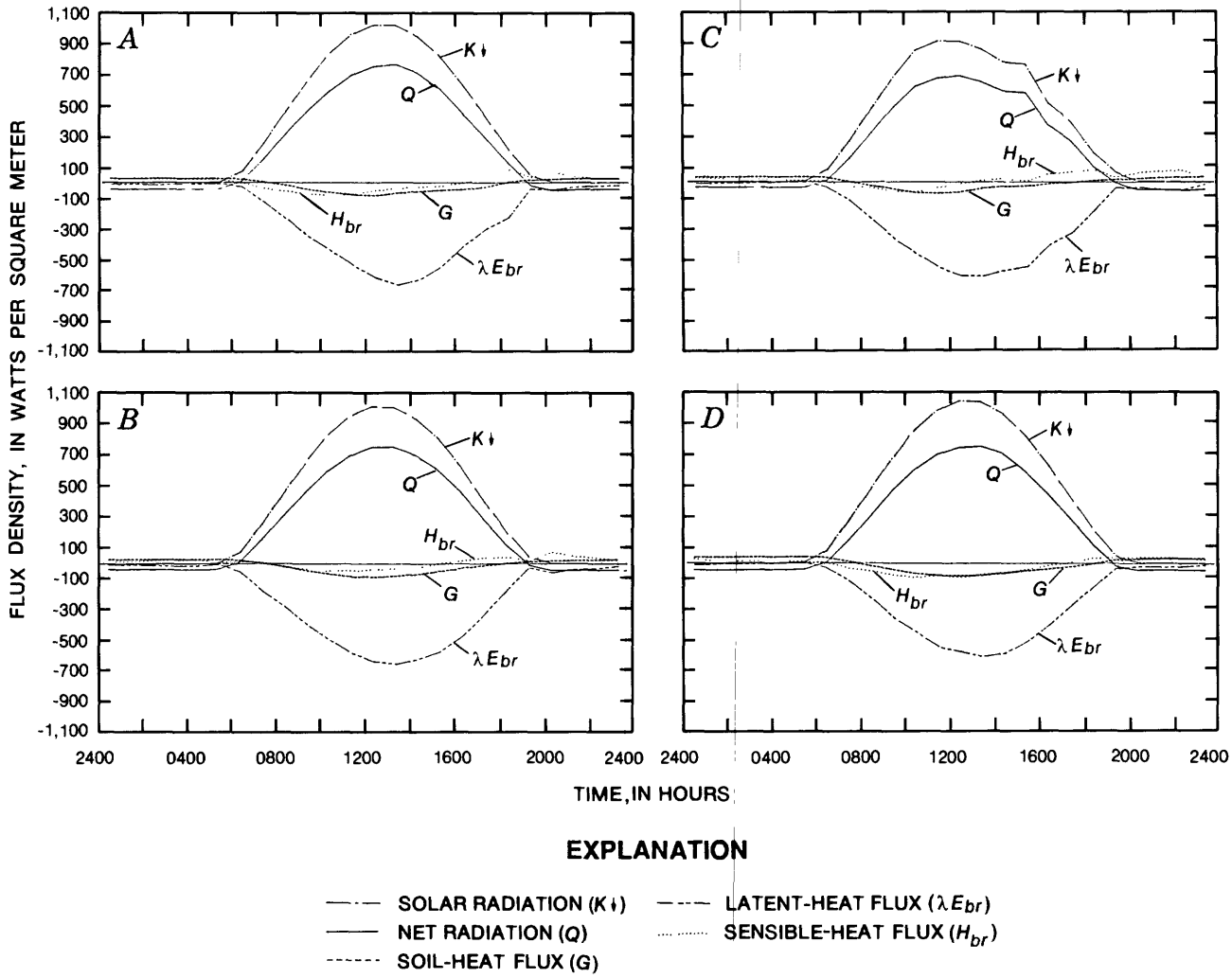

Figure A3. One-hour solar radiation and energy balance at site L, June 2-5, 1986, using the Bowen-ratio method. *A*, June 2. *B*, June 3. *C*, June 4. *D*, June 5.

3 days were used to derive a multivariate model that determined sensible heat during daytime as a function of available energy ($Q + G$), air-temperature difference (ΔT), and horizontal windspeed (U). The model H_{br} = -0.571 ($Q + G$) + 131.13 ΔT -2.38U + 47.97 fit the days of satisfactory data with a correlation coefficient $r^2 = 0.980$ and a standard error of 22.4 W/m^2. This model was used with mean hourly $Q + G$, ΔT, and U to estimate H_{br} for June 3, and λE was then computed from equation A1. The high r^2 and low standard error of this model give confidence in the estimates of λE for June 3 at site C.

The net radiometers and soil-heat-flux plates were calibrated at the U.S. Water Conservation Laboratory, Phoenix, Arizona, in preparation for this study. However, the new calibration coefficient for the net radiometers averaged 20 percent higher than the previous ones. The net-radiation values calculated with these coefficients seem high, as for example the mean rate of 779 W/m^2 at site L for the period, 1330 to 1440 hours, on June 2. Further, the new soil-heat-flux plate coefficients were 12 percent lower than in the past for the four plates used at site C, and 8 percent higher for the two plates used at site L. Confirmation of the appropriate calibration coefficients is needed for these standard sensors.

Table A3. Energy budget and microclimate daily means for sites C and L

[$K\downarrow$, solar radiation, in watts per square meter; Q, net radiation, in watts per square meter; G, soil-heat flux, in watts per square meter; H_{br}, sensible-heat flux, in watts per square meter; λE_{br}, latent-heat flux, in watts per square meter; β, Bowen ratio, dimensionless; T, air temperature, in degree Celsius; e, vapor pressure, in millibars; U, horizontal windspeed, in meters per second; and ET, evapotranspiration, in millimeters per day]

Date	$K\downarrow$	Q	G	H_{br}	λE_{br}	β	T	e	U	ET
					Site C					
June 2	362	198	-10	-118	-69	1.71	25.0	9.7	1.4	-2.45
3	364	198	-9	-124	-64	1.93	25.9	9.9	1.1	-2.27
4	351	188	-3	-119	-66	1.81	24.5	8.0	2.2	-2.32
5	382	196	-3	-128	-65	1.98	21.4	6.4	.7	-2.28
Mean	365	195	-6	-122	-66	1.86	24.2	8.5	1.4	-2.33
					Site L					
June 2	354	232	-8	0	-225	-0.00	24.3	10.6	2.4	-7.92
3	350	235	-8	9	-236	-.04	25.1	10.8	2.3	-8.32
4	326	212	0	15	-226	-.06	22.4	9.3	3.1	-7.96
5	362	229	-5	-14	-209	.07	19.1	7.4	1.6	-7.38
Mean	348	227	-5	3	-224	[1]-0.01	22.7	9.5	2.4	-7.90

[1]Mean β calculated as H_{br} / λE_{br}.

Biased samples of Q and G also will introduce bias into the estimates of H_{br} and λE_{br}. Bias was more likely at site C where the plant canopy is sparse and clumped, than at site L where the cover is much more uniform. The analysis at site C used an equally weighted average of net-radiation measurements made over bare soil, a bush, and sparse grass. Use of this weighted average is thought to yield an adequate estimate of mean Q at site C. An equally weighted average also was used for soil-heat flux at site C; but this average was based on measurements beneath bare soil and beneath a bush. This method probably underestimates mean G at site C.

Calibration and sampling problems for Q and G are important. Because the Bowen-ratio method simply partitions available energy ($Q + G$) into H_{br} and λE_{br}, any errors in net radiation and soil-heat flux will be included in the estimates. Errors in Q and G can arise from calibration and from sampling, and will affect the λE estimates by both the Bowen-ratio and the residual eddy-correlation methods, as well as the closure of the eddy-correlation method. The errors here (if any) probably would be less than 10 percent of the estimated λE.

SUMMARY AND CONCLUSIONS

The instruments operated well in the warm, dry climate of Owens Valley during the study. Measurements were made during a 4-day period at sites C and L. The 4-day mean temperature was 24.2 °C at site C and 22.7 °C at site L, the mean vapor pressure was 8.5 mbar at site C and 9.5 mbar at site L, and the mean windspeed at 2 m above the land surface was 1.4 m/s at site C and 2.4 m/s at site L.

The 12-minute Bowen-ratio measurements at the two sites were generally internally consistent. The daily ET estimates at site C ranged from -2.27 to -2.45 mm and had a mean of -2.33 mm. The daily ET measurements at site L ranged from -7.38 to -8.32 mm and a mean of -7.90 mm. The results are in general agreement with measurements, described in chapters B, C, and D of this report, made by another Bowen-ratio system and by adjacent eddy-correlation systems. Much of the discrepancy between results is attributed to the problem of sampling net radiation and soil-heat flux in areas of discontinuous vegetation.

REFERENCES CITED

Bowen, I.S., 1926, The ratio of heat losses by conduction and evaporation from any water surface: Physical Review, no. 17, p. 779-787.

Denmead, O.T., and McIlroy, I.C., 1970, Measurements of non-potential evapotranspiration from wheat: Agricultural Meteorology, v. 7, p. 285-302.

Dileanis, P.D., Branson, F.A., and Sorenson, S.K., 1985, Methods for determining effects of controlled dewatering of shallow aquifers on desert phreatophytes in Owens Valley, California: Fort Collins, Colorado, U.S. Forest Service General Technical Report, RM-120, Rocky Mountain Forest and Range Experimentation Station, p. 197-200.

Duell, L.F.W., Jr., and Nork, D.M., 1985, Comparison of three micrometeorological methods to calculate evapotranspiration in Owens Valley, California: Fort Collins, Colorado, U.S. Forest Service General Technical Report, RM-120, Rocky Mountain Forest and Range Experimentation Station, p. 161-165.

Gay, L.W., 1988, A portable Bowen ratio system: American Society of Civil Engineering, National Conference on Irrigation and Drainage, New York, Proceedings, p. 625-632.

Groeneveld, D.P., Grate, D.L., Hubbard, P.J., Munk, D.S., Novak, P.J., Tillemans, B., Warren, D.C., and Yamashita, I., 1985, A field assessment of above- and below-ground factors affecting phreatophyte transpiration in the Owens Valley, California: Fort Collins, Colorado, U.S. Forest Service General Technical Report, RM-120, Rocky Mountain Forest and Range Experimentation Station, p. 166-170.

Hartman, R.K., and Gay, L.W., 1981, Improvements in the design and calibration of temperature measurement systems: American Meteorology Society Conference on Agriculture and Forest Meteorology, 15th, Boston, Proceedings, p. 150-151.

Lang, A.R., McNaughton, K.G., Chen, Fazu, Bradley, E.R., and Ohtaki, Eiji, 1983, Inequality of eddy transfer coefficients for vertical transport of sensible and latent heats during advective inversions: Boundary Layer Meteorology, v. 25, p. 25-41.

List, R.J., 1984, Smithsonian meteorological tables, 5th reprint, 6th revision, Washington, D.C., 527 p.

Spittlehouse, D.A., and Black, T.A., 1980, Evaluation of the Bowen ratio/energy balance method for determining forest evapotranspiration: Atmosphere and Oceans, v. 18, p. 98-116.

Tanner, C.B., 1960, Energy balance approach to evapotranspiration from crops: Soil Science Society of America, Proceedings, v. 24, p. 1-9.

Verma, S.B., Rosenberg, N.J., and Bland, B.L., 1978, Turbulent exchange coefficients for sensible heat and water vapor under advective conditions: Journal of Applied Meteorology, v. 17, p. 330-338.

CHAPTER B.--BOWEN-RATIO MEASUREMENTS AT SITES C AND F

By David I. Stannard (U.S. Geological Survey)

INTRODUCTION

Chapter B describes determinations of latent-heat-flux density that were made using the Bowen-ratio method at site C from June 1 to June 3, and at site F from June 3 to June 5, 1986. Adjacent instruments used for measuring Bowen-ratio (Gay, chapter A, this report) and eddy-correlation (Weaver, chapter C, this report) data were operated simultaneously. In this chapter, the direct eddy-correlation latent-heat-flux (λE_{ec}) density and the energy-balance-residual latent-heat-flux (λE_{eb}) densities are used to compare with the Bowen-ratio latent-heat-flux (λE_{br}) density.

Inhomogeneity and sparseness of vegetation probably caused the measured 30-minute-flux densities (from Bowen-ratio and eddy-correlation methods) to differ significantly from the actual value. However, these conditions probably do not produce a bias in the daily totals of flux densities.

The Bowen-ratio equation uses measurements of temperature and vapor density differences above the plant canopy to determine the Bowen ratio (Campbell, 1977):

$$\beta = \frac{H_{br}}{\lambda E_{br}} = \frac{\gamma \Delta T}{\Delta q} \bullet \frac{r_v}{r_h}, \tag{B1}$$

where

β is the Bowen ratio, the ratio of sensible- to latent-heat flux, dimensionless;
H_{br} is sensible-heat flux by the Bowen-ratio method, in watts per square meter;
λE_{br} is latent-heat flux by the Bowen-ratio method, in watts per square meter;
γ is psychrometer constant, in grams per cubic meter per degree Celsius;
ΔT is air temperature difference between two vertically aligned points above the plant canopy, in degrees Celsius;
Δq is vapor-density difference between the same two points, in grams per cubic meter;
r_h is resistance to heat transport during the measurement interval, in seconds per meter; and
r_v is resistance to vapor transport during the measurement interval, in seconds per meter.

The resistance to heat and vapor are assumed to be equal (Campbell, 1977).

Measurements of net radiation and soil-heat flux are used with the computed Bowen ratio to solve the energy-balance equation for latent-heat flux as:

$$\lambda E_{br} = -\frac{Q+G}{1+\beta}, \tag{B2}$$

where

Q is net radiation, in watts per square meter; and
G is soil-heat flux, in watts per square meter.

In using equation B2, the assumptions are made that vegetation is sufficiently extensive (Campbell, 1977), and that the change in energy stored in the plant canopy is negligible (Fritschen, 1965). Both assumptions are valid at the study sites.

INSTRUMENTS AND METHODS

The mechanism used to alternate the positions of temperature sensors (Stannard, 1985) was designed to minimize interference of the airflow past the sensors. Model WVU-7 psychrometers, made by Delta-T Devices in England, and marketed through Campbell Scientific, Inc., in Logan, Utah, were suspended from the ends of a 1-m-long shaft that was rotated "end-over-end" every 5 minutes to remove bias. The psychrometers, positioned 1.6 and 2.6 m above land surface, were used to measure temperature and vapor-density differences. The psychrometers use nonlinear thermistors and the output is linearized by using a 5th-order polynomial in the Campbell Scientific 21X micrologger. The thermistors have a 10-second time constant; aspirator fans maintain a constant airspeed of 3.0 m/s. A cotton wick conducts water from a 20-mL reservoir to the wet bulb. A plated brass cylinder surrounds the thermistor, and is in turn surrounded by a rectangular plated brass housing to provide radiation shielding.

Net radiation (Q) was measured with a Swissteco-type S-1 net radiometer, which had a sensitivity of 22.1 $(W/m^2)/mV$. The radiometer was located 1.6 m above land surface, and was positioned to measure a weighted average of surface representative of the land cover. Inner tubes provided low-pressure air that was passed through a desiccant and used to keep the net-radiometer domes inflated and dry.

Soil-heat flux (G) was measured with four Peltier-cooler type soil-heat-flux plates (Weaver and Campbell, 1985), which had sensitivities that ranged from 14.5 to 16.1 $(W/m^2)/mV$. The plates were buried 1 cm below land surface. Three plates were covered with soil that was exposed to direct sunlight most of the day. One plate was covered with soil that was shaded by vegetation during the day. The plate arrangement was considered to be representative of the average land surface. A copper-constantan thermocouple was used to measure soil temperature at a depth of 1 cm. The soil-heat-flux plates had a small temperature coefficient, and outputs were corrected by using the soil temperature.

MEASUREMENTS

Measurements were made at site C from 1900 hours June 1 to 1500 hours June 3. Instruments were located about 100 m northeast of the remote-sensing plot. The system then was moved to site F, approximately 100 m east of the remote-sensing plot, where measurements were made from 1900 hours June 3 to 1900 hours June 5.

Latent-heat flux (λE_{br}) was calculated on line every 10 minutes. The psychrometers were scanned every 2 seconds for 4.5 minutes, and then positions alternated and allowed to equilibrate for 30 seconds. This cycle was repeated to record unbiased 10-minute temperature and vapor-pressure differences, which were used to calculate β. The net radiometer and soil-heat-flux plates were scanned every 2 seconds, and 10-minute means were used to calculate λE_{br} and H_{br}. Because of a data-logger programming error, instantaneous values of wet- and dry-bulb temperatures, Q and G were recorded every 5 minutes, rather than mean values. (However, λE_{br} was calculated from mean values.) The soil thermocouple used to correct G was scanned and recorded every 5 minutes.

Six 10-minute values of λE_{br} were averaged to produce hourly values. Hourly values of Q and G were based on 12 samples, taken 5 minutes apart. Hourly values of H_{br} were determined using equation A1. Hourly values of all fluxes are reported in tables B1 and B2. Daily totals of λE_{br} were converted to evapotranspiration totals by using a value for latent heat of vaporization (λ) equal to about 2,450 J/g at 20 °C. Daily totals are given in table B3.

Table B1. Hourly flux densities and Bowen ratio at site C

[Q, net radiation, in watts per square meter; G, soil-heat flux, in watts per square meter; H_{br}, sensible heat-flux, in watts per square meter; λE_{br}, latent heat-flux, in watts per square meter; β, Bowen ratio, dimensionless]

Hour	Q	G	H_{br}	λE_{br}	β
		June 1, 1986			
1930	-68.1	60.1	9.7	-1.7	-5.71
2030	-94.3	66.4	52.2	-24.3	-2.15
2130	-94.5	68.1	31.3	-4.9	-6.35
2230	-90.8	67.1	27.5	-3.8	-7.26
2330	-81.0	71.5	9.6	-.2	-43.27
		June 2, 1986			
0030	-82.1	64.5	22.9	-5.4	-4.26
0130	-75.3	65.5	10.1	-.4	-26.31
0230	-72.4	65.5	6.7	.1	130.08
0330	-72.6	61.7	13.6	-2.7	-5.01
0430	-70.5	59.1	14.9	-3.6	-4.20
0530	-61.4	59.6	1.5	.4	4.25
0630	14.3	40.2	-16.5	-38.0	.43
0730	154.5	-13.6	-72.0	-68.9	1.04
0830	292.5	-75.7	-128.8	-88.0	1.46
0930	410.4	-140.0	-173.2	-97.2	1.78
1030	485.7	-182.3	-213.8	-89.5	2.39
1130	523.0	-214.2	-198.1	-110.7	1.79
1230	528.7	-214.0	-179.2	-135.6	1.32
1330	509.4	-183.3	-224.7	-101.4	2.22
1430	458.6	-141.4	-198.0	-119.1	1.66
1530	381.5	-105.5	-175.4	-100.6	1.74
1630	285.4	-70.1	-102.3	-113.0	.91
1730	96.9	-12.1	-36.2	-48.6	.74
1830	48.4	13.9	-13.9	-48.4	.29
1930	-79.7	42.1	23.8	13.7	1.74
2030	-96.4	54.2	69.0	-26.8	-2.57
2130	-91.7	50.5	75.9	-34.7	-2.19
2230	-88.9	55.9	62.6	-29.7	-2.11
2330	-78.9	56.9	40.4	-18.4	-2.20
		June 3, 1986			
0030	-83.0	54.7	51.0	-22.7	-2.25
0130	-76.9	59.7	20.5	-3.3	-6.14
0230	-68.8	66.5	2.8	-.5	-5.53
0330	-71.6	62.2	11.4	-2.0	-5.61
0430	-70.4	61.8	11.0	-2.4	-4.67
0530	-64.0	58.6	7.8	-2.4	-3.20
0630	22.7	40.0	-4.5	-58.2	.08
0730	177.5	-22.0	-69.1	-86.5	.80
0830	307.4	-88.0	-112.5	-107.0	1.05
0930	406.7	-142.4	-153.6	-110.8	1.39
1030	477.3	-186.6	-199.7	-91.1	2.19
1130	518.3	-211.7	-199.9	-106.8	1.87
1230	529.9	-213.3	-173.6	-143.0	1.21
1330	510.4	-183.3	-204.3	-122.8	1.66
1430	468.0	-139.7	-221.2	-107.1	2.07
1530	326.8	-97.0	-142.2	-87.6	1.62

Table B2. Hourly flux densities and Bowen ratio at site F

[Q, net radiation, in watts per square meter; G, soil-heat flux, in watts per square meter; H_{br}, sensible heat-flux, in watts per square meter; λE_{br}, latent heat-flux, in watts per square meter; β, Bowen ratio, dimensionless]

Hour	Q	G	H_{br}	λE_{br}	β
		June 3, 1986			
1930	-62.9	21.1	51.0	-9.2	-5.54
2030	-91.8	44.7	77.8	-30.8	-2.53
2130	-82.6	49.4	72.2	-39.0	-1.85
2230	-78.8	51.2	55.8	-28.3	-1.97
2330	-77.5	50.4	46.2	-19.1	-2.42
		June 4, 1986			
0030	-67.8	54.8	20.9	-7.9	-2.67
0130	-68.6	54.8	28.5	-14.7	-1.94
0230	-69.5	50.3	36.8	-17.6	-2.09
0330	-65.4	53.1	19.9	-7.5	-2.66
0430	-65.4	55.7	16.2	-6.5	-2.51
0530	-57.2	57.5	-.5	.2	-2.60
0630	11.7	41.2	-46.9	-5.9	7.90
0730	135.3	-4.4	-47.7	-83.2	.57
0830	247.9	-67.8	-64.3	-115.8	.55
0930	343.0	-117.8	-126.8	-98.4	1.29
1030	428.8	-149.1	-212.6	-67.1	3.17
1130	481.6	-159.5	-251.1	-71.0	3.54
1230	431.3	-136.4	-226.7	-68.3	3.32
1330	448.2	-95.4	-283.5	-69.3	4.09
1430	368.9	-93.2	-215.5	-60.3	3.57
1530	378.0	-90.2	-225.4	-62.4	3.61
1630	339.5	-62.6	-245.6	-31.3	7.84
1730	223.3	-35.0	-136.3	-52.0	2.62
1830	63.3	-6.6	-38.1	-18.6	2.05
1930	-54.9	20.7	44.7	-10.5	-4.26
2030	-103.7	45.3	74.8	-16.4	-4.55
2130	-103.6	50.9	62.3	-9.6	-6.51
2230	-98.3	60.1	57.0	-18.7	-3.04
2330	-89.2	65.1	30.8	-6.6	-4.63
		June 5, 1986			
0030	-91.3	64.9	39.5	-13.1	-3.02
0230	-77.7	70.8	9.2	-2.3	-3.95
0330	-75.9	69.9	8.8	-2.8	-3.11
0430	-72.2	68.8	3.9	-0.5	-7.40
0530	-65.7	69.7	-3.7	-0.3	11.23
0630	5.0	51.3	-13.9	-42.4	.33
0730	130.8	-1.7	-57.1	-72.0	.79
0830	244.2	-63.8	-94.5	-85.9	1.10
0930	339.6	-114.5	-130.6	-94.5	1.38
1030	409.8	-152.1	-185.2	-72.6	2.55
1130	448.5	-173.0	-224.7	-50.8	4.42
1230	471.1	-175.0	-198.3	-97.8	2.03
1330	466.8	-150.9	-206.3	-109.7	1.88
1430	436.2	-127.4	-236.9	-71.9	3.30
1530	377.1	-95.1	-197.5	-84.6	2.33
1630	295.5	-66.8	-164.9	-63.8	2.59
1730	189.4	-29.5	-111.7	-48.2	2.32
1830	55.5	5.6	-38.9	-22.2	1.75

Table B3. Daily totals of energy-flux densities and evapotranspiration for sites C and F from Bowen-ratio and eddy-correlation methods

[Subscripts indicate values determined by following methods: *br*, Bowen ratio, *eb*, energy balance; *ec*, eddy correlation. *Q*, net radiation, in megajoules per square meter per day; *G*, soil-heat flux, in megajoules per square meter per day; *H*, sensible-heat-flux, in megajoules per square meter per day; λE, latent-heat flux, in megajoules per square meter per day; *ET*, evapotranspiration, in millimeters per day]

Site	Date	Q	G	H_{br}	λE_{br}	ET_{br}	ET_{ec}	ET_{eb}
C	June 2, 1986	11.95	-2.38	-5.01	-4.56	-1.82	-1.38	-1.60
F	June 4, 1986	11.00	-1.47	-6.22	-3.31	-1.32	--	-1.45
F	June 5, 1986	10.64	-1.57	-5.46	-3.61	-1.44	-1.35	-1.21

Generally, evaporation continues at a greatly reduced rate at night. Sensible-heat flux is often directed downward at night, resulting in negative Bowen ratios. Equation B2 is arithmetically unstable for Bowen ratios near -1.0, producing erroneous large (positive or negative) values of λE_{br}. In this analysis, λE_{br} was set equal to zero when the Bowen ratio was between -0.7 and -1.3. Very little error resulted through the use of this technique because evaporation is known to be near zero at night.

Eddy-correlation measurements, λE_{ec} and H_{ec}, were made adjacent to the Bowen-ratio instruments during the same measurement periods (Weaver, chapter C, this report). λE_{ec} was a direct measure of vapor flux, proportional to the covariance between vapor density and vertical windspeed. A second energy balance residual estimate, λE_{eb}, was obtained by measuring H_{ec} and determining λE_{eb} using equation A1. The residual was calculated using hourly means of the 5-minute instantaneous values of Q and G.

RESULTS

A 24-hour time series of the 1-hour mean energy balance data (Q, G, H_{br}, and λE_{br}) at site C on June 2 is shown in figure B1*A*. Although Q and G were smooth functions through most of the day, variability in the measured Bowen ratio produced somewhat jagged traces of λE_{br} and H_{br}. The inhomogeneity and sparseness of the plant canopy was probably the primary source of the variability. Figure B1*B* is a 24-hour time series of the 1-hour mean energy balance data (Q, G, H_{br}, and λE_{br}) at site F on June 4. The morning of June 4 was sunny, and partial cloudiness developed in the afternoon. Peak λE_{br} was at 0830 hours; λE_{br} then remained at about 60 percent of its peak value for the rest of the day.

Figure B2 is a 24-hour time series of the 1-hour mean estimates of λE_{br}, λE_{ec}, and λE_{eb} at site C on June 2. The discrepancy between the λE_{ec} and λE_{eb} is not fully resolved (Weaver, chapter C, this report), but is caused in part by storage of energy in the top 1 cm of soil. The Bowen-ratio method apportions this "magnified energy storage discrepancy" to both λE_{br} and H_{br}, and therefore often produces a λE_{br} estimate between the λE_{ec} and λE_{eb} (fig. B2).

λE_{br} probably was an overestimate just prior to midnight on three evenings (two at site C and one at site F). Figure B2 shows the most extreme example of this, when the estimate averaged -26 W/m^2 for a 5-hour period at site C on June 2. During this time, the available energy (Q + G) was approximately -33 W/m^2, and the Bowen ratios generally ranged from -1.5 to -3.0. Correction for heat stored in the top 1 cm of soil would have reduced the magnitude of the available energy only by about 10 W/m^2.

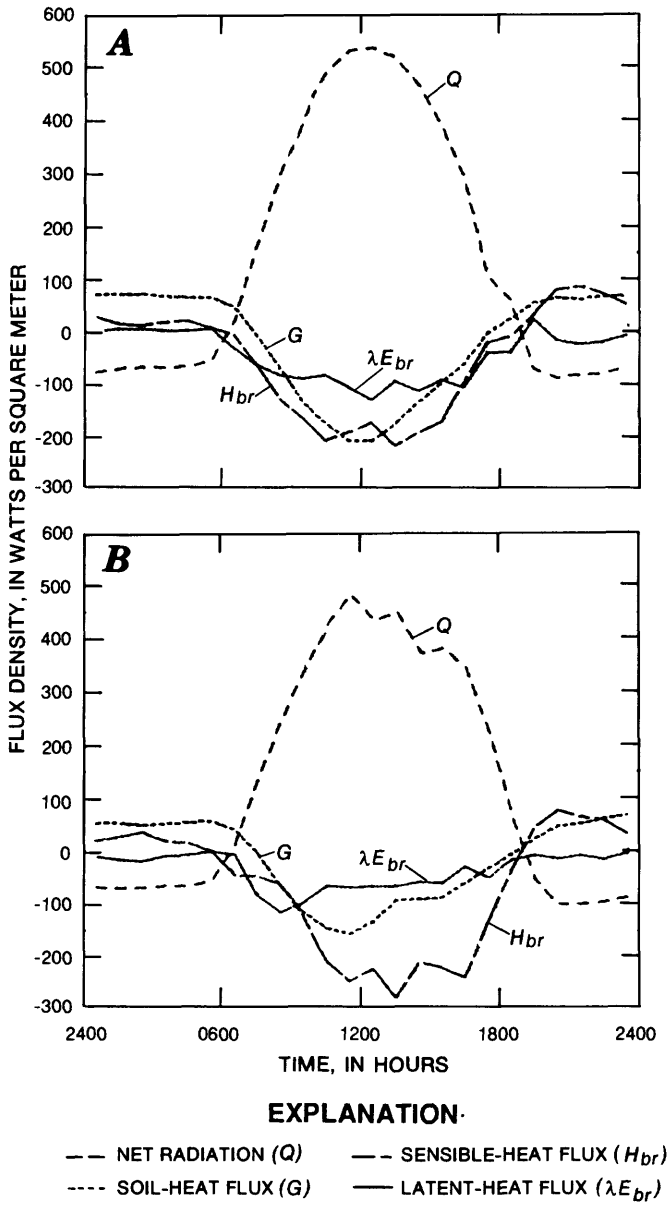

Figure B1. One-hour energy balance at sites C and F, using the Bowen-ratio method. *A*, Site C, June 2, 1986. *B*, Site F, June 4, 1986.

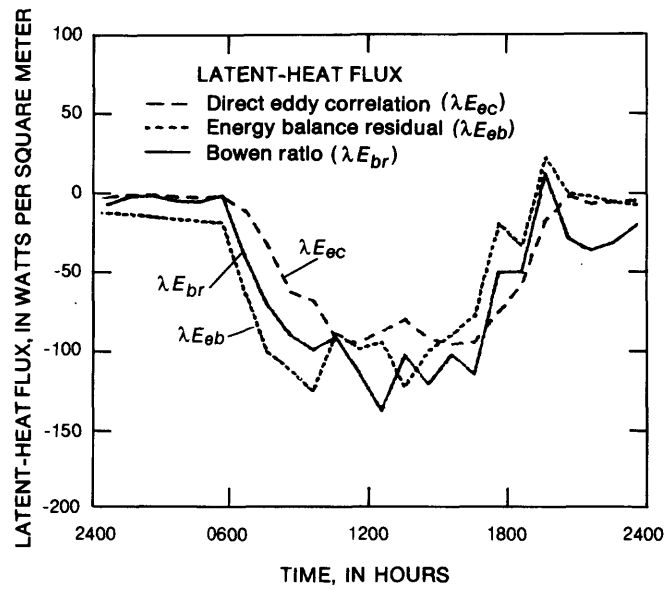

Figure B2. Three estimates of 1-hour latent-heat flux at site C, June 2, 1986.

The temperature and vapor-density differences during this period were very small. The vapor-density differences, in particular, may have been within the limits of resolution of the sensors. However, the 10-minute measurements of Bowen ratios were uniform during this time; ranging, for example, from -1.9 to -2.5 during the hour beginning at 2200 hours. This stability in the Bowen ratio lends credibility to the measured temperature and vapor-density differences.

Another explanation for λE_{br} being an overestimate at night is bias in the net-radiation or soil-heat-flux density measurements caused by the subjective placement of the instruments. This bias would be relatively unimportant during the day when fluxes are large, and would become more apparent at night, when available energy is near zero and Bowen ratios are often negative. Correcting for such a bias also could change the reported near-zero values of available energy in the following predawn hours to significantly positive values. However, this would have almost no effect on the corresponding values of λE_{br} because the Bowen ratios were large negative and positive numbers during that period.

A third explanation may be the inequality of the eddy-diffusion coefficient for heat transport (K_h) with the eddy-diffusion coefficient for vapor transport (K_v) during stable conditions (Lang and others, 1983). However, because no consistent relations between K_h and K_v have been determined, this correction was not investigated. The large nighttime values of λE_{br} are probably the result of energy storage in the top 1 cm of soil and slightly biased measurements of Q and G.

Daily totals of energy-flux densities and evapotranspiration are in table B3. On June 5, measurements were concluded at 1900 hours and data from the previous evening were substituted for the missing values. On June 3, Bowen-ratio measurements were concluded at site C at 1600 hours, so no totals for that day are reported. Totals for June 2 and 4 are based on measurements from midnight to midnight.

The largest disagreement between values of *ET* by the Bowen-ratio method (ET_{br}) and *ET* by the direct eddy-correlation method (ET_{ec}) was on June 2, when unusually high nighttime values of λE_{br} were calculated. A second value of ET_{br} was determined for June 2 by setting four of the large nighttime values of λE_{br} equal to λE_{ec}. The modified value of ET_{br} was 1.66 mm/d, only slightly greater than *ET* by the energy-balance-residual eddy-correlation method (ET_{eb}).

On June 2 and 3, at site C, the Bowen ratio decreased significantly during the hour beginning at about 1200 hours and to a lesser degree during the following and preceding hours (table B1). A time series of the Bowen ratio and the eddy-correlation Bowen ratio (equal to H_{ec} divided by λE_{ec}) shows satisfactory correlation except for the hours near noon on both days (Weaver, chapter C, this report). It is thought that the upper psychrometer was shading the lower psychrometer during this period, reducing the radiation loading on the lower one. Such shading reduces the temperature difference more than it does the vapor-pressure difference, reducing the calculated Bowen ratio. Correction for this measurement error would further reduce ET_{br} on June 2, probably to a value between ET_{eb} and ET_{ec}.

This phenomenon did not occur at site F, probably because of different alignment of the psychrometers. On June 4, ET_{eb} was greater than ET_{br}, which was the result normally expected (table B3). On June 5, ET_{br} was about 7 percent greater than ET_{ec}, but ET_{eb} was about 10 percent less than ET_{ec}. Weaver suggested (chapter C, this report) that advected sensible heat may have caused ET_{ec} to be greater than ET_{eb}. If so, advection may have affected measurements of gradients differently than it did measurements of covariances.

In general, agreement between the three estimates of evapotranspiration is satisfactory, especially if the high value of ET_{br} at site C on June 2 is lowered to 1.66 mm/d as noted above.

REFERENCES

Campbell, G.S., 1977, An introduction to environmental biophysics: New York, Springer-Verlag, 159 p.

Fritschen, L.J., 1965, Accuracy of evapotranspiration determinations by the Bowen-ratio methods: Bulletin of the International Association of Scientific Hydrology, v. 2, 38 p.

Lang, A.F.G., McNaughton, K.G., Chen, Fazu, Bradley, E.F., and Ohtaki, Eiji, 1983, Inequality of eddy transfer coefficients for vertical transport of sensible and latent heats during advective inversions: Boundary-Layer Meteorology, v. 25, p. 25-41.

Stannard, D.I., 1985, Design and performance of machines used in the calculation of Bowen ratios: National Water Well Association Conference on Characterization and Monitoring of the Vadose Zone, November 1985, Proceedings, p. 143-156.

Weaver, H.L., and Campbell, G.S., 1985, Use of Peltier coolers as soil-heat flux transducers: Soil Science Society of America Journal, v. 49, no. 4, p. 1065-1067.

CHAPTER C.--EDDY-CORRELATION MEASUREMENTS AT SITES C AND F

By Harold L. Weaver (U.S. Geological Survey)

INTRODUCTION

Chapter C describes eddy-correlation measurements used to provide estimates of evapotranspiration (*ET*) at sites C and F to compare with *ET* estimates determined by other methods. The other methods included Bowen ratio (Gay, chapter A, this report; Stannard, chapter B, this report), porometry (Groeneveld and Warren, chapter E, this report), and remote sensing (Moran and others, chapter G, this report). The period of comparison was June 2-5, midnight to midnight.

THEORY

The eddy-correlation method depends on the relation between the direction of air movement near the land surface and properties of the atmosphere, such as temperature and humidity. During daylight hours, for example, upward-moving airmasses tend to be warmer and moister than downward-moving airmasses. The covariance between vertical windspeed (w) and a scalar property of air such as water-vapor density (q) expresses this relation, as indicated by the following equation:

$$ET \approx - \overline{w'q'} \ , \tag{C1}$$

where

ET is evapotranspiration rate, in grams per square meter per second;
w is vertical windspeed, in meters per second;
q is water-vapor density, in grams per cubic meter;
$'$ signifies the deviation from the mean; and
$\overline{\quad}$ indicates averaging.

Equation C1 is not exact because a correction term is used that may change its value by as much as 20 percent to account for the changes in air density caused by warming or cooling at the surface.

$$ET = -\left(\overline{w'q'} + \frac{\overline{q}}{\overline{T}\ (\mathrm{K})} \overline{w'T'} \right), \tag{C2}$$

where $\overline{T}$ (K) is mean air temperature, in kelvin.

The covariance between vertical windspeed, w, and air temperature, T, when multiplied by the volumetric heat capacity of air, ρC_p, yields the direct eddy-correlation measurement of sensible-heat flux (H_{ec}).

$$H_{ec} = -\rho C_p \overline{w'T'}, \quad \text{(C3)}$$

where

H_{ec} is sensible-heat flux by the eddy-correlation method, in watts per square meter;
ρ is the air density, in grams per cubic meter; and
C_p is the heat capacity of air, in Joules per gram per degree Celsius.

A principal use of this equation is in a surface energy balance,

$$Q + G + H_{ec} + \lambda E_{eb} = 0, \quad \text{(C4)}$$

where

Q is net radiation, in watts per square meter;
G is soil-heat flux, in watts per square meter;
λ is latent heat of vaporization, equal to about 2,450 J/g at 20 °C; and
λE_{eb} is the energy-balance-residual estimate of *ET* by the eddy-correlation method, in grams per square meter per second.

INSTRUMENTS AND METHODS

Sites for the eddy-correlation instruments were chosen according to three criteria: (1) Typical vegetation densities both locally (5-m radius) and upwind (200 m); (2) minimal upwind physical activity, structures, and other measurement systems; and (3) avoidance of north-south and east-west remote-sensing flight paths and the remote-sensing ground plot. At site C, the eddy-correlation instruments were approximately 100 m northeast of the remote-sensing ground plot and 50 m northeast of an electric generator-equipped site where plant-water and reflectance experiments were being conducted. At site F, the eddy-correlation instruments were approximately 100 m east of the remote-sensing ground plot. At both sites, fetch was 500+ m, exclusive of an unimproved road less than 15 m wide about 100 m north of site F.

The micrometeorological instruments were positioned 1.0 to 2.1 m above the base of the instrument mast. However, sand hummocks at site F made determination of instrument height above the land surface difficult. Soil-heat-flux plates were buried approximately 1 cm below the surface. Each site had an array of four soil-heat-flux plates arranged in proportion to the estimated shaded part of the surface at time of installation. This resulted in three flux plates being buried well away from shrubs; one or two of the plates were occasionally in the partial shade of grass blades. The fourth was shaded by a shrub most of the day. The net radiometer was positioned above an area that was subjectively judged to be typical of conditions.

The eddy-correlation instruments included a Campbell Scientific model-Q A 27-T sonic anemometer for measurement of vertical windspeed (w) and a Campbell Scientific Lyman-alpha hygrometer (Tanner and others, 1985) for measurement of water-vapor density (q). A fine-wire thermocouple built into the sonic anemometer provided a measurement of air temperature (T). The signals from these instruments were sampled at a rate of 10 Hz by a Campbell Scientific 21X data logger. This data logger calculated 5-minute means and variances for ρ, w, and T, and covariances, $\overline{w'T'}$ and $\overline{w'q'}$.

Additional measurements were taken to provide a surface energy balance. Net radiation, Q, was measured by Swissteco net radiometers. Soil-heat flux, G, was provided by soil-heat-flux plates adapted from Peltier coolers (Weaver and Campbell, 1985). Solar radiation ($K\downarrow$) was measured using an Eppley Precision pyranometer, model PSP; soil-surface temperature (T_s) was measured at a depth of 0.5 cm with a copper-constantan thermocouple. Windspeed (w) and wind direction (Az_u) were measured by using a Young model 03001 anemometer and wind vane. These additional measurements were sampled every 10 seconds and averaged over 5-minute intervals by the same data logger that collected eddy-correlation data. Wind direction was sampled at 5-minute intervals.

RESULTS AND DISCUSSION

Continuous eddy-correlation monitoring of H_{ec} and latent-heat flux (λE_{ec}) at site C included the period 1900 hours, June 1 to 2045 hours, June 5. At site F, the monitoring period was from 1400 hours, June 2, to 1930 hours, June 5. Daily totals were used for the period from midnight to midnight, so data substituted were from the evening of June 4 for the missing hours during the evening of June 5 at both sites. Conditions were similar for both evenings.

During the afternoons of June 2, 3, and 4, the hygrometer at site F malfunctioned but returned to normal operation at about 1800 hours on June 2 and 3. Prior to 1800 hours on June 4, the windows on the Lyman-alpha hygrometer were cleaned with distilled water. This seemed to correct the problem immediately, but some measurements during the subsequent hour were too large. Thereafter the malfunction did not recur. The problem is noted because it occurred under dry conditions. Moisture sometimes short circuits the detector tube of these Lyman-alpha hygrometers, but a check of the zero offset indicated a short was not present. It is unusual that the malfunction resulted in increased λE_{ec} (fig. C1); all previous malfunctions decreased λE_{ec}. The very large values of λE_{ec}, together with energy-balance analysis, made it easier to determine those periods when λE_{ec} was in error.

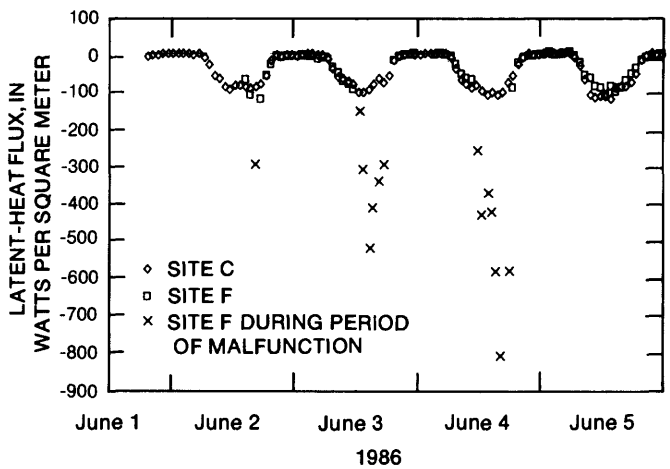

Figure C1. One-hour direct eddy-correlation measurements of latent-heat flux at sites C and F, June 1-5, 1986.

A comparison of λE_{ec} and energy-balance-residual latent-heat flux λE_{eb} is shown for sites C and F in figure C2. The λE_{eb} was computed from an energy balance (eq. C4) by using the H_{ec}. The λE_{ec} estimates increased from June 2 to June 5. The λE_{eb} estimates increased from June 2 to June 4, and decreased somewhat on June 5 (figs. C2*A*-C2*D*). The same trends can be observed at site F (fig. C2*E*).

A detailed examination of figure C2 shows that λE_{eb} is usually greater than λE_{ec} in the late morning and less than λE_{ec} in the afternoon. At a time prior to noon and midnight both tend to be equal. The quantity of λE_{eb} - λE_{ec} is similar to a heat-storage term, but its absolute value is larger than the estimated heat storage of the 1-cm-thick soil layer above the soil-heat flux sensor. This is a commonly observed phenomena and has no explanation at this time. Because λE_{eb} - λE_{ec} is like heat storage, integrating λE_{ec} and λE_{eb} for 24 hours may provide a more satisfactory comparison because the effects of heat storage should then diminish.

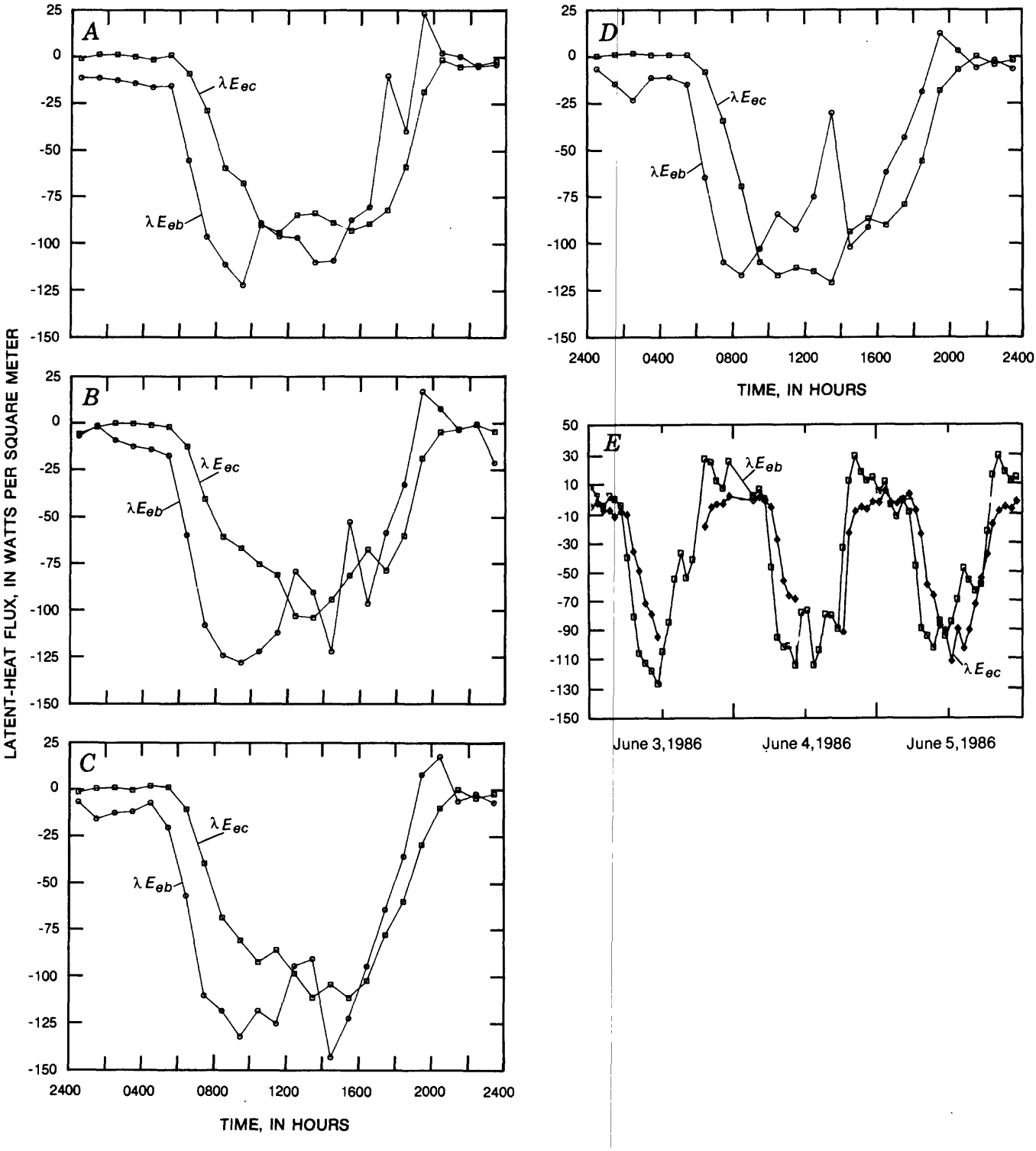

Figure C2. One-hour direct eddy-correlation (λE_{ec}) and energy-balance residual eddy-correlation (λE_{eb}) latent-heat flux for sites C and F, June 2-5, 1986. *A*, Site C, June 2. *B*, Site C, June 3. *C*, Site C, June 4. *D*, Site C, June 5. *E*, Site F, June 3-5.

Integration of all flux values are presented in table C1, where the daily total of λE_{eb} at site C is greater than that of λE_{ec} for all days except June 5. Thus daily *ET* estimated by the energy-balance-residual eddy-correlation method (ET_{eb}) exceeds daily *ET* by the direct eddy-correlation method (ET_{ec}) by 16 to 26 percent on June 2-4 at site C. Here ET_{ec} and ET_{eb} denote integration over 24 hours of λE_{ec} and λE_{eb}, respectively, by the latent heat of vaporization, λ (about 2,450 J/g at 20 °C), and converted to depth of water per day.

A comparison of λE_{ec} and λE_{eb} for site C (figs. C2*A*-C2*D*) is facilitated by appropriate scaling of the figures; all questionable large values of λE_{ec} have been excluded beyond the boundaries of the figure. Although a 24-hour integration was not possible because of a hygrometer malfunction, it appears from figures C2*A*-C2*D* that $\lambda E_{ec} \approx \lambda E_{eb}$. Some λE_{eb} estimates during the evening suggest condensation rather than evaporation. This is not credible, but it is a frequent occurrence with measurement of λE_{eb}. The lagged response of *G* and *H* to the change in sign of net radiation is other evidence of heat-storage effects on the energy balance. This response, together with the inherent noisiness of λE_{eb}, makes λE_{eb} less useful than λE_{ec} for short-term *ET* analysis. The most meaningful quantitative comparison of λE_{eb} to other fluxes is for a 24-hour period.

Daily *ET* for both sites also are shown in table C1. *ET* at site C appears to be about 30 percent higher than site F, assuming that $\lambda E_{ebC} / \lambda E_{ebF}$[1] is valid and that sensible heat advection did not differ significantly between the two sites. But the $\lambda E_{eb} / \lambda E_{ec}$ ratio declined at site C and, quite probably, at site F on June 5. Sensible-heat advection could cause this decrease.

The ratio, $\lambda E_{eb} / \lambda E_{ec}$, was smallest at site F on June 5. This may have been caused by a calibration error in the hygrometer at site F, resulting in high estimates of *ET*, even though the calibration error did not greatly amplify measurements of *ET* on June 5. A later comparison in Kansas under conditions when the vapor density was about three times higher than that at Owens Valley indicated that the hygrometer at site F did have a tendency to overestimate *ET*. This is possible because the calibration factor is a function of vapor density in such a way that a minor propensity for high estimates of *ET* at lower vapor densities (as in Owens Valley) would be greater than under conditions of high vapor density. Therefore, the conclusion is that even on June 5, when the eddy-correlation measurement of *ET* at site F was not grossly in error, it was nonetheless about 10 percent too high.

To compare the results of the eddy-correlation method with the Bowen-ratio method, the ratio of H_{ec} and λE_{ec} was computed for the eddy-correlation data and plotted in figure C3 against Bowen-ratio data. When there is disagreement between the measurement of *Q* and *G*, as there was between the values reported here and those reported by Gay (chapter A, this report), this comparison bypasses the discrepancy. The agreement between $H_{ec} / \lambda E_{ec}$ and the Bowen ratio measured by Bowen-ratio instruments is satisfactory. The ratio comparisons are least satisfactory for a Bowen ratio of ≈ 2, when the difference is about 25 percent. This produces differences on the order of 20 percent in *ET* values if the measurements of *Q* and *G* were the same for both systems. Because Gay's (chapter A, this report) Bowen-ratio instruments were located about 100 cm from the eddy-correlation instruments, it is possible that spatial variability accounts for most of a 20-percent difference in *ET* values.

The $H_{ec} / \lambda E_{ec}$ ratios tend to be lower than the hourly Bowen ratios of Gay (chapter A, this report) and higher than the hourly Bowen ratios computed by averaging 5-minute Bowen-ratio values (fig. C4) (Stannard, chapter B, this report). Only daytime Bowen ratios were used for comparison in figure C4 because nighttime Bowen ratios are more variable.

All energy-balance fluxes using λE_{ec} and H_{ec} for site C are shown in figure C5 and those for site F are shown in figure C6.

---

[1] $\lambda E_{ebC} / \lambda E_{ebF}$ are ratios of corresponding quantities for sites C and F.

Table C1. Daily totals of energy fluxes and evapotranspiration for sites C and F, based on eddy-correlation measurements, June 2-5, 1986

[Sign conventions for fluxes conform to equation C4. Q, net radiation, in megajoules per square meter per day; G, soil-heat flux, in megajoules per square meter per day; H_{ec}, sensible-heat flux, in megajoules per square meter per day; λE_{ec}, direct eddy-correlation latent-heat flux, in megajoules per square meter per day; λE_{eb}, energy-balance residual eddy-correlation latent-heat flux, in millimeters per day; ET_{ec}, direct eddy-correlation evapotranspiration, in millimeters per day; ET_{eb}, energy-balance residual eddy-correlation evapotranspiration, in millimeters per day; ET_{ecC}/ET_{ecF}, comparison of direct eddy-correlation evapotranspiration for sites C and F; ET_{ebC}/ET_{ebF}, comparison of energy-balance residual eddy-correlation evapotranspiration for sites C and F]

Date	Site C							Site F							ET_{ecC}/ET_{ecF}	ET_{ebC}/ET_{ebF}
	Q	G	H_{ec}	λE_{ec}	λE_{eb}	ET_{ec}	ET_{eb}	Q	G	H_{ec}	λE_{ec}	λE_{eb}	ET_{ec}	ET_{eb}		
June 2	11.9	-2.4	-5.4	-3.5	-4.0	-1.38	-1.60	--	--	--	--	--	--	--	--	--
June 3	11.7	-2.1	-5.2	-3.4	-4.2	-1.33	-1.68	11.8	-2.6	-5.9	--	-3.3	--	-1.31	--	-1.28
June 4	11.3	-1.3	-5.2	-3.8	-4.9	-1.55	-1.96	11.0	-1.5	-5.9	--	-3.6	--	-1.45	--	-1.35
June 5	10.4	-1.3	-5.2	-3.9	-3.9	-1.57	-1.56	10.6	-1.6	-6.0	-3.4	-3.0	-1.35	-.21	-1.16	-1.28

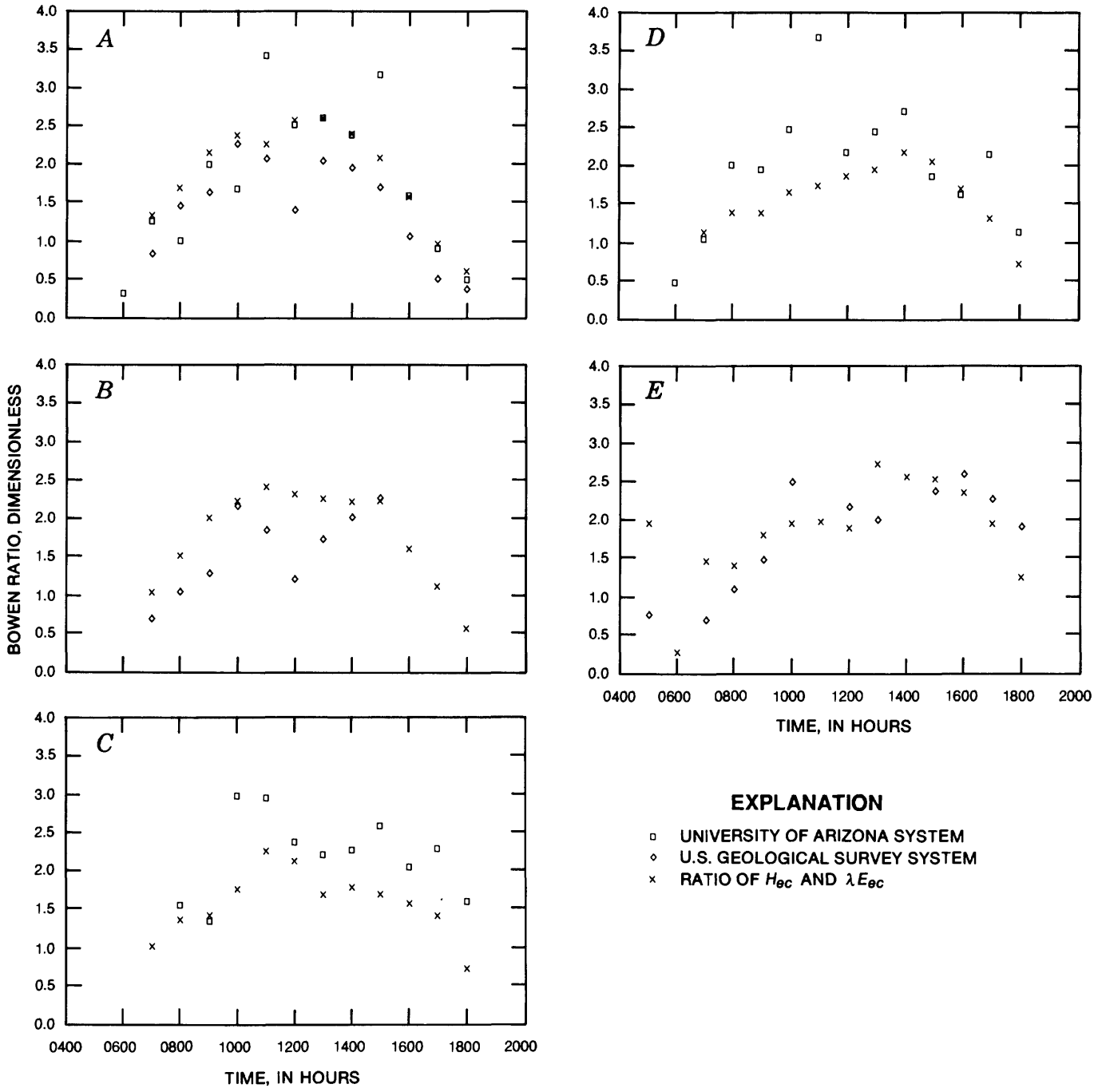

Figure C3. Daytime 1-hour Bowen ratios measured by the University of Arizona system and the U.S. Geological Survey system, and eddy-correlation measurements of sensible-heat (H_{ec}) and latent-heat (λE_{ec}) flux ratios at site C, June 2-5, 1986, and at site F, June 5, 1986. *A*, Site C, June 2. *B*, Site C, June 3. *C*, Site C, June 4. *D*, Site C, June 5. *E*, Site F, June 5.

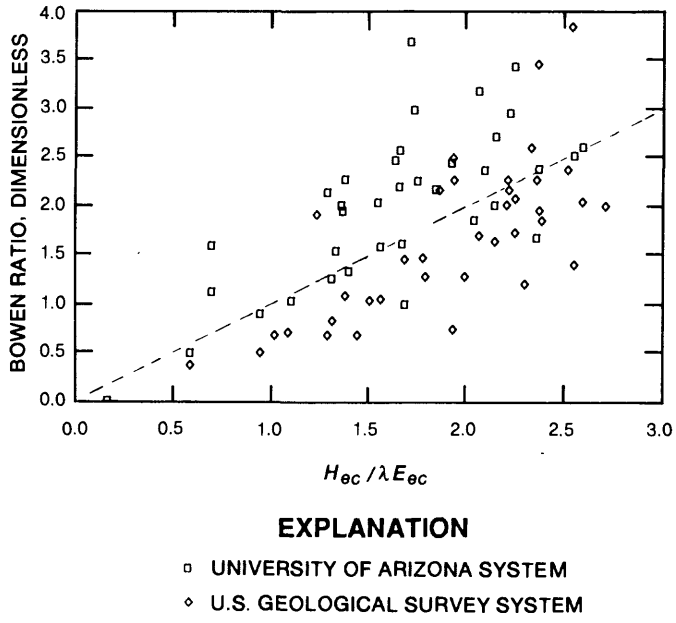

Figure C4. Bowen ratios measured by the University of Arizona system and the U.S. Geological Survey system compared with eddy-correlation measurements of sensible-heat (H_{ec}) and latent-heat (λE_{ec}) flux ratios during daytime periods when sensible-heat flux had negative values.

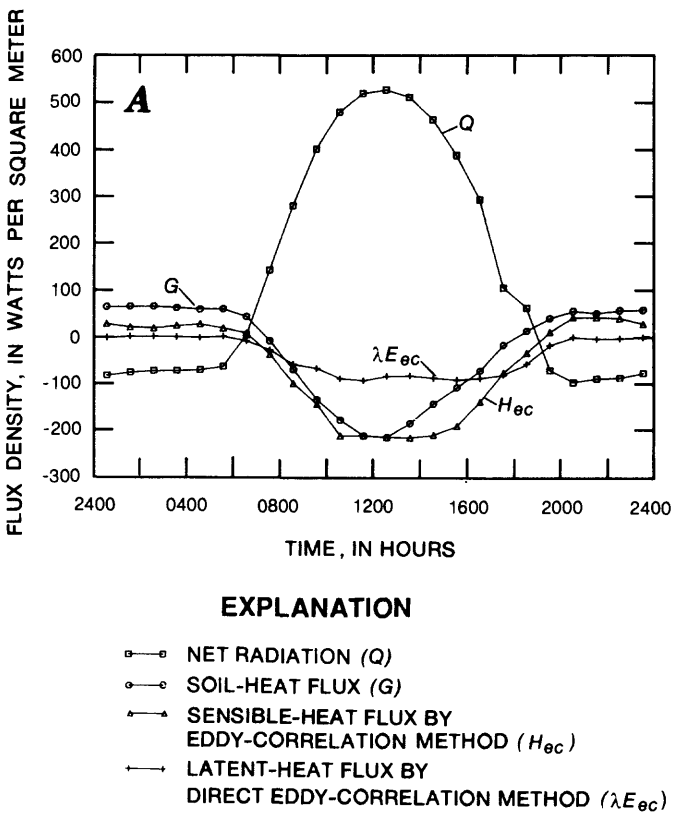

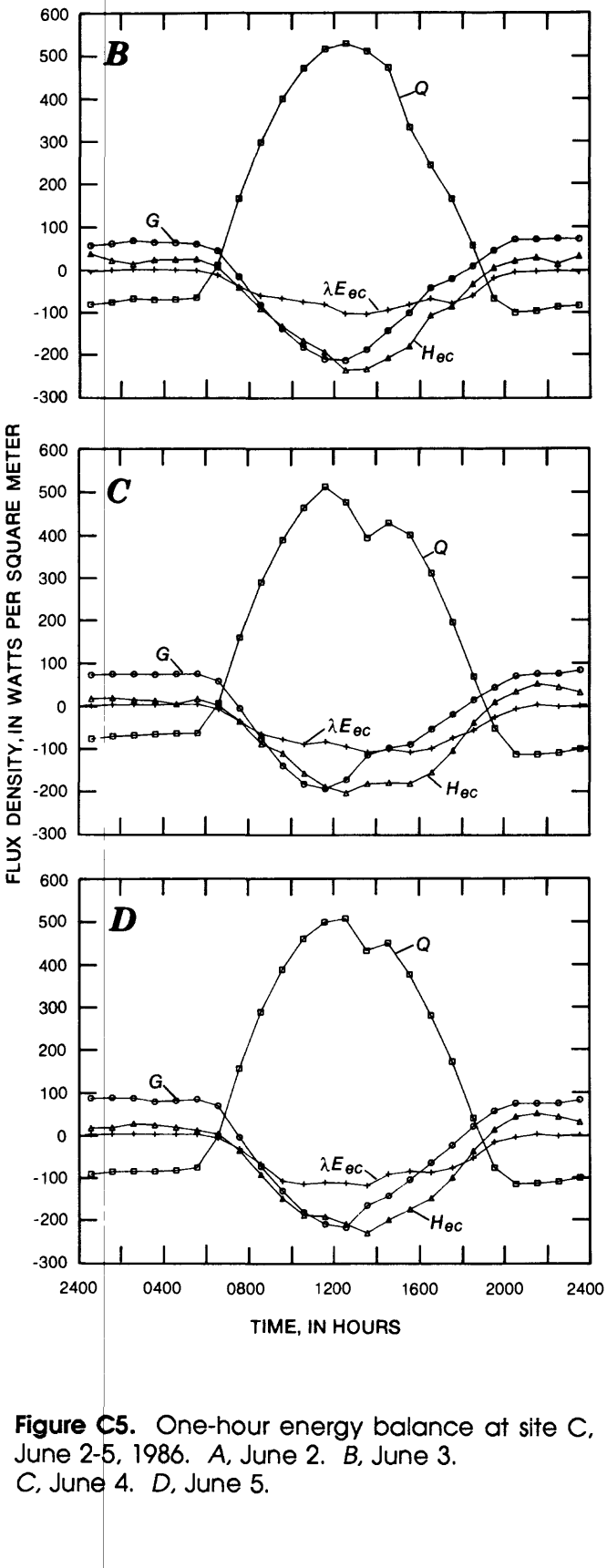

Figure C5. One-hour energy balance at site C, June 2-5, 1986. *A*, June 2. *B*, June 3. *C*, June 4. *D*, June 5.

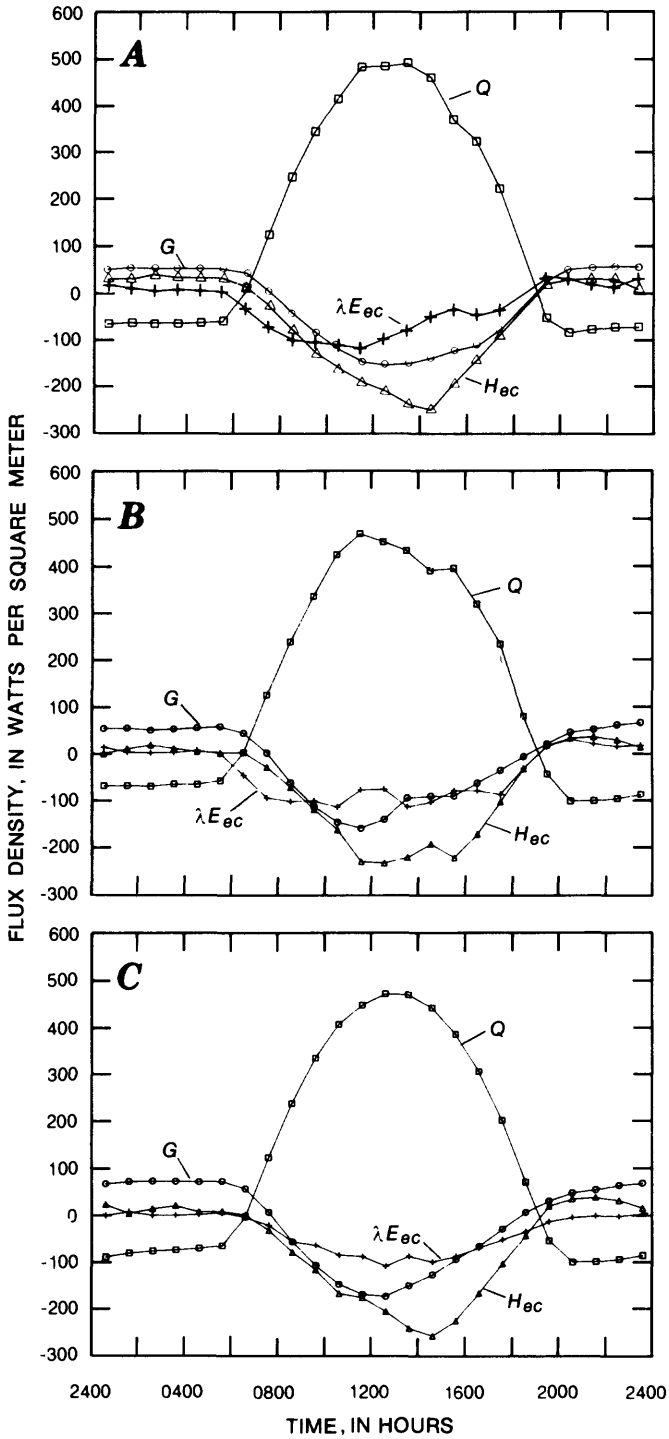

Figure C6. One-hour energy balance at site F, June 3-5, 1986. *A*, June 3. *B*, June 4. *C*, June 5.

CONCLUSIONS

The eddy-correlation instruments at sites C and F performed adequately except for malfunction of the hygrometer at site F in the afternoons of June 2-4. Estimates of λE_{eb} permit reasonable estimates of *ET* during the periods of hygrometer malfunction. For the diurnal *ET* cycle, the ET_{ec} are probably better than the ET_{eb} estimates. Integrated over 24 hours the two kinds of values converge somewhat, with the ET_{eb} estimates tending to be approximately 20 percent higher than the corresponding ET_{ec} estimates. Comparison of H_{ec} / λE_{ec} to the Bowen ratios produced by Bowen-ratio method is quite satisfactory. This indicates that *ET* estimates by either method should be in fairly good agreement for identical flux densities of net radiation and soil heat.

Site C had about 30 percent more *ET* than site F. For the June 2 to June 5 measurement period, the respective values are about 1.6 mm/d and 1.2 mm/d based on ET_{ec}.

REFERENCES

Tanner, B.D., Tanner, M.S., Dugas, W.A., Campbell, E.C., and Bland, B.L., 1985, Evaluation of an operational eddy correlation system for evapotranspiration measurements, *in* Advances in Evapotranspiration: National Conference on Advances in Evapotranspiration, Chicago, Illinois, December 16-17, 1985: St. Joseph, Michigan, American Society of Agricultural Engineers, Publication 14-85, p. 87-99.

Weaver, H.L., and Campbell, G.S., 1985, Use of Peltier coolers as soil-heat flux transducers: Soil Science Society of America Journal, v. 49, no. 4, p. 1065-1067.

CHAPTER D.--EDDY-CORRELATION MEASUREMENTS AT SITE L

By Lowell F. W. Duell, Jr. (U.S. Geological Survey)

INTRODUCTION

Chapter D describes the methods and instruments used to estimate evapotranspiration (*ET*) by the eddy-correlation method at site L (fig. 1) from May 31 to June 6, 1986. Two sets of instruments were used simultaneously. This paper presents two latent-heat-flux (λE) estimates for each set of instruments using the direct eddy-correlation method (λE_{ec}) and the energy-balance-residual eddy-correlation method (λE_{eb}). These *ET* estimates are compared with previous estimates made by the U.S. Geological Survey in May, June, and July 1984 and 1985 at site L.

METHODS

The net transfer of energy into and out of any given physical system at the Earth's surface can be expressed in terms of an energy budget. The elements of the energy budget represent flux densities (energy per unit of area per unit of time). If photosynthesis, respiration, and heat storage in the crop canopy are neglected, the equation for the energy budget at the Earth's surface can be expressed as:

$$Q + G + H + \lambda E = 0, \tag{D1}$$

where

Q is net radiation, in watts per square meter;
G is soil-heat flux, in watts per square meter;
H is sensible-heat flux, in watts per square meter; and
λE is latent-heat flux, in watts per square meter, which is equal to:
  λ is latent heat of vaporization, equal to about 2,450 J/g at 20 °C; and
  E is quantity of water evapotranspired, in grams per square meter per second.

Two estimates of the quantity of water evapotranspired at a particular site can be made using the eddy-correlation method and measuring additional energy-budget components. The first method discussed in this chapter is the direct eddy-correlation method measuring λE_{ec}. The second method discussed is the energy-balance-residual eddy-correlation method calculating λE_{eb} as a residual of the energy balance.

Swinbank (1951) used the eddy-correlation method to estimate both sensible-heat flux (H_{ec}) and λE_{ec}. For the eddy-correlation method, H_{ec} and λE_{ec} can be estimated independent of two other energy-budget components: net radiation (Q) and soil-heat flux (G). In this study, H_{ec} was calculated from the covariance of fluctuating vertical windspeed and air temperature, and λE_{ec} was calculated from the covariance of fluctuating water-vapor density and vertical windspeed. Equations for H_{ec} and λE_{ec} (Campbell, 1977) follow:

$$H_{ec} = -\rho a\ C_p\ \overline{w'T'}, \tag{D2}$$

and

$$\lambda E_{ec} = -\overline{w'q'}, \tag{D3}$$

where

H_{ec} is sensible-heat flux by the eddy-correlation method, in watts per square meter;
ρa is corrected air density, in grams per cubic meter, which is equal to:

$$\rho \frac{\text{station barometric pressure, in millibars}}{\text{sea level barometric pressure, in millibars}}, \tag{D4}$$

where ρ is air density, equal to 1,203 grams per cubic meter;

C_p is heat capacity of air, equal to 1.01 joules per gram per degree Celsius;
w is vertical windspeed, in meters per second;
T is air temperature, in degrees Celsius;
λE_{ec} is latent-heat flux by the eddy-correlation method, in watts per square meter;
q is water-vapor density, in grams per cubic meter;
$'$ signifies the instantaneous deviation from the mean; and
$\overline{\quad}$ signifies the averages taken during a 5-minute period.

The energy-budget residual method is the second method of estimating *ET* used in this study. Theoretically, *ET* can be calculated by estimating all the other elements (*Q*, *G*, and *H*) in the energy-budget equation D1. Latent-heat flux (λE_{eb}) was calculated as a residual of the other energy-budget components by rearranging equation D1:

$$\lambda E_{eb} = \lambda E = Q + G + H, \tag{D5}$$

where λE_{eb} is the latent-heat flux by the energy-balance-residual eddy-correlation method, in watts per square meter.

INSTRUMENTS

The instruments used for the eddy-correlation measurements (H_{ec} and λE_{ec}) included a Lyman-alpha hygrometer, a sonic anemometer, a fine-wire thermocouple, and a computing data logger. The energy budget components of *Q* and *G* were simultaneously measured using a net radiometer and soil-heat-flux plates. Additional micrometeorological data collected during this study, but not used in calculating *ET*, include wet- and dry-bulb temperature, horizontal windspeed, and solar radiation. Two duplicate sets of instruments were used to collect all data, with the exception of solar radiation. Duell (1990) described the instruments in more detail. The sets of instruments are referred to in this paper as masts 1 and 2.

LYMAN-ALPHA HYGROMETER

The Lyman-alpha hygrometer measured fluctuating water-vapor density (q, eq. D3). This method is based on the principle that water vapor strongly absorbs energy at certain wavelengths and not at other wavelengths. The source of the Lyman-alpha radiation is a partially evacuated tube that contains a small amount of hydrogen gas energized by a high-voltage electrostatic field. The adjacent detector tube contains nitric oxide and senses the strength of the incoming Lyman-alpha radiation. The relative attenuation of the Lyman-alpha signal is proportional to the q between the Lyman-alpha source and the detector (Buck, 1976). These instruments were placed 2 m above land surface.

The Lyman-alpha source strength drifted with time; therefore, the instrument was not considered reliable for absolute q measurements. This drift was negligible, however, for the short periods of time necessary for determination of water-vapor flux. The Lyman-alpha hygrometers were calibrated by the manufacturer prior to the start of this study.

SONIC ANEMOMETER

The sonic anemometer measured fluctuating vertical windspeed (w, eq. D2 and D3). It measured the phase shift generated by convected translation of emitted soundwaves caused by the wind. Because the velocity of sound is affected by temperature, the acoustic transducers were switched 160 times per second and the net phase shift was used to compute windspeed. These anemometers were placed 2 m above land surface.

FINE-WIRE THERMOCOUPLE

The fine-wire thermocouple measured fluctuating air temperature (T, eq. D2). The instrument is attached to the sonic anemometer and consists of a fine-wire (diameter 12.7 μm) chromel-constantan thermocouple. The thermocouple has a rapid response time. The instruments were placed 2 m above land surface.

NET RADIOMETER

Net radiation (Q, eq. D1 and D5) was measured with a modified Fritschen net radiometer that used a 22-junction manganin-constantan thermopile in circuit with a temperature-compensated thermistor. The instrument has a blackened sensitive surface and is enclosed within a hemispherically shaped polyethylene dome 50 mm in diameter. Manufacturer specifications indicate a sensitivity of 5 $(W/m^2)/\mu V$, an internal resistance of 200 ohms, and a time constant of approximately 12 seconds. These instruments were calibrated prior to this study and placed 2 m above land surface.

SOIL-HEAT-FLUX PLATE

Soil-heat flux (G, eq. D1 and D5) was measured with three soil-heat-flux plates and the data were averaged. The soil-heat-flux plates used in this study were made by Melcor Inc. and are used commercially as cooling devices. The plates, described by Weaver and Campbell (1985), produce millivolt potential, which is converted to G by using a calibration factor. The plates were individually calibrated for this study and sealed with epoxy. The plates were placed horizontally in a layer of 10-mm thick undisturbed soil.

PSYCHROMETER

Wet- and dry-bulb temperatures were measured with psychrometers made by the Delta-T Corporation. These data were used to calculate vapor pressure. The psychrometers were ventilated by fans powered by 6-volt direct-current motors and used two Fenwal Electronics nonlinear thermistors. The data logger provided a fifth-order polynomial function specifically regressed for these thermistors, converting voltage to temperature readings. The psychrometers were placed 2 m above land surface.

ANEMOMETER

Horizontal windspeed (U) was measured with a three-cup anemometer. Magnetic reed switches measured the rotating cups, and the switch closures were sensed by the pulse-counting channel in the data logger. These instruments were placed 2.5 m above land surface.

PYRANOMETER

Solar radiation ($K\downarrow$) was measured with an Eppley-Precision Spectral pyranometer. These data were not used in any calculations; however, the data can be used to indicate cloud cover. One pyranometer was used during this study and placed 1 m above land surface.

DATA LOGGER

The data loggers used for this study were models CR-7 and CR-21X manufactured by Campbell Scientific Inc. The eddy-correlation instruments were scanned by the data logger every 0.1 second for millivolt potential. A mathematical algorithm stored in the data logger computed the means and covariance of the voltage from each instrument and stored the data for intervals of 5 minutes. The values within the data logger were converted to actual readings in watts per square meter by the use of the appropriate multiplier. Calibration to absolute values with the eddy-correlation instruments was not as critical as the system accurately measuring and tracking rapidly changing wind, water-vapor, and air-temperature fluxes. All other instruments were scanned by the data logger every 10 seconds, and 5-minute averages were calculated by the data logger and recorded. All data were recorded on cassette tape for later transfer to a computer.

RESULTS

The average hourly and daily net radiation, soil-heat flux, sensible-heat-flux, direct eddy-correlation latent-heat-flux, energy-balance residual eddy-correlation latent-heat-flux, air temperature, vapor pressure, horizontal windspeed, and solar radiation data are given in table D2 (at end of chapter). Wet- and dry-bulb temperature data were not obtained when the psychrometer reservoirs became dry or fans were turned off. Sensible-heat-flux density, direct water-vapor latent-heat-flux, energy-budget residual latent-heat-flux, air temperature, vapor pressure, and windspeed data for mast 2 were not collected from May 31 through June 2, 1986.

The eddy-correlation method provides two estimates of *ET*. Because two eddy-correlation instruments (masts 1 and 2) were used, a total of four estimates of *ET* were determined. The λE_{ec} data for mast 1 were consistently lower than the other three *ET* estimates because the Lyman-alpha hygrometer used on mast 1 apparently malfunctioned during the study. Because the estimates of λE_{ec} for mast 1 do not agree with the other three estimates, they were assumed to be in error and not used. Estimates of daily *ET* for this study ranged from 5.9 to 7.3 mm. Average hourly λE_{eb} at mast 1 and λE_{ec} and λE_{eb} at mast 2 are included in figure D1. The data compare well.

Micrometeorological and latent-heat-flux data collected at site L for May, June, and July 1984 and 1985 by Duell (1990) are shown in table D1. For that study, λE was estimated using the Penman-combination method. The average daily *ET* estimates for May, June, and July were 7.6, 7.8, and 6.2 mm in 1984 and 6.1, 8.1, and 7.0 mm in 1985. The data show that the range of *ET* estimated during this study was similar to the 1984 and 1985 average daily estimates and that micrometeorological conditions were similar.

Average hourly estimates of sensible-heat-flux density compare well for both masts as shown in figure D2. Average daily estimates of H_{ec} are consistently lower than Q, λE_{ec}, or λE_{eb} (table D2).

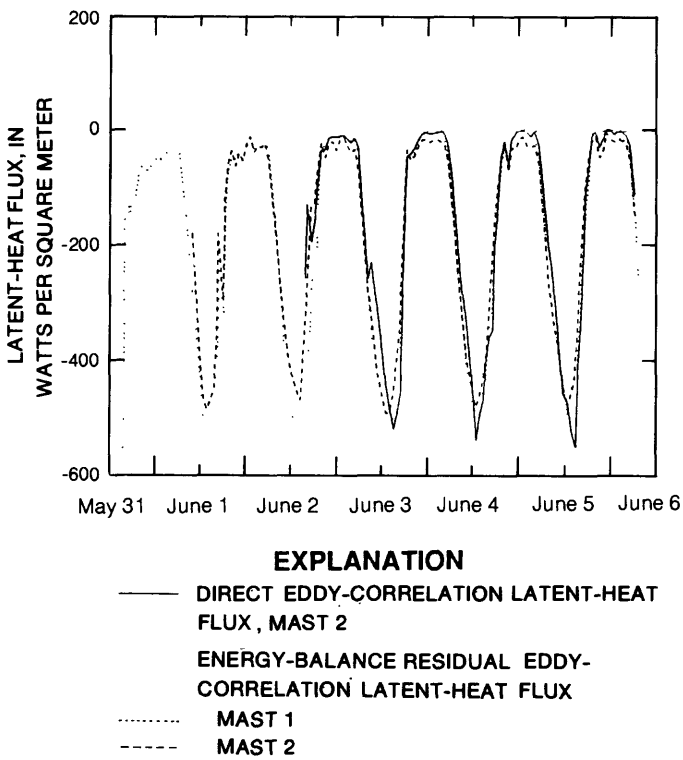

Figure D1. One-hour latent-heat flux from 1400 hours, May 31 to 0900 hours, June 6, 1986, at site L.

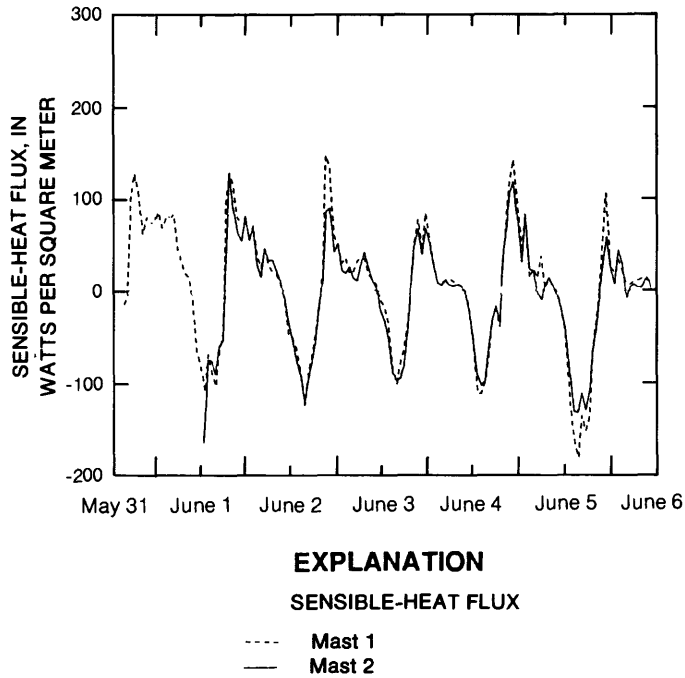

Figure D2. One-hour sensible-heat flux from 1400 hours, May 31 to 0900 hours, June 6, 1986, at site L.

Table D1. Daily maximum and minimum, and average monthly net radiation, soil-heat flux, latent-heat flux, air temperature, vapor pressure, windspeed, and solar radiation for May, June, and July 1984-85, at site L

[Q, net radiation, in watts per square meter; G, soil-heat flux, in watts per square meter; λE, latent-heat flux, in watts per square meter; T, air temperature, in degree Celsius; q, vapor pressure, in millibars; U, horizontal windspeed, in meters per second; and $K\downarrow$, solar radiation, in watts per square meter]

Month and year	Q			G			λE			T			q			U			$K\downarrow$	
	Maximum	Minimum	Mean	Maximum	Minimum	Mean	Maximum	Minimum	Mean	Maximum	Minimum	Mean	Maximum	Minimum	Mean	Maximum	Minimum	Mean	Maximum	Mean
May 1984	225	149	196	34	15	27	252	171	216	25.5	16.3	21.8	9.7	3.0	5.5	5.1	2.4	3.5	369	345
June 1984	218	130	193	19	6	15	234	207	221	21.1	19.1	19.9	9.5	6.0	7.6	6.3	3.4	4.4	374	325
July 1984	226	121	176	21	-2	10	249	110	176	26.4	19.4	23.5	17.5	4.6	12.6	3.5	1.8	2.6	351	278
May 1985	198	146	180	21	6	15	197	125	172	20.9	12.9	18.1	8.2	3.1	5.2	6.4	2.1	3.7	375	344
June 1985	212	96	192	27	1	19	276	102	231	27.8	9.3	23.2	10.9	4.4	7.1	4.6	1.9	2.8	374	347
July 1985	201	112	166	24	0	16	260	126	197	29.2	22.6	26.0	20.1	5.0	11.8	3.7	2.0	2.6	370	299

SUMMARY

The direct and energy-balance-residual eddy-correlation methods were used to estimate *ET* at site L. Two sets of instruments were used simultaneously. Eddy-correlation data from masts 1 and 2 compare well except for λE_{ec} from mast 1. The λE_{ec} from mast 1 was consistently lower and was not used in this study. Daily *ET* estimates at site L ranged from 5.9 to 7.3 mm. These *ET* estimates were similar to average daily estimates from a previous study for May, June, and July 1984-85 which ranged from 6.1 to 8.1 mm.

Micrometeorological data collected for this study from mast 1 and 2 at site L compare well. Data collected were net radiation, soil-heat flux, air temperature, vapor pressure, windspeed, and solar radiation. These data were similar to previous data collected in 1984-85 during the months of May through July at site L.

REFERENCES

Buck, Arden, 1976, The variable-path Lyman alpha hygrometer and its operating characteristics: Bulletin of American Meteorological Society, v. 57, p. 1113-1118.

Campbell, G.S., 1977, An introduction to environmental biophysics: New York, Springer-Verlag, 159 p.

Duell, L.F.W., Jr., 1990, Estimates of evapotranspiration in alkaline scrub and meadow communities of Owens Valley, California, using the Bowen-ratio, eddy-correlation, and Penman-combination methods: U.S. Geological Survey Water-Supply Paper 2370-E, 39 p.

Swinbank, W.C., 1951, The measurement of vertical transfer of heat and water vapor by eddies in the lower atmosphere: Journal of Meteorology, v. 8, no. 3, p. 125-145.

Weaver, H.L., and Campbell, G.S., 1985, Use of Peltier coolers as soil-heat flux transducers: Soil Science Society of America Journal, v. 49, no. 4, p. 1065-1067.

Table D2. Average hourly and daily flux densities for two sets of instruments from 1400 hours, May 31, 1986, through 0900 hours, June 6, 1986, at site L

[Q, net radiation, in watts per square meter; G, soil-heat flux, in watts per square meter; H_{ec}, sensible heat flux, in watts per square meter; λE_{ec}, direct eddy-correlation latent-heat-flux, in watts per square meter; λE_{eb}, energy-balance residual eddy-correlation latent-heat flux, in watts per square meter; T, air temperature, in degree Celsius; q, vapor pressure, in millibars; U, horizontal windspeed, in meters per second; and $K\downarrow$, solar radiation, in watts per square meter]

Time	Q	G	H_{ec}	λE_{ec}	λE_{eb}	T	q	U	$K\downarrow$
				Mast 1, May 31, 1986					
1400	712.9	-100.4	-15.0	-96.8	-597.5	33.6	8.9	3.57	994.0
1500	581.0	-119.9	-4.8	-71.0	-456.3	33.8	9.3	2.85	824.4
1600	61.6	-11.1	98.6	109.8	-149.1	28.9	9.3	7.34	128.4
1700	32.7	21.0	129.6	75.6	-183.3	27.8	8.4	7.73	81.8
1800	-9.9	19.4	109.8	145.5	-119.3	26.9	8.4	4.32	16.5
1900	45.5	7.6	62.6	108.2	-115.7	26.3	9.7	3.21	114.8
2000	-20.0	16.0	81.1	42.1	-77.1	24.5	9.7	3.32	39.0
2100	-50.1	31.0	76.0	55.3	-56.9	22.3	9.8	2.96	.0
2200	-28.2	25.3	73.9	27.7	-70.9	22.8	10.3	5.57	.0
2300	-41.6	20.4	86.5	4.5	-65.3	22.0	11.3	9.61	.0
2400	-40.2	22.9	68.9	5.7	-51.6	20.7	11.2	8.82	.0
				Mast 1, June 1, 1986					
0100	-55.3	23.4	80.2	7.0	-48.3	20.6	10.9	8.59	0.0
0200	-54.8	24.8	79.3	9.4	-49.4	20.0	11.0	6.23	.0
0300	-54.4	24.6	84.1	7.7	-54.4	19.8	--	5.60	.0
0400	-51.5	28.2	46.8	5.7	-23.4	17.9	--	3.18	.0
0500	-47.1	32.0	30.3	6.9	-15.2	15.9	--	2.27	.0
0600	-38.4	36.6	18.0	3.7	-16.2	14.9	--	2.31	5.7
0700	2.5	22.0	14.2	11.1	-38.6	16.8	--	1.59	87.5
0800	139.7	-7.4	-17.6	-27.5	-114.7	19.1	--	1.58	282.2
0900	303.2	-38.0	-66.1	-74.1	-199.1	21.8	12.9	.85	484.0
1000	461.2	-62.7	-82.2	-116.4	-316.3	24.9	12.7	1.48	678.9
1100	595.5	-91.0	-109.5	-216.9	-395.0	27.6	12.6	1.91	854.8
1200	691.3	-105.7	-70.1	-191.4	-515.4	29.3	12.1	2.25	966.8
1300	729.5	-120.0	-91.2	-263.6	-518.2	30.5	11.4	1.94	1,020.9
1400	729.7	-129.3	-104.2	-327.6	-496.2	32.3	11.7	1.53	1,032.8
1500	689.3	-115.9	-69.0	-272.2	-504.3	33.5	10.9	1.67	972.8
1600	575.9	-98.5	-47.3	-175.7	-430.1	33.8	10.7	1.87	824.2
1700	173.1	-22.5	94.3	101.1	-244.8	30.6	10.7	4.10	261.6
1800	195.4	-2.9	129.7	243.5	-322.2	28.6	9.8	5.89	290.7
1900	22.7	14.3	115.6	59.4	-152.6	27.7	9.4	5.87	93.9
2000	-28.1	20.7	78.7	87.5	-71.2	26.8	8.8	3.10	24.3
2100	-56.3	29.0	77.5	30.8	-50.3	24.1	9.6	4.23	.0
2200	-55.1	28.6	76.5	24.7	-50.1	22.6	10.3	4.04	.0
2300	-52.7	29.9	57.5	20.7	-34.7	20.8	10.5	3.41	.0
2400	-52.3	30.4	71.7	22.0	-49.8	20.1	10.7	3.58	.0
Average daily values	198.5	-18.7	16.5	-42.7	-196.3	24.2	--	3.30	328.4
				Mast 1, June 2, 1986					
0100	-45.5	34.2	39.1	28.2	-27.8	19.0	--	2.53	0.0
0200	-45.4	33.3	25.0	15.1	-12.9	18.0	--	2.16	.0
0300	-46.6	32.9	45.5	15.8	-31.8	16.8	--	3.07	.0
0400	-45.4	33.1	27.2	9.1	-15.0	16.2	--	2.47	.0
0500	-44.7	34.7	20.0	5.6	-9.9	15.1	--	2.54	.0

Table D2. Average hourly and daily flux densities for two sets of instruments from 1400 hours, May 31, 1986, through 0900 hours, June 6, 1986, at site L--*Continued*

Time	Q	G	H_{ec}	λE_{ec}	λE_{eb}	T	q	U	$K\downarrow$
				Mast 1, June 2, 1986--*Continued*					
0600	-39.3	33.9	17.6	7.7	-12.1	14.9	--	2.17	6.0
0700	7.4	25.3	6.9	10.1	-39.7	16.0	--	1.95	94.4
0800	136.0	-.9	-10.9	-16.4	-124.1	20.2	--	2.26	272.4
0900	302.8	-28.0	-48.1	-82.7	-226.7	23.0	--	2.22	477.2
1000	468.7	-46.9	-51.4	-123.7	-370.4	24.1	--	2.15	678.6
1100	600.8	-76.8	-63.4	-200.8	-460.6	27.3	11.5	1.56	851.1
1200	680.8	-91.1	-88.1	-227.8	-501.6	29.5	10.9	1.33	966.9
1300	718.8	-99.9	-124.6	-292.0	-494.4	31.4	10.8	2.42	1,025.6
1400	732.7	-99.8	-90.4	-162.0	-542.5	31.1	11.0	4.39	1,019.6
1500	679.0	-107.6	-71.2	-129.0	-500.1	32.9	11.3	4.50	953.5
1600	579.7	-101.7	-45.8	-110.6	-432.2	33.6	10.8	3.53	832.8
1700	439.8	-75.6	-11.8	-15.1	-352.5	--	--	1.79	658.7
1800	284.8	-47.8	21.8	114.3	-258.7	--	--	1.95	462.4
1900	119.1	-6.5	148.7	158.8	-261.2	--	--	5.62	249.9
2000	-22.0	9.1	136.3	114.0	-123.4	--	--	4.17	49.8
2100	-53.0	18.0	60.4	262.5	-25.4	--	--	2.44	.2
2200	-44.0	22.9	49.7	312.5	-28.6	--	--	1.94	.0
2300	-41.2	26.2	29.9	82.0	-14.9	--	--	2.37	.0
2400	-40.8	25.4	36.1	58.9	-20.7	--	--	2.36	.0
Average daily values	220.1	-18.9	2.4	-6.9	-203.6	--	--	2.66	358.3
				Mast 1, June 3, 1986					
0100	-36.1	29.0	18.7	39.0	-11.6	--	--	1.47	0.0
0200	-35.1	25.7	21.0	83.8	-11.5	--	--	1.81	.0
0300	-39.2	25.6	32.4	77.2	-18.9	--	--	2.02	.0
0400	-40.7	24.8	36.3	34.4	-20.4	--	--	2.37	.0
0500	-41.8	24.2	34.8	31.1	-17.2	--	--	2.29	.0
0600	-34.0	27.2	17.2	22.5	-10.4	--	--	1.89	3.2
0700	8.4	18.2	12.7	35.2	-39.2	--	--	1.80	98.0
0800	154.6	.1	6.7	6.7	-161.4	--	--	3.19	295.1
0900	325.1	-22.1	-11.4	-10.0	-291.6	--	--	2.58	501.2
1000	482.8	-54.2	-18.0	-104.2	-410.5	28.0	10.7	2.27	690.0
1100	603.3	-91.6	-36.4	-146.6	-475.3	30.1	11.0	1.92	847.6
1200	676.8	-98.3	-85.0	-282.2	-493.4	31.5	11.3	1.64	959.3
1300	722.8	-101.0	-102.3	-321.2	-519.5	32.7	11.6	2.60	1,018.8
1400	720.6	-111.2	-80.8	-281.1	-528.5	33.4	11.5	3.19	1,011.3
1500	674.2	-110.2	-64.5	-179.3	-499.5	33.7	11.5	3.60	951.4
1600	581.2	-92.6	-34.9	-82.1	-453.7	33.7	11.1	4.15	830.1
1700	450.9	-68.2	9.7	21.1	-392.4	33.5	11.1	4.93	662.0
1800	275.4	-40.8	54.7	75.3	-289.3	32.8	11.0	4.78	446.6
1900	109.0	-17.3	78.4	98.9	-170.1	31.0	11.6	3.63	232.8
2000	-12.5	5.6	49.0	264.1	-42.1	28.0	11.5	2.30	45.0
2100	-45.7	17.4	85.6	281.5	-57.3	27.6	10.6	2.42	.0
2200	-41.5	21.8	57.3	233.7	-37.6	26.4	10.4	1.84	.0
2300	-37.7	28.8	29.7	194.1	-20.8	22.6	10.4	1.81	.0
2400	-35.4	32.6	7.5	100.4	-4.7	21.3	9.6	1.36	.0
Average daily values	224.4	-21.9	4.9	8.0	-207.4	--	--	2.58	358.0

Table D2. Average hourly and daily flux densities for two sets of instruments from 1400 hours, May 31, 1986, through 0900 hours, June 6, 1986, at site L--*Continued*

Time	Q	G	H_{ec}	λE_{ec}	λE_{eb}	T	q	U	$K\downarrow$
				Mast 1, June 4, 1986					
0100	-37.4	35.1	8.3	122.6	-6.0	16.9	9.7	1.63	0.0
0200	-37.3	35.5	10.3	33.8	-8.2	15.5	10.2	1.99	.0
0300	-36.3	36.2	13.0	52.3	-13.0	15.2	9.6	1.91	.0
0400	-36.5	37.8	10.0	49.1	-11.3	13.8	9.7	1.75	.0
0500	-35.2	40.0	6.7	17.3	-11.5	12.5	9.7	1.27	.0
0600	-31.5	41.5	5.1	8.4	-15.1	11.4	9.3	1.00	3.6
0700	8.8	34.9	2.0	5.1	-45.7	12.5	10.3	1.08	103.1
0800	143.1	10.1	-18.9	-35.0	-134.3	19.3	11.4	.98	301.0
0900	316.1	-16.7	-54.0	-114.0	-245.5	23.5	10.6	1.58	509.3
1000	485.2	-39.1	-112.6	-233.9	-333.4	26.3	11.0	2.07	709.8
1100	605.6	-61.1	-112.4	-276.5	-432.1	28.5	10.8	1.88	871.0
1200	653.4	-78.8	-98.9	-260.0	-475.8	30.1	10.8	2.85	937.9
1300	661.3	-90.1	-75.3	-152.6	-496.0	31.1	9.6	4.44	943.8
1400	595.1	-79.5	-32.5	-58.6	-483.2	31.0	9.6	6.08	845.9
1500	547.7	-68.5	-20.6	-26.9	-458.7	30.9	9.2	6.76	787.8
1600	540.0	-67.0	-40.2	-37.5	-432.8	30.6	10.2	7.72	775.7
1700	363.6	-41.6	32.3	30.8	-354.3	30.1	10.0	7.38	551.4
1800	256.0	-27.1	79.6	40.5	-308.6	30.4	8.9	7.88	437.6
1900	83.0	-5.3	122.2	76.5	-199.9	29.1	8.8	6.37	211.9
2000	-15.4	8.3	143.8	86.6	-136.8	27.5	8.1	5.68	63.1
2100	-54.9	21.4	100.9	102.9	-67.5	24.6	7.3	3.21	2.1
2200	-50.5	32.1	47.2	203.9	-28.7	23.8	5.7	1.83	.0
2300	-58.4	36.0	84.6	197.2	-62.2	21.2	5.6	2.89	.0
2400	-46.0	42.8	13.8	153.5	-10.6	19.3	5.7	1.60	.0
Average daily values	200.8	-6.8	4.8	-0.6	-198.8	23.1	9.2	3.41	335.6
				Mast 1, June 5, 1986					
0100	-45.9	46.6	24.4	140.4	-25.0	13.0	6.2	1.87	0.0
0200	-44.9	49.0	13.5	79.7	-17.6	10.5	6.1	1.66	.0
0300	-41.7	51.6	38.0	401.9	-47.9	9.5	6.1	1.35	.0
0400	-41.4	52.3	1.9	40.2	-12.7	7.2	6.2	1.64	.0
0500	-45.9	50.4	12.8	-8.3	-17.4	6.8	6.2	2.15	.0
0600	-39.9	49.1	3.6	13.1	-12.8	7.4	6.2	1.86	4.0
0700	3.9	43.9	-.3	14.7	-47.5	9.2	7.3	1.08	103.2
0800	150.1	19.0	-20.0	-47.8	-149.0	15.9	8.2	.61	310.5
0900	327.9	-8.3	-45.3	-123.5	-274.3	21.1	8.0	1.68	523.3
1000	478.7	-32.8	-123.0	-256.2	-322.8	23.1	7.9	1.48	715.9
1100	601.0	-55.5	-162.4	-385.8	-383.2	24.9	8.0	1.51	876.7
1200	686.5	-72.2	-182.1	-454.5	-432.2	26.5	7.2	1.49	994.0
1300	724.8	-89.5	-136.3	-458.4	-499.1	27.6	7.0	1.40	1,052.7
1400	716.9	-104.9	-152.9	-485.9	-459.1	28.8	7.7	2.53	1,043.6
1500	673.0	-103.7	-137.0	-328.2	-432.3	29.2	8.1	3.81	975.9
1600	567.2	-85.4	-68.7	-214.7	-413.2	29.3	7.9	2.83	844.8
1700	427.3	-61.5	-34.7	-129.2	-331.1	30.1	7.3	2.10	670.3
1800	264.2	-40.4	-.9	23.6	-223.0	30.2	7.9	1.84	464.1
1900	101.4	-15.1	59.1	153.4	-145.5	28.8	7.9	2.20	243.3
2000	-27.0	12.8	106.7	138.6	-92.5	25.2	7.9	3.26	49.5
2100	-48.0	27.8	25.2	110.1	-5.0	20.5	7.8	2.06	.0

Table D2. Average hourly and daily flux densities for two sets of instruments from 1400 hours, May 31, 1986, through 0900 hours, June 6, 1986, at site L--*Continued*

Time	Q	G	H_{ec}	λE_{ec}	λE_{eb}	T	q	U	$K\downarrow$
				Mast 1, June 5, 1986--*Continued*					
2200	-43.1	34.1	19.6	445.4	-10.6	19.4	7.8	1.95	0.0
2300	-44.4	37.3	33.9	137.5	-26.8	17.9	8.2	1.75	.0
2400	-43.0	37.4	20.7	119.1	-15.1	16.2	8.3	1.77	.0
Average daily values	219.1	-6.6	-29.3	-44.8	-183.2	19.9	7.4	1.91	369.7
				Mast 1, June 6, 1986					
0100	-41.8	39.9	7.5	44.0	-5.7	12.9	8.1	2.00	0.0
0200	39.4	40.4	5.9	29.9	-6.9	12.3	7.9	1.92	.0
0300	-39.9	41.7	10.1	28.3	-12.0	11.5	7.6	2.05	.0
0400	-40.9	41.9	10.5	28.7	-11.5	11.7	7.6	1.96	.0
0500	-39.3	43.7	12.6	7.7	-17.1	9.3	7.6	2.07	.0
0600	-39.6	41.2	14.6	16.5	-16.2	10.1	7.8	2.26	3.8
0700	7.7	35.4	9.6	28.8	-52.8	12.5	8.3	1.52	103.3
0800	153.4	14.1	-16.4	-32.2	-151.2	18.0	8.9	2.04	304.2
0900	223.4	-8.5	-17.0	-77.3	-297.9	20.1	8.5	2.07	511.8
				Mast 2, May 31, 1986					
1600	61.5	20.9	--	--	--	--	--	--	--
1700	23.5	21.0	--	--	--	--	--	--	--
1800	-10.5	21.9	--	--	--	--	--	--	--
1900	34.1	6.7	--	--	--	--	--	--	--
2000	-28.3	21.8	--	--	--	--	--	--	--
2100	-48.3	35.2	--	--	--	--	--	--	--
2200	-26.5	25.0	--	--	--	--	--	--	--
2300	-41.9	21.7	--	--	--	--	--	--	--
2400	-39.4	23.9	--	--	--	--	--	--	--
				Mast 2, June 1, 1986					
0100	-54.4	24.8	--	--	--	--	--	--	--
0200	-53.0	26.0	--	--	--	--	--	--	--
0300	-52.5	25.7	--	--	--	--	--	--	--
0400	-49.3	30.0	--	--	--	--	--	--	--
0500	-44.7	34.5	--	--	--	--	--	--	--
0600	-35.5	37.3	--	--	--	--	--	--	--
0700	13.6	15.3	--	--	--	--	--	--	--
0800	144.7	-20.3	--	--	--	--	--	--	--
0900	297.4	-55.0	--	--	--	--	--	--	--
1000	452.9	-90.5	--	--	--	--	--	--	--
1100	583.4	-106.7	--	--	--	--	--	--	--
1200	658.6	-117.8	-76.0	--	-464.9	29.5	12.3	2.38	--
1300	694.5	-128.8	-77.5	--	-488.3	31.3	11.6	2.02	--
1400	699.2	-137.6	-91.4	--	-470.2	33.1	11.8	1.62	--
1500	641.0	-127.2	-61.4	--	453.4	33.8	11.4	1.83	--
1600	532.0	-110.3	-55.4	--	-366.2	34.3	11.2	2.03	--
1700	154.8	-17.6	42.5	--	-178.7	30.9	11.0	4.21	--
1800	165.2	3.9	129.3	--	-298.5	29.0	10.0	6.00	--
1900	15.2	20.5	89.9	--	-125.6	27.9	9.5	6.05	--
2000	-29.7	26.6	63.4	--	-60.3	27.0	--	3.26	--

Table D2. Average hourly and daily flux densities for two sets of instruments from 1400 hours, May 31, 1986, through 0900 hours, June 6, 1986, at site L--*Continued*

Time	Q	G	H_{ec}	λE_{ec}	λE_{eb}	T	q	U	$K\downarrow$
				Mast 2, June 1, 1986--*Continued*					
2100	-54.1	34.0	54.7	--	-34.4	24.4	--	4.38	--
2200	-53.2	33.2	82.2	--	-62.3	22.8	--	4.07	--
2300	-50.5	34.8	55.4	--	-39.7	21.0	--	3.46	--
2400	-50.2	33.9	69.7	--	-53.4	20.4	--	3.70	--
Average daily values	188.6	-22.1	--	--	--	--	--	--	--
				Mast 2, June 2, 1986					
0100	-43.2	38.4	27.7	--	-22.9	19.2	--	2.62	--
0200	-42.7	37.5	14.5	--	-9.3	18.2	--	2.27	--
0300	-44.8	35.6	47.0	--	-37.9	17.0	--	3.14	--
0400	-43.0	37.2	32.7	--	-26.9	16.4	--	2.56	--
0500	-42.5	38.3	33.7	--	-29.4	15.3	--	2.66	--
0600	-37.1	37.3	21.8	--	-22.0	15.0	--	2.27	--
0700	24.8	21.8	10.9	--	-57.5	16.3	--	2.05	--
0800	157.7	-15.6	-7.9	--	-134.2	20.4	--	2.44	--
0900	311.7	-51.3	-33.8	--	-226.6	23.2	--	2.37	--
1000	460.8	-82.3	-53.3	--	-325.2	25.6	--	2.26	--
1100	580.6	-115.8	-75.4	--	-389.4	27.8	11.9	1.69	--
1200	656.3	-135.2	-91.4	--	-429.7	30.0	11.2	1.42	--
1300	714.8	-139.8	-121.8	--	-453.2	31.8	11.1	2.60	--
1400	701.7	-132.2	-96.3	-283.0	-473.1	32.5	11.2	4.52	--
1500	600.8	-121.8	-79.3	-297.8	-399.7	33.0	11.3	4.72	--
1600	482.4	-109.2	-55.3	-267.0	-317.9	34.1	10.8	3.66	--
1700	334.1	-89.1	-12.2	-129.6	-232.8	--	--	1.97	--
1800	180.9	-55.1	10.5	-195.2	-136.3	--	--	2.14	--
1900	37.5	1.4	87.1	-155.4	-126.0	--	--	5.63	--
2000	-44.5	17.5	90.8	-88.6	-63.8	--	--	4.28	--
2100	-51.2	29.4	42.8	-34.0	-21.0	--	--	2.55	--
2200	-40.1	35.9	52.3	-33.3	-48.1	--	--	2.05	--
2300	-38.3	39.3	21.8	-11.8	-22.8	--	--	2.46	--
2400	-38.0	37.2	18.8	-10.0	-18.0	--	--	2.45	--
Average daily values	199.1	-26.7	-4.8	--	-167.7	--	--	2.78	--
				Mast 2, June 3, 1986					
0100	-32.1	40.7	26.4	-10.7	-34.9	--	--	1.62	--
0200	-32.9	35.1	13.1	-8.9	-15.4	--	--	1.89	--
0300	-36.7	36.4	10.7	-7.0	-10.3	--	--	2.09	--
0400	-37.9	35.5	28.9	-14.0	-26.5	--	--	2.43	--
0500	-38.7	34.5	42.3	-21.1	-38.0	--	--	2.35	--
0600	-31.3	37.9	25.9	-12.6	-32.6	--	--	2.01	--
0700	48.8	18.8	10.6	-28.6	-78.2	--	--	1.87	--
0800	213.8	-19.3	2.6	-154.9	-197.1	--	--	3.26	--
0900	366.6	-57.5	-22.5	-259.1	-286.6	--	--	2.69	--
1000	459.4	-71.1	-33.4	-230.7	-354.9	28.0	11.5	2.32	--
1100	570.8	-89.8	-53.0	-299.2	-427.9	30.1	11.5	1.93	--
1200	657.8	-102.4	-89.1	-361.9	-466.4	31.6	11.8	1.74	--
1300	711.2	-116.8	-98.3	-441.2	-496.2	32.6	11.9	2.72	--
1400	707.7	-119.1	-95.5	-489.0	-493.1	33.5	11.6	3.25	--

Table D2. Average hourly and daily flux densities for two sets of instruments from 1400 hours, May 31, 1986, through 0900 hours, June 6, 1986, at site L--*Continued*

Time	Q	G	H_{ec}	λE_{ec}	λE_{eb}	T	q	U	$K\downarrow$
				Mast 2, June 3, 1986--*Continued*					
1500	656.0	-112.8	-82.7	-523.2	-460.5	33.9	11.6	3.65	--
1600	553.9	-97.4	-44.6	-494.1	-411.9	34.1	11.1	4.38	--
1700	418.8	-70.7	6.8	-459.6	-354.9	33.5	11.3	5.11	--
1800	239.0	-43.2	50.4	-307.8	-246.1	33.1	11.0	4.80	--
1900	80.4	-10.1	67.7	-166.2	-138.0	31.6	11.4	3.74	--
2000	-19.9	13.8	39.8	-45.7	-33.7	28.2	11.3	2.33	--
2100	-43.5	27.5	68.7	-41.2	-52.7	27.9	10.4	2.46	--
2200	-39.4	31.9	51.9	-30.6	-44.3	26.5	10.2	1.98	--
2300	-35.7	37.8	26.2	-15.5	-28.3	22.8	10.3	1.91	--
2400	-33.9	41.4	8.3	-5.5	-15.9	21.5	9.5	1.48	--
Average daily values	220.9	-21.6	-1.6	-184.5	-197.7	--	--	2.67	--
				Mast 2, June 4, 1986					
0100	-34.9	44.4	5.0	-2.4	-14.6	17.1	9.7	1.70	--
0200	-35.5	44.9	11.2	-4.6	-20.7	15.7	10.3	2.06	--
0300	-34.2	44.5	5.8	-4.0	-16.1	15.4	9.7	2.02	--
0400	-34.9	46.2	4.2	-4.1	-15.6	14.1	9.8	1.81	--
0500	-33.9	47.7	5.8	-1.5	-19.6	12.6	9.9	1.37	--
0600	-30.6	49.2	4.8	-2.6	-23.5	11.5	9.7	1.08	--
0700	17.8	39.3	-.6	-24.0	-56.5	12.8	10.8	1.22	--
0800	151.6	8.3	-21.8	-79.6	-138.0	19.6	12.1	1.04	--
0900	319.2	-23.5	-52.8	-184.5	-242.9	23.7	10.8	1.64	--
1000	477.8	-54.4	-92.9	-277.2	-330.4	26.4	10.9	2.13	--
1100	593.0	-82.9	-103.8	-332.8	-406.4	28.8	10.6	1.92	--
1200	644.8	-96.2	-98.1	-424.1	-450.5	30.1	11.0	2.86	--
1300	645.4	-95.5	-63.8	-543.7	-486.1	30.9	9.4	4.70	--
1400	574.6	-76.1	-32.6	-499.1	-465.9	31.3	9.2	6.27	--
1500	524.0	-66.1	-17.2	-475.0	-440.7	30.2	9.4	7.00	--
1600	506.2	-69.3	-35.6	-407.8	-401.2	30.9	9.8	7.94	--
1700	331.5	-44.8	37.2	-364.8	-323.9	30.9	9.7	7.40	--
1800	209.1	-31.5	69.8	-351.3	-247.4	30.7	8.5	7.95	--
1900	52.3	-.5	108.4	-198.9	-160.1	29.4	8.5	6.40	--
2000	-26.1	13.4	119.3	-134.7	-106.6	27.7	7.8	5.66	--
2100	-54.0	28.5	79.9	-50.5	-54.4	24.8	7.0	3.29	--
2200	-48.7	41.6	30.8	-19.2	-23.7	24.0	5.3	2.02	--
2300	-56.3	44.6	84.1	-58.9	-72.3	21.3	5.2	2.98	--
2400	-44.2	51.8	22.7	-13.1	-30.3	19.5	5.9	1.68	--
Average daily values	192.2	-5.7	2.9	-185.8	-189.5	23.3	9.2	3.52	--
				Mast 2, June 5, 1986					
0100	-43.2	55.6	21.0	-6.2	-33.5	13.2	--	1.94	--
0200	-41.5	58.5	-2.0	1.3	-14.1	10.7	--	1.76	--
0300	-39.0	60.3	-10.4	6.5	-10.9	9.7	--	1.46	--
0400	-38.9	60.8	5.6	-1.9	-27.4	7.5	--	1.74	--
0500	-43.2	59.3	13.9	-10.9	-30.0	6.9	--	2.21	--
0600	-37.4	57.5	5.4	-1.6	-25.5	7.7	--	1.93	--
0700	20.9	46.3	-5.1	-24.6	-62.2	9.5	--	1.18	--
0800	168.3	15.4	-20.7	-100.5	-162.9	16.3	--	.72	--

Table D2. Average hourly and daily flux densities for two sets of instruments from 1400 hours, May 31, 1986, through 0900 hours, June 6, 1986, at site L--*Continued*

Time	Q	G	H_{ec}	λE_{ec}	λE_{eb}	T	q	U	$K\downarrow$
				Mast 2, June 5, 1986--*Continued*					
0900	325.8	-16.4	-41.9	-196.0	-267.6	21.3	--	1.81	--
1000	478.3	-49.9	-89.6	-250.9	-338.8	23.2	--	1.58	--
1100	588.7	-78.3	-132.1	-342.7	-378.3	25.1	7.4	1.63	--
1200	674.4	-97.4	-133.0	-462.9	-444.0	26.8	6.7	1.58	--
1300	710.1	-112.8	-111.9	-474.0	-485.4	27.9	6.4	1.50	--
1400	713.8	-119.7	-130.1	-530.2	-465.0	29.1	7.2	2.60	--
1500	664.3	-110.6	-110.0	-556.0	-443.7	29.4	7.7	3.91	--
1600	545.4	-99.4	-69.0	-435.6	-376.9	28.9	8.0	2.89	--
1700	404.2	-84.9	-43.6	-360.4	-275.7	30.1	7.1	2.16	--
1800	238.7	-53.9	-6.5	-261.2	-178.4	30.7	7.2	1.95	--
1900	77.3	-8.4	30.7	-113.8	-99.5	29.3	7.4	2.27	--
2000	-33.8	23.4	58.9	-66.5	-48.5	25.4	7.4	3.31	--
2100	-43.9	39.4	23.7	-8.5	-19.2	20.7	7.5	2.16	--
2200	-40.3	44.8	6.5	-1.3	-11.0	19.7	7.5	2.05	--
2300	-42.0	46.3	44.5	-29.9	-48.7	18.1	8.0	1.84	--
2400	-40.4	46.4	28.8	-14.8	-34.8	16.3	8.1	1.83	--
Average daily values	215.3	-9.1	-27.8	-176.8	-178.4	20.2	--	2.0	--
				Mast 2, June 6, 1986					
0100	-38.8	49.3	-8.2	3.2	-2.3	13.2	8.0	2.06	--
0200	-36.8	49.2	3.4	1.9	-15.8	12.6	7.8	2.03	--
0300	-36.9	50.2	6.4	-6.6	-19.7	11.7	7.6	2.11	--
0400	-37.9	50.7	2.4	-1.1	-15.2	12.0	7.5	2.00	--
0500	-36.9	52.0	3.1	-1.5	-18.2	9.5	7.6	2.16	--
0600	-37.3	49.4	12.0	-8.0	-24.1	10.3	8.0	2.34	--
0700	10.8	39.7	8.7	-27.8	-58.2	12.9	--	1.65	--
0800	147.3	11.3	-6.3	-113.4	-152.3	18.3	--	2.15	--

CHAPTER E.--TOTAL TRANSPIRATION FROM LAND AREAS ESTIMATED FROM HAND-HELD POROMETER MEASUREMENTS

By David P. Groeneveld (Inyo County Water Department) *and*
Daniel C. Warren (University of Arizona, Tucson)

INTRODUCTION

A null-balance hand-held porometer has been used for measuring transpiration of shallow ground-water plants in Owens Valley, California. The primary goal for these measurements has been to compare plant transpiration under relatively steady-state conditions of soil water with transpiration when soil water becomes depleted after water-table decline due to regional ground-water pumping. The results of past plant-water-balance studies in the valley suggest that the hand-held porometer also may be used to accurately estimate plant transpiration over large areas with known vegetation species composition and cover (Groeneveld and others, 1986a). The extrapolation of porometer data to the land surface is possible because of three factors:

1. Most (>90 percent) of the vegetation covering the parts of the Owens Valley floor that are underlain by ground water less than 4-m deep is dominated by five species of phreatophytes (Los Angeles Department of Water and Power, 1987).

2. From data collected when the water table was under steady-state conditions, transpiration per unit leaf area could be accurately modeled for each of the dominant Owens Valley floor species using the day of the year as the independent variable. The presence of shallow ground water tends to buffer against severe soil-water depletion and, under natural conditions, tends to support phreatophyte transpiration through the entire season.

3. Data suggest that the dominant valley floor phreatophytes tend to adjust leaf area to the available soil water (Groeneveld and others, 1986b). During droughts, leaf area will tend to decrease dramatically and increase during wet periods. Transpiration per leaf area will tend to remain the same during wet or dry conditions.

The water use and growth of the five dominant shrub and grass phreatophytes of the Owens Valley floor have received intensive investigation (Groeneveld and others, 1986a,b) and this study uses these data for estimation of land-surface transpiration. The estimates of land-surface transpiration were partly or entirely simulated from data collected in 1984 and 1985.

For estimating land-surface transpiration, three factors were necessary:

1. Leaf area index for the projected area of canopy cover of each species,
2. The fractional cover of the canopies of each species, and
3. A daily transpiration rate for each species.

For both the estimates of land-surface transpiration, partly and entirely simulated, factors 1 and 2 were treated the same. For the entirely simulated estimate of transpiration, the transpiration data for factor 3 were taken from seasonal curves calculated from data collected during 1984 and 1985. For the partly simulated estimates, transpiration data were obtained from hand-held porometer measurements at sites C and L concurrently with evapotranspiration measurements made by micrometeorological techniques (Bowen ratio and eddy correlation).

The intent of this part of the study was to (1) confirm that estimating land-surface transpiration using hand-held porometer data was valid by comparing estimates to micrometeorologic measurements of land-surface *ET* (this comparison is made in chapters G and H, this report) and (2) determine how accurately land-surface transpiration could be simulated entirely from existing data.

STUDY SITES

The two sites chosen for study are referred to here as site C (scrub site), and site L (alkaline meadow site). The five species monitored in this study were those that dominate the Owens Valley floor and included three shrubs: Nevada saltbush (*Atriplex torreyi*), rubber rabbitbrush (*Chrysothamnus nauseosus*), and greasewood (*Sarcobatus vermiculatus*), and two grasses: saltgrass (*Distichlis spicata*) and alkali sacaton (*Sporobolus airoides*) (Munz and Keck, 1959).

Table E1 gives species composition at the two study sites measured in 1984 by a modified toe-point transect technique (Evans and Love, 1957). Although sites C and L contain many of the same species, their ecology is very different. Site C is relatively dry and sandy, and depth of the water table is in excess of 3 m. The vegetation cover of site L is atypical for meadow sites in the Owens Valley because the site received irrigation during several seasons prior to this study. This irrigation helped to maintain the water
table at a depth of about 1 m.

Table E1. Vegetative cover by species, as a decimal fraction, at the two study sites

[Numbers in parentheses indicate percentage of vegetation which received or lacked transpiration measurements]

	Site C	Site L
Atriplex torreyi	0.032	0.005
Chrysothamnus nauseosus	.108	0
Sarcobatus vermiculatus	.039	.002
Distichlis spicata	0	.212
Sporobolus airoides	.113	.118
Total for species with transpiration measured	0.292 (91)	0.337 (46)
Total for species with transpiration not measured	0.030 (9)	0.403 (54)
Total vegetative cover	0.322	0.740

The comparatively wet soil at site L supported over three times the cover of site C and numerous plant species that have high water requirements. These species compose the 54-percent cover that did not receive transpiration monitoring. Their transpiration was estimated on the basis of measured species at the site.

METHODS

A null-balance porometer Model LI-1600 manufactured by Li-Cor, Inc. (Beardsel and others, 1972), was used to monitor transpiration rates on five branchlets for each shrub and 10 leaves for each grass species. These measurements were made at approximately 2-hour intervals through the day from sunrise to sunset. The instrument was calibrated for the dry Owens Valley climate in a range of relative humidity from 12 to 50 percent. The properties measured by the instrument were

transpiration, diffusive resistance, cuvette relative humidity, cuvette temperature, and photosynthetically active radiation (wave length ranging from 0.4 to 0.7 μm). Ambient relative humidity and temperature also were measured using a sling psychrometer.

Grass leaves were selected randomly to reflect the "average" appearance of viable leaves at the site and were not marked for remeasurement. Adaxial and abaxial surfaces of grasses were sampled separately because only one surface at a time could be measured by the cuvette-porometer combination designed for the measurement on grasses. These measurements were summed to yield transpiration on the basis of projected leaf area.

The cuvette chamber used for the shrub measurements consisted of a hinged and bisected polycarbonate cylinder which was clamped over the leafy stems. Cuvette positions on the shrub branches were marked with plastic flagging tape for later measurements on the same leafy material.

The shrub branch samples had variable leaf area which required that a correction factor for actual leaf area be determined following a diurnal measurement course on the shrubs. To estimate the leaf area of each shrub branch sample following a diurnal monitoring suite, the leaves were removed from the stems and placed as a single layer on a grid field of 1-cm^2 cells. Their area was estimated to the nearest millimeter using the grid field and stereologic techniques (Weibel, 1980). The measured transpiration was then corrected to actual unit-leaf-area transpiration using these estimates.

Prior to taking transpiration measurements, the porometer was placed in the shade and turned on for 10 minutes to acclimate to ambient relative humidity and temperature. The cuvette chamber was shaded during each measurement and kept shielded from the sun as much as possible between measurements to minimize the possibility of data biased by temperature gradients. Most of the transpiration measurements were accomplished within 30 seconds. Precalibration observations indicated that shading for periods of 1 minute has little effect on the leaf conductance for the species monitored in this study.

Following each transpiration measurement with the porometer, a relative irradiance value of photosynthetically active radiation (PAR) was measured at the branchlet or grass blade. This was done by holding the PAR sensor (Li-Cor, Inc., LI-1905-1), located on the porometer head, horizontally and adjacent to the measured leaves. The horizontal position was used as a convenience because it was impractical to assess the actual radiation impinging on shrub branchlets and grass canopies owing to the complex alignment of leaf surfaces.

Transpiration data collected by a hand-held porometer may have measurement errors that arise primarily from accidental breaking of branchlets during measurement or an incomplete seal of the chamber during windy conditions. To reduce scatter induced by measurement errors, data were screened by deriving a mean and standard deviation for each block of semihourly measurements (five per shrub or grass blade surface). Those records that lay outside one standard deviation to either side of the mean were then eliminated from the data set. Although this two-standard deviation interval for accepting data was somewhat arbitrary, by experience this data filtering tended to remove extreme values resulting from sampling broken branches or leakage of ambient air into the chamber during measurement. With the exception of the extreme values, most data points tended to cluster about the mean.

Diurnal curves of transpiration for these species tend to form downward opening parabolas and this permits accurate mathematical description using polynomial regression. Measurements of transpiration and leaf conductance before sunrise and after sunset have shown that the stomata of these species close in the absence of light (Groeneveld and others, 1986a). To set the zero points on the parabolic diurnal transpiration curves, the sunrise and sunset times determined from a table published for Bishop (U.S. Naval Observatory, undated) were added to the transpiration data. Polynomial regression was then used to calculate quadratic curves of transpiration for each species at both sites. The curves were integrated through the day to provide unit-leaf-area transpiration for each species as a total daily volume that could be multiplied by the estimated leaf area for that species at that site.

A Scholander-type pressure chamber (Scholander and others, 1964) was used to measure the xylem pressure potential of shoots of the plants monitored at each of the study sites. This method is commonly used in field studies of plant water physiology because it provides an assessment of the total water status of a plant (Ritchie and Hinckley, 1975). Measurements were made on pieces of shrub stem approximately 10 cm in length and on culms of the grass species.

Soil water at the study sites was monitored by a neutron probe through a series of access tubes. The access tubes were implanted in the drip lines of three shrub canopies at site C and through two grass plots at site L. A master calibration curve developed for the Owens Valley was used to convert the neutron probe counts to volumetric soil water content. Because transpiration, plant-cover, and leaf-area measurements from 1984 and 1985 were used in this study to estimate land-surface transpiration in 1986, soil-water measurements from 1984 through 1986 were compared to determine whether soil-water content may have had an influence on these plant responses. According to the neutron probe data, soil-water contents during a 1-month period surrounding the first week of June remained relatively stable through the 3-year period, thus confirming the appropriateness of using transpiration data measured during this earlier period.

RESULTS OF PHYSIOLOGICAL MONITORING FOR EACH SPECIES

Figure E1 presents the results of porometer and pressure chamber measurements at site C on June 3 and 4. Figure E2 shows the same measurements from grasses at site L on June 5. Each data point on the plots of transpiration and leaf conductance represents an average (outliers deleted) for each semihourly suite of 5 measurements for each shrub and 10 measurements for each grass species. Each point on the plots of shoot potential represents an arithmetic average of three measurements.

The transpiration data (figs. E1 and E2) illustrate that a quadratic model to represent transpiration for each species through a diurnal period is appropriate. Equation E1 presents the curve used to express transpiration rate ($\hat{T}$) as a function of time.

$$\hat{T}_i = \beta_{0_i} + \beta_{1_i} t + \beta_{2_i} t^2, \qquad \text{(E1)}$$

where

$\hat{T}$ is transpiration, in micrograms per square centimeter per second;
i refers to the ith species;
β_0, β_1, β_2 are regression coefficients, dimensionless; and
t is time of day, in hours.

From the data, transpiration rates through the day correlate better with solar radiation rather than with either ambient relative humidity or temperature. These curves suggest that transpiration processes for these species are controlled largely by the temperature gradient induced by the solar radiation received by the leaves. Such transpiration responses may be attributed to the presence of the shallow water table, which provides soil water greatly in excess of the 10- to 15-cm average annual precipitation received on the Owens Valley floor. The relatively abundant soil water may permit the plants to maintain near-optimal leaf conductance for photosynthesis. This relation may be moderated somewhat by climatic factors because diurnal leaf conductance for these species apparently correlates with relative humidity. Stomatal regulation in response to relative humidity has been observed for many species (Losch and Tenheunen, 1981).

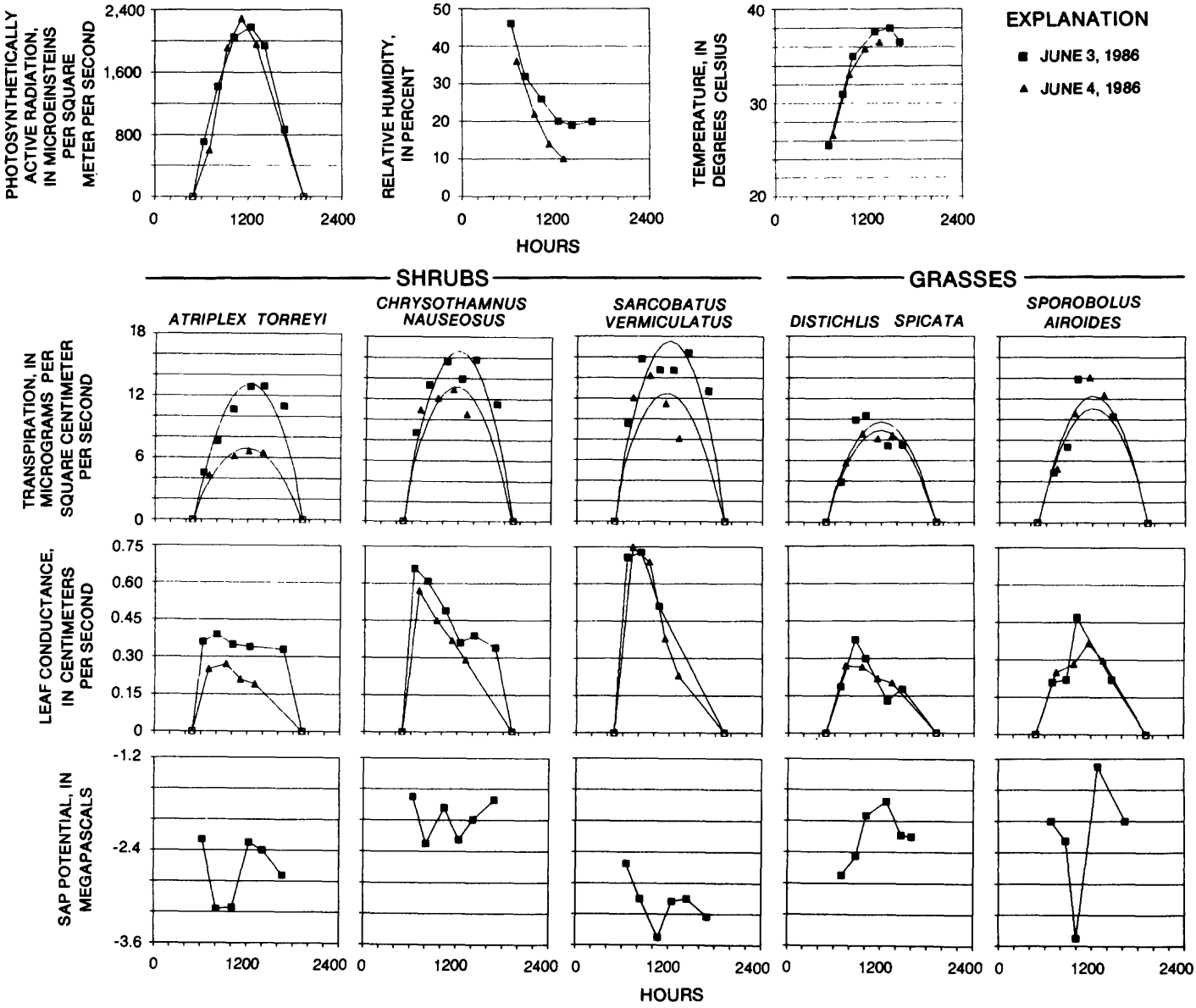

Figure E1. Results of monitoring ground-water plants at site C, June 3 and 4, 1986.

Measurements of sap potential obtained with the Scholander pressure chamber (figs. E1 and E2) are of interest because stomatal aperture and thus leaf conductance are partly regulated by leaf-water potential (Davies and others, 1981). These data show that midday decreases in leaf conductance correlate with recovery of the water potential of measured shoots. However, stomatal closure alone cannot account for the recovery of water potential because the greatest diurnal transpiration rates were recorded during the period of apparent recovery. Another factor (probably osmotic) may be operative, which could induce recovery of water potential during midday to the extent observed for *Atriplex torreyi*, *Distichlis spicata*, and *Sporobolus airoides* on June 3 (fig. E1). For these plants, midday water potentials are as high or higher than those recorded just before sunrise. Syvertsen and others (1975) suggested that this phenomenon in *Larrea tridentata* was caused by diurnal movement of soil-water vapor responding to solar heating of the soil surface. For this system, this explanation may be inadequate because at shallow ground-water sites, the available soil water due to capillarity would diminish the influence of diurnal water vapor movement in the soil.

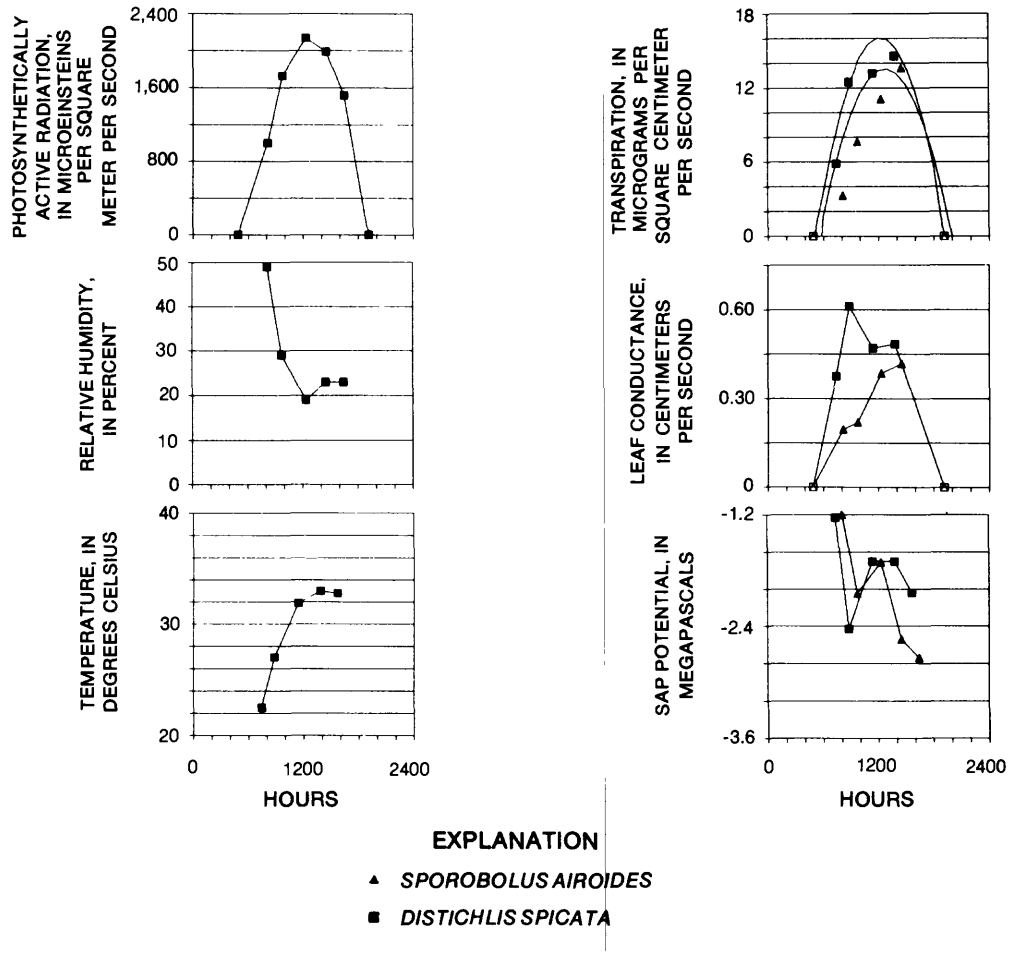

Figure E2. Results of monitoring ground-water plants at site L, June 5, 1986.

The results for measurements at site L are shown in figure E2. Transpiration rates of *Distichlis spicata* and *Sporobolus airoides* at site L were much greater than was recorded at site C (fig. E1). This result confirms earlier Owens Valley work that showed that transpiration for the two grasses was substantially greater for sites with high clay content soils such as site L than for sites with sandy soil textures such as site C (Groeneveld and others, 1986a).

CALCULATIONS OF TRANSPIRATION FOR THE STUDY SITES

Transpiration from the land surface may be estimated from porometric data using the statistically derived transpiration curves as shown in figures E1 and E2 and measured leaf area for each species. Total leaf area per land area for each species was the basis for estimating land-surface transpiration because transpiration was measured and modeled in terms of unit leaf area.

Measurement of leaf area at the study sites during June 1986 was beyond the scope of this investigation, so the required per species factors were partly simulated on the basis of data collected during 1984 and 1985. Leaf area of selected shrub or grass plots of each of the five dominant species were

repeatedly measured by a method that used vertically aligned pins whose locations were aligned by permanent markers (Groeneveld and others, 1986a). These measurements were used to determine leaf area to be combined with the species composition data in table E1 to calculate leaf area per ground area, which is known as leaf area index (*LAI*) (Brown and Blaser, 1968).

To model leaf area through the growing season for shrubs, leaf-area indexes for projected canopy areas (*LAIP*s) were calculated for the three species using data collected during 1984 through 1985. *LAIP* was calculated by taking the leaf area for a discrete shrub canopy and dividing by the projected area of canopy cover. Simple *LAI* generally is used to describe the average number of leaf layers covering a site (Brown and Blaser, 1968) and does not permit characterization by species or comparison among sites with different species composition. *LAIP* was used because the Owens Valley species tend to be distributed in discrete clumps or patches, commonly with bare ground in between. Also, the use of *LAIP* enabled combining data for each species from additional sites that had varying species composition.

For grasses, leaf area data were collected from permanently marked plots. Because the projected area of the canopy of the grasses was taken to be the area of each plot, *LAIP* for grasses measured in plots is equivalent to *LAI*.

LAIP yields the leaf-area index for the site when multiplied by the species composition data at the site (table E1). Analysis of the 1984 through 1985 data indicated that leaf area on a per plant or plot basis varied seasonally as a normal curve which is described mathematically in equation E2.

$$LAIP = a\, e^{-c(J-b)^2}, \tag{E2}$$

where

J is the day of year
e is vapor pressure, in millibars;
a is the maximum leaf area recorded;
b is the day of year on which the maximum leaf area was likely to occur; and
c is a coefficient determined by iteration for best fit of the curve to the data.

Equation E2 was used to determine the *LAIP* for each species by substituting the desired day of year. The constants used for describing the per species *LAIP* are given in table E2. The productivity of the grasses at the two sites was sufficiently different to warrant calculation of different curves for each site.

The empirical factors for equation E2 described a modeled leaf-area index for a desired date that could be multiplied by the species composition (table E1) to yield an estimate of per-species leaf cover at the desired site on the desired date. The resultant product was then multiplied by the daily total transpiration for each species measured at the site and the final products were then summed for all species. The mathematical notation for this operation is given in equation E3.

$$\hat{T}_j = \sum_{i=1}^{n} SC_{i_j} * \left[a_i e^{-c_i(J-b)_i^2}\right] * \int_{t=0}^{m} \left[\beta_{0_i}+\beta_{1_i}t+\beta_{2_i}t^2\right]dt, \tag{E3}$$

where

i is the ith species

j is the jth site;

SC_{i_j} is species composition (table E1);

$\left[a_i e^{-c_i(J-b)_i^2}\right]$ is projected leaf area index (eq. E2); and

$\int_{t=0}^{m}\left[\beta_{0_i}+\beta_{1_i}t+\beta_{2_i}t^2\right]dt$ is total transpiration (integral of eq. E1) evaluated between sunrise $t = 0$ and sunset (m).

Table E2. Constants derived from 1984-85 to describe projected leaf-area curves for five dominant species

[Data derived by using specimens from 10 widely different sites. *n*, number of samples used for each curve; *a*, maximum leaf area recorded; *b*, day of year on which the maximum leaf area was likely to occur; *c*, coefficient determined by iteration for best fit of the curve to the data]

Species	*n*	*a*	*b*	*c*
Atriplex torreyi	10	1.76	196.4	0.000105
Chrysothamnus nauseosus	9	1.91	182.7	.000111
Sarcobatus vermiculatus	11	2.34	187.5	.000170
Distichlis spicata				
Site C	2	1.19	175.4	.000226
Site L	3	5.67	195.0	.000471
Sporobolus airoides				
Site C	2	1.35	192.9	.000206
Site L	5	2.65	190.0	.000244

To compare to the transpiration estimate made using the porometer data measured during the 3 days of testing, transpiration also was simulated entirely from seasonal transpiration models. The seasonal models used a modification of equation E3 to estimate a value of total daily transpiration during any day from quadratic curves fitted by day of year. Fitted seasonal transpiration curves for each species used in this calculation were taken from data combined from a suite of several sites, including sites C and L, during 1984 and 1985 (Groeneveld and others, 1986a). Table E3 presents these curves. The time factor "*t*" of equation E1 was changed to day of year to represent diurnal total transpiration on an annual basis. For this calculation, transpiration was evaluated on the appropriate day of year when the field measurements took place. Other factors for the land-surface transpiration estimate in equation E3, species composition, and leaf area, remained the same.

Land-surface transpiration estimates for the two sites made using the June measurements combined with the simulated leaf areas from 1984 and 1985 are presented in table E4 along with estimates of transpiration that were simulated entirely from the 1984-85 data.

Table E3. Modeled factors for 1984-85 data to describe seasonal transpiration, in liters per square meter of leaf area per day, for each species

[Data derived from a total of 10 sites with widely differing soils and depths to water table. *n*, number of samples used for each curve]

Species	*n*	β_0	β_1	β_2	R^2
Atriplex torreyi	10	-2.29	0.0462	-0.000125	0.61
Chrysothamnus nauseosus	9	-4.14	.0898	-.000250	.55
Sarcobatus vermiculatus	11	-4.78	.0823	-.000205	.51
Distichlis spicata					
Site C	2	-2.47	.0496	-.000132	.72
Site L	3	-5.33	.106	-.000291	.63
Sporobolus airoides					
Site C	2	-2.84	.0516	-.000137	.74
Site L	5	-5.50	.101	-.000279	.81

DISCUSSION

The results (table E4) show close agreement between the completely simulated estimate of land-surface transpiration and the corresponding estimate based on measured transpiration rates and simulated leaf area. Though error bars are not provided because of the complexity of the calculation, the two data sets fit within the expected span of one standard error above and below the estimates. The estimates of land surface transpiration for June 3 at site C that used measured transpiration lie near the expected upper error bound.

Table E4. Calculated land-surface transpiration for each species based on model results from 1984 and 1985, and on measurements during June 1986

[The two columns of D were derived by multiplying one of the columns of A with columns B and C. The transpiration and *LAIP* of the unmeasured species at site L were estimated by taking the average of the two known species and added to the calculations because these species comprise 54 percent of the plant cover at the site. The land-surface estimates, in millimeters, at each site are presented as the totals beneath the set for each date]

Species	A		B	C	D	
	Transpiration (mm/d)		*LAIP*	Fractional ground cover[2]	Transpiration (mm/d)	
	Measured	Modeled[1]			Measured	Modeled
Site C - June 3, 1986						
Atriplex torreyi	3.64	1.86	1.46	0.032	0.17	0.09
Chrysothamnus nauseosus	4.68	3.76	1.74	.108	.88	.71
Sarcobatus vermiculatus	4.97	3.03	1.93	.039	.37	.23
Distichlis spicata	2.70	2.03	1.07	.113	.33	.25
Sporobolus airoides	3.06	1.86	.99	.035	.11	.06
Total					1.86	1.34
Site C - June 4, 1986						
Atriplex torreyi	1.90	1.87	1.47	0.032	0.09	0.09
Chrysothamnus nauseosus	3.69	3.77	1.75	.108	.70	.71
Sarcobatus vermiculatus	3.50	3.05	1.96	.039	.27	.23
Distichlis spicata	2.46	2.05	1.08	.113	.30	.25
Sporobolus airoides	3.33	1.87	1.00	.035	.12	.07
Total					1.48	1.35
Site L - June 5, 1986						
Distichlis spicata	4.38	4.21	2.70	0.212	2.51	2.41
Sporobolus airoides	3.68	3.55	2.00	.118	.87	.84
All other species	[3]4.03	[3]3.88	[4]2.35	.403	3.82	3.67
Total					7.20	6.92

[1]Modeled from 1984 and 1985.
[2]Measurements from 1984.
[3]Transpiration estimated as average of known species.
[4]*LAIP* estimated as the average of known species.

The estimates of land-surface transpiration in table E4 are close to those reported for micrometeorological techniques but, overall, tend to be slightly low (Reginato and Jackson, Chapter H, table H1, this report). This may be due to the failure to include an estimate of land-surface evaporation. This certainly was a factor because the late-winter period prior to the fieldwork was relatively wet (National Climatic Data Center, 1986).

Although the estimates of seasonal transpiration made on the basis of hand-held porometer data are relatively accurate, large errors can arise in estimating the rate for any single day. This is because the quadratic model for transpiration is statistically based and does not account for fluctuations in weather. Because weather affects transpiration directly, variability of cloud cover, relative humidity, or temperature may induce divergence from the modeled "average" transpiration.

Even though the data and analysis in this work largely ignore plant physiology, graphs of the data show that leaf area apparently follows curves of set shape and magnitude. Transpiration is essentially a passive loss of water that occurs when plants open stomata for photosynthetic gas exchange. The leaf conductance that results is proportional to photosynthesis (Wong and others, 1979) and transpiration takes place simply as evaporation driven by the vapor pressure deficit between saturated conditions in the leaf and the atmosphere outside. Water-use efficiency, a ratio between photosynthesis and transpiration, is a useful concept for comparing leaf area and water use by plants.

The parabolic shape of seasonal unit-leaf area transpiration curves of these species follows the rise and fall of the atmosphere's evaporative power induced by vapor density deficit. Thus, on a leaf area basis, water tends to remain relatively nonlimiting for transpiration. Two factors may be responsible for this: (1) stabilizing of soil water due to subirrigation from the water table and (2) feedback mechanisms to optimize leaf area to the available soil water and thus maintain a set water-use efficiency. The latter is suggested by the acceptable accuracy of seasonal unit leaf-area transpiration models combined from specimens of each shrub species at sites with disparate soils (table E3). Similar support for this proposed optimization is in data obtained for these species during water stress showing that transpiration rates tended to be maintained while leaf area decreased markedly (Groeneveld and others, 1986b).

Micrometeorological techniques require far less effort than the statistical-porometric technique reported here. However, data from such studies have almost never been reported with sufficient vegetation information to permit accurate extrapolation to other areas.

The porometric-statistical technique presented here should be considered as a viable alternative to micrometeorologic techniques. Although development of a data base suitable for application to land-surface estimates is time consuming, this technique is valid, if the intended application of the data is for estimating transpiration from large areas of mixed phreatophyte cover. In addition, once curves of expected transpiration are developed for a species, these curves may be adapted to other areas where these plants grow by using the same leaf conductance relations but correcting for vapor density deficit. However, it should be noted that this technique is generally applicable only for areas where the growing season weather tends to be hot, dry, and sunny.

Although this study did not provide estimates of evaporation, consumptive use by phreatophytes generally is reported in terms of evapotranspiration rather than in transpiration alone. Evaporation from the soil surface or water surface can be simulated relatively accurately with sufficient climatological data to yield evapotranspirational flux from the system. Judging from a comparison of porometer-based measurements with micrometeorological measurements in table H1, soil-surface evaporation from Owens Valley floor range sites was a minor component of evapotranspiration. Therefore, errors in land-surface consumptive use induced by estimating evaporation will tend to be relatively low.

SUMMARY

The results confirm that transpiration measurements made using a hand-held porometer can be used to estimate land-surface transpiration for a daily or seasonal period with acceptable accuracy for the plant-soil-water system of the Owens Valley floor. Because these estimates are made on a unit-leaf-area basis for each species, this technique can be applied to any site with known species composition and cover. The technique is particularly useful for the Owens Valley floor because more than 90 percent of the plant cover consists of the five species measured for this study.

REFERENCES

Beardsel, M.F., Jarvis, P.G., and Davidson, B., 1972, A null balance diffusion porometer suitable for use with leaves of many shapes: Journal of Applied Ecology, v. 9, p. 677-690.

Brown, R.G., and Blaser, R.E., 1968, Leaf area index and pasture growth: Herbage Abstracts, v. 1, p. 1-9.

Davies, W. J., Wilson, J.A., Sharp, R.E., and Osonubi, O., 1981, Control of stomatal behavior in water-stressed plants, *in* Jarvis, P.G., and Mansfield, T.A. (eds.), Stomatal Physiology, Society of Experimental Biology Seminar Series 8: New York, Cambridge University Press, p. 163-186.

Evans, R.A., and Love, R.M., 1957, The step-point method of sampling--A practical tool in range research: Journal of Range Management, v. 10, p. 208-212.

Groeneveld, D.P., Warren, D.C., Hubbard, P.J., and Yamashita, I.S., 1986a, Transpiration processes of shallow groundwater shrubs and grasses in the Owens Valley, California, Phase 1: Steady-state conditions, study jointly funded by Los Angeles Department of Water and Power, Inyo County, and the California State Water Resources Control Board 205J Grant Program, Contract no. 3-081-225-0, unpublished report.

Groeneveld, D.P., Warren, D.C., Hubbard, P.J., Yamashita, I.Y., and Manning, S.J., 1986b, Transpiration processes of shallow groundwater shrubs and grasses in the Owens Valley, California, Phase 2: Soil water changes and plant responses induced by altered depth to the water table, study jointly funded by Los Angeles Department of Water and Power, Inyo County, and the California State Water Resources Control Board 205J Grant Program, Contract no. 3-081-225-0, unpublished report.

Los Angeles Department of Water and Power, 1987, Unpublished data from a vegetation inventory of the Owens Valley in the files of Inyo County Water Department.

Losch, R., and Tenheunen, J.D., 1981, Stomatal responses to humidity--phenomenon and mechanism, *in* Jarvis, P.G., and Mansfield, T.A. (eds.), Stomatal Physiology, Society of Experimental Biology Seminar Series 8: New York, Cambridge University Press, p. 137-162.

Munz, D.A., and Keck, D.D., 1959, A California flora: Berkeley, University of California Press, 1681 p., Supplement, 224 p.

National Climatic Data Center, 1986, Local climatological data, annual summary with comparative data, Bishop, California: 8 p.

Ritchie, G.A., and Hinckley, T.M., 1975, The pressure chamber as an instrument for ecological research: Advances in Ecological Research, v. 9, p. 165-254.

Scholander, P.F., Hammel, H.T., Hemmingsen, E.A., and Bradstreet, E.D., 1964, Hydrostatic pressure and osmotic potential in leaves of mangroves and some other plants: Proceedings of the National Academy Science, v. 52, p. 119-125.86

Syvertsen, J.P., Cunningham, G.L., and Feather, T.V., 1975, Anomalous diurnal patterns of stem xylem water potentials in *Larrea tridentata*: Ecology, v. 56, p. 1423-1428.

U.S. Naval Observatory [n.d.], Sunrise and sunset at Bishop, California, Pacific Standard Time: Publication No. 1030, 1 p.

Weibel, E.R., 1980, Stereological methods, Volume 1. Practical methods for biological morphometry: San Diego, California, Academic Press, 415 p.

Wong, S.C., Cowan, I.R., and Farquhar, G.D., 1979, Stomatal conductance correlates with photosynthetic capacity: Nature, v. 282, p. 424-426.

CHAPTER F.--THEMATIC MAPPER VEGETATION COVER MODEL

By Susan L. Ustin (University of California, Davis)

INTRODUCTION

Attempts to model regional estimates of evapotranspiration are complex because of the inherent difficulty of extrapolating point data over large nonhomogeneous spatial areas for long periods of time. Because of a synoptic view, remotely sensed data measured from aircraft or satellite offer an opportunity to obtain spatially distributed information about biophysical processes for near-instantaneous time intervals. For estimates of evapotranspiration, some energy-balance numerical parameters require ground-based microclimatological measurements. Other components, however, such as solar radiation fluxes and apparent surface temperatures, can be directly obtained by using remote-sensing instruments.

The Bowen-ratio and eddy-correlation methods generally used for the determination of evapotranspiration do not require information on the type or characteristics of vegetation for calculations. However, greater accuracy in modeling on a regional scale and further insight into patterns of plant water use would be possible if characteristics of vegetation were better understood. During the dry Mediterranean summer, a substantial amount of the evaporation in semiarid environments, such as Owens Valley, is transpiration from the perennial vegetation canopy. A better understanding of the spatial distribution of vegetation and patterns of plant water use as functions of environmental conditions would improve interpretation of regional evapotranspiration models. Spatial distribution of vegetation includes factors such as percentage of canopy cover, leaf area, biomass, distribution of species, and abundance. Patterns of plant water use include transpiration and stomatal conductance. A study of patterns of plant water use and the distribution of vegetation as affected by factors such as light, temperature, and vapor-pressure deficit would provide a basis for assessing accuracy of regional evapotranspiration estimates.

Recent studies in Owens Valley by the University of California, Davis, consisted of an investigation of visible and infrared spectral characteristics of soils and perennial native vegetation from scrub communities. This chapter includes a brief review of the data base available and a summary of methods used in these studies.

The contributions of other investigators are acknowledged. The Thematic-Mapper mixing analyses were developed in cooperation with Drs. Milton Smith and John Adams, University of Washington; access to the spectral library at the Space Sciences Laboratory, University of California, Berkeley, was provided by Dr. Barrett Rock, Jet Propulsion Laboratory, Pasadena; the turbulent-flux energy-budget model was developed by Dr. Kyaw Tha Paw U, University of California, Davis; and field vegetation sampling was conducted with the help of Dr. Roy Woodward, University of California, Davis.

METHODS AND RESULTS

FIELD GAS EXCHANGE

The portable null-balance open gas-exchange system permits simultaneous measurement of photosynthesis and transpiration on attached leaves. The system (Armstrong Enterprises) is modified from the design of Field and others (1982). The system permits control and measurement of temperature, humidity, and carbon dioxide concentration and also allows measurement of either ambient conditions or manipulation of environmental variables. As an example, typical response curves are shown in figure F1. Carbon dioxide concentrations are measured by using an ADC portable carbon dioxide analyzer, water vapor is measured with a Vaisala Humicap sensor, and carbon dioxide mixing and flow rates are determined by using Tylan flow controllers. Temperature is regulated with a Peltier cooling block and heater.

Field-measured gas-exchange rates made during the (evapotranspiration) *ET* experiment, June 1-4, 1986, were not valid. The new equipment was assembled just prior to the *ET* experiment and had not been fully tested. As a result, various equipment malfunctions made interpretation impossible. The primary source of difficulty was temperature related and will be corrected for future field experiments. This type of measurement permits a detailed analysis of physiological conditions for a relatively small number of plant samples. These measurements could be supplemented with porometer measurements for leaf conductance or transpiration rates, or data obtained by using commercially available drawdown-type photosynthesis chambers, to obtain a larger statistical sample.

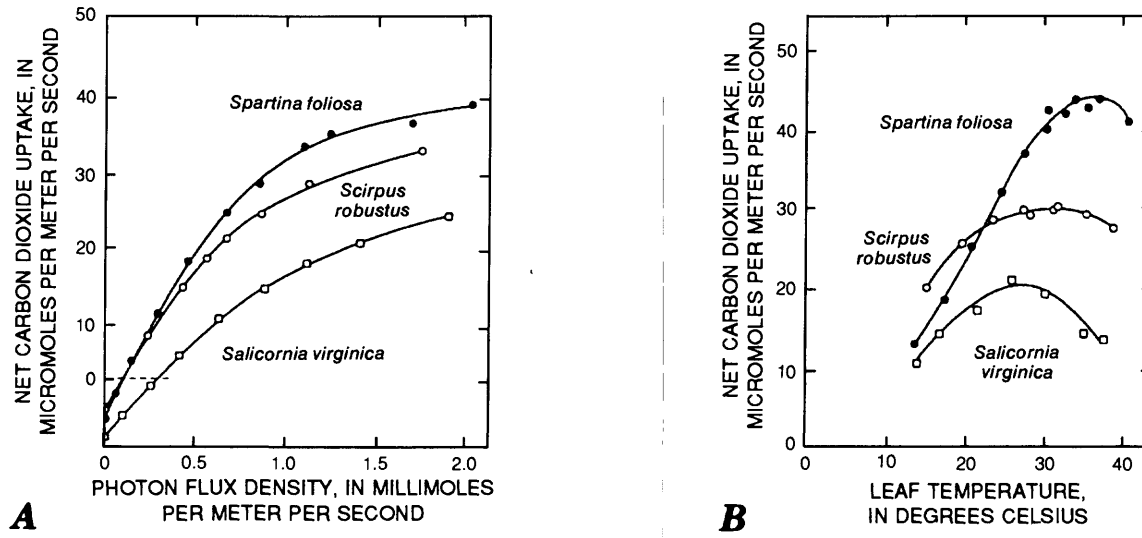

Figure F1. Typical photosynthetic response curves for light, temperature, and carbon dioxide concentration for *Spartina foliosa, Scirpus robustus,* and *Salicornia virginica.* Data from Pearcy and Ustin (1984). *A,* Net carbon dioxide uptake as a function of photosynthetically active radiation. *B,* Photosynthetic carbon dioxide uptake as a function of leaf temperature. *C,* Effect of soil salinity, in milliequivalent cations per cubic centimeter, on net carbon dioxide uptake. *D,* Effect of salinity, in milliequivalents per liter, on leaf and mesophyll conductance. *E,* Photosynthetic carbon dioxide uptake for plants grown at various salt concentrations as a function of intercelluar carbon dioxide pressure. Atmospheric concentration of carbon dioxide in 1989 is about 25 Pa. Arrows indicate the intercellular $p(CO_2)$ and photosynthetic rate at an atmospheric $p(CO_2)$ of 32.5 ± 1.0 Pa.

COMPUTER-BASED METHODS OF THE MODEL

A new approach for determining and separating the spectral components of a heterogeneous surface in satellite-pixel data has been developed (Adams and Adams, 1984; Smith and Adams, 1985; Adams and others, 1985, 1986; Ustin and others, 1986). A basic assumption of this method is that pixel-spectral variation results from linear mixtures of the spectra of surface materials and shade. The model is represented by the equation:

$$DN_b = f_n EM_{nb'}, \tag{F1}$$

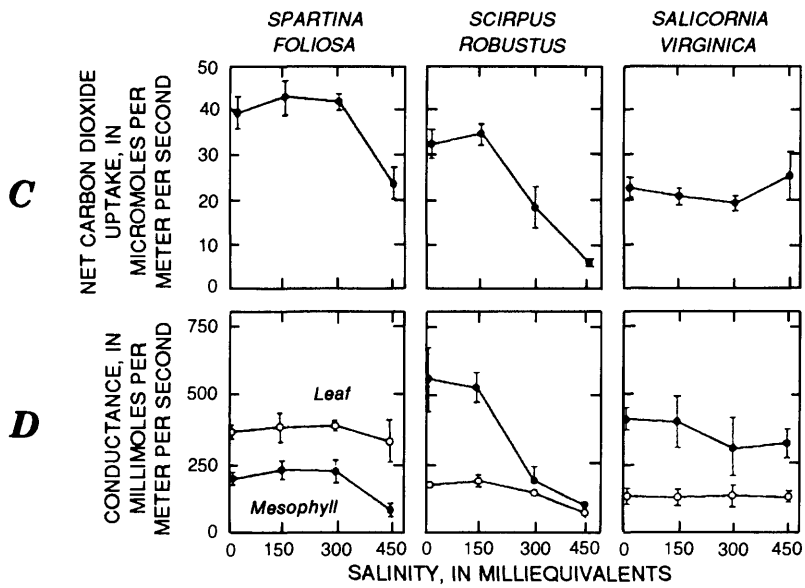

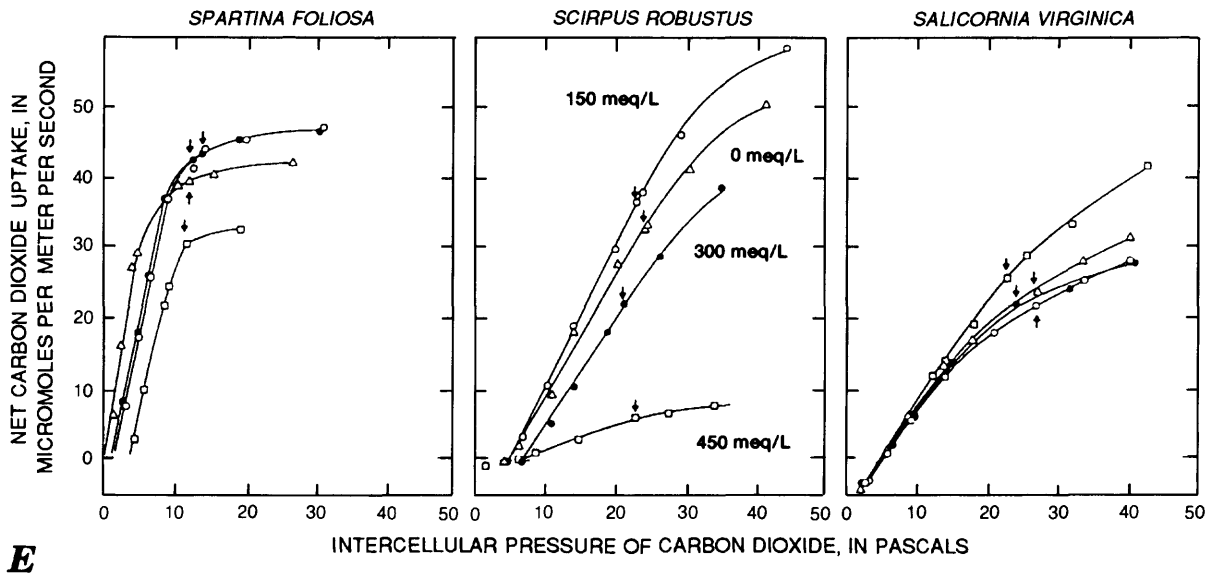

Figure F1.--Continued.

where

DN_b is the digital number (*DN*) brightness of an image pixel for each band *b*, in *DN* units;
f_n is the fraction of endmember *n*; and
$EM_{nb'}$ is the nth image endmember for each band *b*, in *DN* units (Adams and others, 1986; Smith and others, 1990a).

Analysis was done for a part of a Thematic Mapper (TM) scene (1,708 by 2,673 pixels, six minimum picture resolution elements) collated on May 16, 1985, in Owens Valley. Unmixing of the pixel spectra was done by using the six visible and reflected infrared TM bands. Image endmember spectra represent actual surface types (soils, plant species, and stage), which are identified in the radiometrically calibrated image data by the inversion of an Eigen matrix derived from an analysis of principal components (Smith and others, 1985). Image endmember spectra are then identified with actual surface types by comparison of the generated image endmember pseudospectra with plant and soil spectra contained in an interactive computer library. Library spectra (Beckman DK-2A Spectrophotometer) include rock, soil, and vegetation samples obtained from many locations, including Owens Valley. Library hemispherical reflectance spectra have been adjusted to fit bidirectional reflectance using gain and offset values for each band (Adams and others, 1986; Smith and others, 1990a). Ideally, both unique and acceptable solutions match image endmembers with library spectra.

Image endmembers are then fit to the TM data in a pixel-by-pixel analysis and the proportion of each endmember determined for each pixel (endmember proportions sum to 1). Potential image solutions for each endmember are examined to determine if spatial patterns were satisfactory, based on other information about the image (topography, soils, and vegetation) and by examination of the root mean square error (approximately zero) for spatial pattern. When this iterative process is completed, the resulting models best fit the spectral six-dimensional space and conform to known surface conditions (fig. F2). Models developed for the valley floor are live (green) vegetation, dry vegetation (nongreen canopy), soil, and shade-shadow. In order to display the entire area in one image, the scene has been subsampled and only every fifth pixel is shown. Therefore, full resolution is actually five times greater. Parts of the image can be displayed at full resolution and enlarged for more detailed examination. Working with the digital numbers, vegetation models can be color mapped by percentage cover, and interactions between models can be examined by assigning each model a color and displaying them together as a false-color image.

FIELD SAMPLING

Efforts to determine the accuracy of the image endmember for vegetation cover have involved quantitative measurements (line-intercept transects and measurements of pixel-sized plots), and qualitative visual assessments (Ustin and others, 1986; Smith and others, 1990a). Additional vegetation data for the fans near Independence were provided by Inyo County Water District and the U.S. Bureau of Land Management. The Los Angeles Department of Water and Power has drafted a vegetation map for lands included in the U.S. Geological Survey, Independence, California, 7.5-minute topographic quadrangle.

MODELING

Seasonal patterns of *ET* variation could be determined by using TM or Thematic-Mapper Simulator (TMS) data with appropriate meteorological data, or by site-specific testing of energy-balance data collected in June 1986, using the turbulence model of Paw U and others (1985).

A

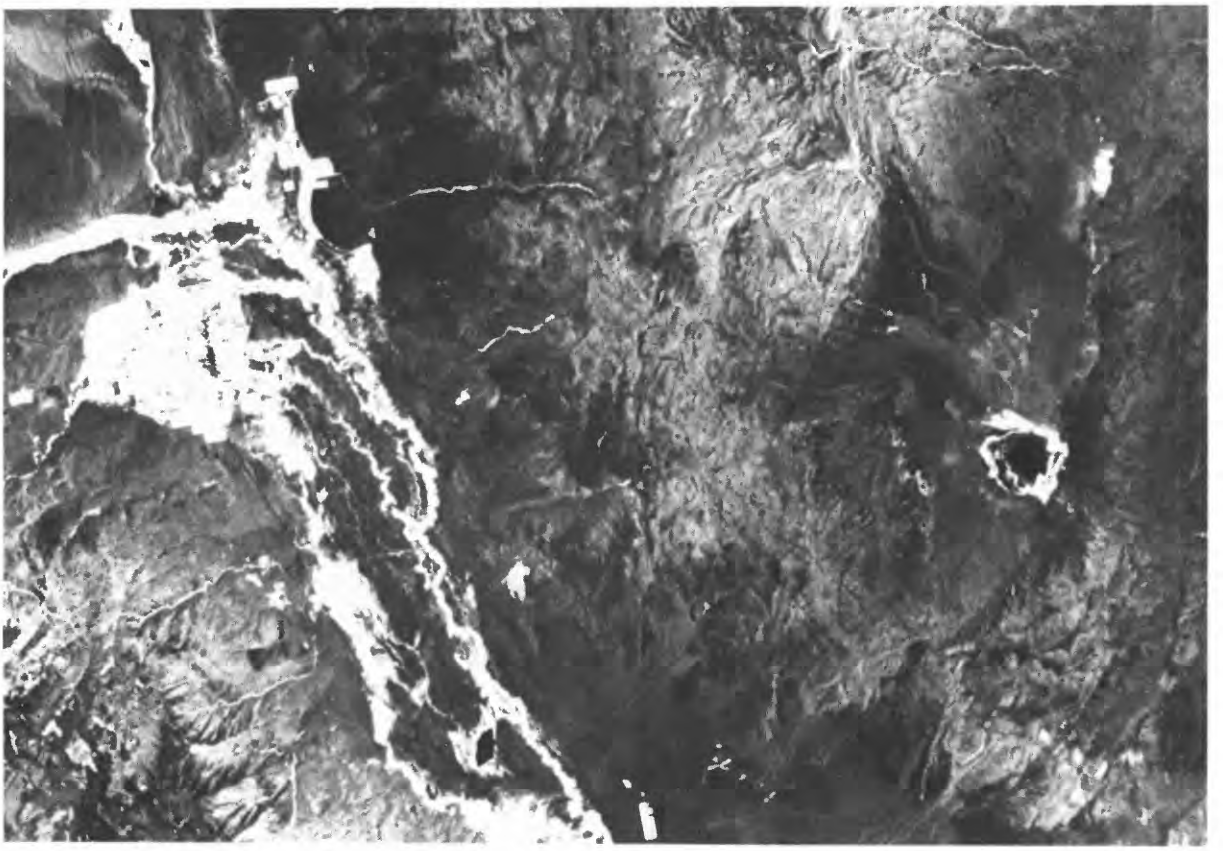

B

Figure F2. Thematic mapper endmember models. *A*, Live vegetation. *B*, Dry vegetation. *C*, Bright soil. *D*, Shade. Each image shows the endmember as gray shades varying from white to black. Geographic features identified in *C* are Fish Slough (**A**), Bishop (**B**), Deep Springs playa (**C**), Klondike Lake (**D**), and Owens River (**E**).

C

D

Figure F2.--Thematic mapper endmember models. *A*, Live vegetation. *B*, Dry vegetation. *C*, Bright soil. *D*, Shade. Each image shows the endmember as gray shades varying from white to black. Geographic features identified in *C* are Fish Slough (**A**), Bishop (**B**), Deep Springs playa (**C**), Klondike Lake (**D**), and Owens River (**E**).--Continued.

SPECTRAL DATA

GROUND SPECTRAL DATA

Generally, monthly inspections were made between March 1984 and August 1985 to obtain field-collected spectra of several dominant shrub species and soils. Among those of interest for modeling valley floor vegetation were *Artemisia tridentata*, *Sarcobatus vermiculatus*, and *Atriplex parryii*. These spectra were made by using either the Jet Propulsion Laboratory's portable field reflectance spectrometer (PFRS) or a visible infrared intelligent spectrometer (VIRIS) (Ustin and others, 1985; 1986b). Both spectrometers obtain high spectral resolution contiguous spectra between 0.4 and 2.4 μm. All species show significant increases in reflectance in red and shortwave infrared wavelengths during the growing season, common for aging leaves that have lower chlorophyll and water content on an area basis. Infrared wavelengths for *Artemisia tridentata* and *Purshia glandulosa* are shown in figure F3.

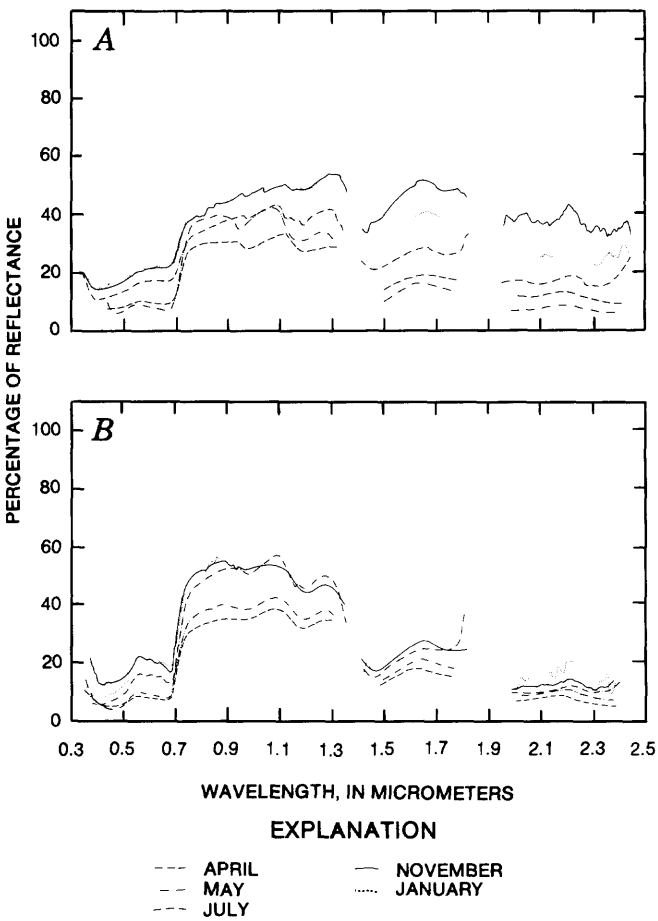

Figure F3. Seasonal reflectance spectra for two shrub species in Owens Valley. Spectra are characteristic for healthy leaves within the canopy for each month. Data from Ustin and others (1986). *A, Artemisia tridentata. B, Purshia glandulosa.*

AIRBORNE SPECTRAL DATA

Thematic-Mapper Simulator (TMS) and Airborne Imaging Spectrometer (AIS) data have been acquired for several flightlines over the central Sierra Nevada alluvial fans in Owens Valley and for areas around the southern shore of Owens Lake. The TMS has bands matching the seven TM bands plus an additional shortwave infrared band centered near 1.2 μm. In contrast, the AIS has 128 contiguous spectral bands between 1.1 and 2.4 μm or 0.85 and 2.1 μm (exact wavelength segments depend on flight specifications). Flight altitude was about 5.25 km above the terrain; pixel size is about 14 m for TMS and 10 m for AIS. Dates of data acquisition were July 10, 1984; October 30, 1984; April 2, 1985; May 22-23, 1985; and May 15, 1986 (includes a flightline across the *ET* study area on the valley floor, from near Lone Pine to Bishop).

SATELLITE THEMATIC-MAPPER DATA

Thematic-Mapper data for Owens Valley are available for December 12, 1982 (row 35, pass 41); July 17, 1984; October 10, 1984; and May 16, 1985 (rows 34, 35; pass 41).

RESULTS AND DISCUSSION OF THEMATIC-MAPPER MODELS OF SPECTRAL COVER TYPES

Percentages of live (green canopy) cover, dry (nongreen canopy) cover, bright soil cover and shade-shadow cover, were developed by linear mixture analysis of a May TM image for the valley floor region

included in the *ET* experiment. Live cover is best modeled by a green-leaf spectrum. The bright soil type is typical of the valley floor alkali sediments. Shade-shadow endmembers include all topographic effects, but in the absence of topography, shadows are primarily caused by vegetation canopies (Ustin and others, 1986). Because of heavy spring rain and moderate temperature in 1986, the condition of vegetation during the *ET* experiment was probably comparable with the 1985 May TM date.

Although estimates of percentage cover have not been rigorously tested on this image, we expect that model predictions are accurate to within 10 percent of the actual cover, on the basis of a more thorough testing of other vegetation models for the shrub-dominated fans near Independence (Ustin and others, 1986, 1987; Smith and others, 1990a). Greater accuracy is difficult to determine because of substantial heterogeneity on the ground. Unpublished results of actual ground measurements of all shrubs on entire pixels show that moving the plot position by as little as 5 m could produce a substantial plant cover error for the plot. On the alluvial fans near Independence, this resulted in cover estimates ranging from 14 to 25 percent cover. Despite these difficulties, with a large sample size, there was a linear relation between digital numerical values (for pixels in the image) and plant cover.

The results (fig. F2) show significant spatial variation in live (green) vegetation, dry vegetation, soil, and shade-shadow, which have a substantial impact on estimates of regional evapotranspiration. For orientation of the images, several reference points are indicated in figure F2*C*. Owens Valley is located between the Sierra Nevada to the west and the White-Inyo Mountains to the east. In this view, the northern end of Owens Valley trends from the upper left to the lower center of the images. Fish Slough (**A**) is a freshwater marsh at the top left of the image trending south towards the city of Bishop (**B**), near the center-left margin. Deep Springs Valley is located just east of the White-Inyo Mountains; it is oriented from the center right and trends toward the upper right of the images. The Deep Springs playa (**C**) is the nearly circular feature seen in the center right of the images. Within Owens Valley, the most obvious features in the images are the Klondike Lake (**D**) and the city of Bishop. The Owens River reaches Fort Independence at the bottom center of the image. Standing water found in the center of the Deep Springs playa and the Owens River (**E**), lower center, stands out as black features in figure F2*A*. Few pixels are composed of only one surface material, thus most of the images are gray tones and indicate the complex surface structure that must be considered in modeling climate processes.

Figure F2*A* shows the fractional abundance of green vegetation for the northern part of Owens Valley. The tonal variation in this image indicates the relative concentration of green vegetation and its spatial distribution. Areas having high plant cover are white in the image and areas having low or no plant cover are black; gray tones represent intermediate levels of live plant cover. The image brightness levels vary linearly with canopy cover from 0 to 100 percent on the valley floor (Ustin and others, 1987; Smith and others, 1990a). The image endmembers were modeled for the valley floor vegetation, which is "greener" than the typical vegetation on the fans (Smith and others, 1990a,b); therefore the image may underrepresent actual vegetation concentrations on the fans or in the mountains relative to the valley floor. Areas having high concentrations of green vegetation (nearly pure pixels) are distinctly zoned on the valley floor and associated with sites of permanent water. Irrigated agricultural land is distinctly visible due to the sharp rectangular boundaries. Nonirrigated areas on the valley floor, which do not have ground-water access, have significantly lower amounts of vegetation. Most pixels are shades of gray and indicate mixtures of all surface components, with green vegetation usually present in low but varying amounts in the valley. The sharp gradients and diverse conditions of vegetation on the valley floor that are observed in the images demonstrate the difficulty in extrapolating valleywide estimates of *ET* from a few point measurements.

The relative distribution of the dry-vegetation endmember is shown in figure F2*B*. The spectral signature of this plant material is that of dry litter and similar to a cellulose spectrum. Although much of the image, particularly the regions near stream channels, shows similarities (although opposite in tone) to the green-vegetation endmember, close inspection reveals contrasting differences. This is not unexpected because regions having more live green cover also are likely to have less dead canopy litter in the total biomass, even when there is more canopy litter on an absolute basis because of differences in total biomass. Thus, the dry-vegetation image is not

simply the reciprocal of the green-vegetation image. Because these images have not been normalized with respect to each other, differences in brightness intensity between images should be used for comparisons of general spatial patterns only and not for estimates of allocation of biomass.

Figure F2*C* shows the distribution of the soil endmember. The soil type selected for this report is a sandy-clay type and is spectrally brighter than the alluvium typical of the Sierran fans. Because of the relatively low spectral contrast between this soil type and the dry-vegetation endmember, there may be some misclassification of the proportions, although the spatial patterns should be clear. Darker soil types may be misclassified as the shade endmember.

The shade endmember is indicated in figure F2*D*. In this image, the shade (and shadow) concentrations are shown as in the other images, with the areas having the highest concentrations of shade as white and areas of least shade as black (opposite to ones usual perception). To the eye, the shade endmember resembles a black and white photograph because of the topographic information. In addition to the surficial texture of the alluvial fans, considerable tonal variation is apparent on the valley floor. These shadow-casting features are considered to correspond to changes in canopy height and density of the vegetation. When better understood, this information may provide the key to estimating canopy biomass (or canopy volume) when related to the percentage of live cover and the litter estimates. Frequently, the cover and shade patterns are positively correlated, although grasslands tend to show low shade, but high cover concentrations.

The canopy vegetation-cover patterns present in these images may relate to subsurface hydrologic patterns, disturbance, soil salinity, or to other unknown causes. However, the images demonstrate that the source locations for evapotranspirative flux are not uniformly distributed. These images allow some inference regarding the representativeness of the sites chosen for measurement of microclimate variables. Because of the spatial heterogeneity in arid regions, such as Owens Valley, and the dynamic response to environmental conditions, it will be difficult to develop detailed hydrological models. The development of satellite-based *ET* estimates, either independently or integrated with ground measurements, provides a means to improve the reliability of *ET* estimation.

The interaction between the canopy components on these images have been evaluated (Ustin and others, 1987; Smith and others 1990a,b) and the distribution of vegetation as estimated by the live-canopy-cover image (fig. F2*A*) remains stable between winter and summer TM scenes (Smith and others, 1990a). Furthermore, the May live-cover endmember image can be used as an approximation of spatial distribution of *ET* (Smith and others, 1990b).

Seasonal changes in reflectance of shrub canopies for two species in Owens Valley, *Artemisia tridentata* (Big sagebrush) and *Purshia glandulosa* (blackbrush) are shown in figure F3. Reflectance is lowest in the visible spectrum (0.5-0.7 μm) during the spring and higher when less green foliage is present in the canopy during other seasons. Differences such as these permit discrimination of some vegetation characteristics within the spectral resolution of the TM scanner.

FUTURE RESEARCH

This type of approach has potential for expanding the current estimates of *ET* by using empirically derived calibrations from ground stations. Spectral mixing analyses are less sensitive to scene-dependent classification than are other commonly used analytical techniques. To develop this potential application, the mixing method needs to be tested in other seasons and in other localities. The recent development of new sensors capable of acquiring data in new wavelength regions (such as thermal and microwave) at high spatial and spectral resolutions has greatly increased the potential usefulness of satellite-based *ET* modeling because of the possibility of determining a larger set of endmembers within a scene.

REFERENCES

Adams, J.B., and Adams, J.D., 1984, Geologic mapping using Landsat MMS and TM images: Removing vegetation by modeling spectral mixtures, in International Symposium on Remote Sensing Environment 3rd Thematic Conference: Remote Sensing for Exploration Geology, Ann Arbor, Michigan, Environmental Resources Institute, Proceedings, p. 615-622.

Adams, J.B., Smith, M.O., and Johnson, P.E., 1985, Viking Lander I: A new map of rock and soil types, Abstract Lunar Planetary Scientific Conference 16th, Proceedings.

-----1986, Spectral mixture modeling: A new analysis of rock and soil types at the Viking Lander I site: Journal of Geophysical Research, v. 91, p. 8098-8119.

Field, C., Berry, J.A., Mooney, H.A., 1982, A portable system for measuring carbon dioxide and water vapor exchange of leaves: Plant, Cell and Environment, v. 5, p. 179-186.

Paw U, K.T., Shaw, R.H., and Meyers, T.P., 1985, Evapotranspiration as modeled by a higher order closure scheme, *in* Advances in Evapotranspiration: National Conference on Advances in Evapotranspiration, American Society of Agricultural Engineers Publication 14-85, St. Joseph, Michigan, p. 43-50.

Pearcy, R.W. and Ustin, S.L., 1984, Effects of salinity on growth and photosynthesis of three California tidal marsh species: Oecologia, v. 62, p. 68-73.

Smith, M.O., and Adams, J.B., 1985, Interpretation of AIS Images of Cuprite, Nevada using constraints of spectral mixtures: Airborne Imaging Spectrometer Data Analysis Workshop, April 8-10, 1985, Jet Propulsion Laboratory Publishing 85-41, Proceedings, p. 62-67.

Smith, M.O., Johnson, P.E., and Adams, J.B., 1985, Quantitative determination of mineral types and abundances from reflectance spectra using principal components analysis: Lunar Planetary Science Conference 15th, Proceedings, p. C707-C804.

Smith, M.O., Ustin, S.L., Adams, J.B., and Gillespie, A.R., 1990a, Vegetation in deserts. 1. A regional measure of abundances from multispectal images: Remote Sensing of Environment, v. 29, p. 1-26.

-----1990b, Vegetation in deserts. 2. Environmental influences on regional abundance: Remote Sensing of Environment, v. 29, p. 27-52.

Ustin, S.L., Adams, J.B., Evlidge, C.D., Rejmanek, M., Rock, B.N., Smith, M.O. Thomas, R.W., and Woodward, R.A., 1986, Thematic Mapper studies of semiarid shrub communities: BioScience, v. 34, p. 446-452.

Ustin, S.L., Rock, B.N., and Woodward, R.A., 1985, Analysis of substrate and plant spectral features of semi-arid shrub communities in the Owens Valley, California, International Symposium Remote Sensing Environment 4th Thematic Conference: Remote Sensing Exploration Geological Environment Research Institute Michigan, Proceedings, p. 347-359.

-----1986, Use of remote sensing techniques in the analysis of semi-arid shrub communities, *in* Natural History of the White-Inyo Range, Eastern California and Western Nevada and High Altitude Physiology: Bishop, University of California White Mountain Research Station Symposium, v. 1, August 23-25, 1985, p. 84-98

Ustin, S.L., Smith, M.O., and Adams, J.B., 1987, Vegetation patterns derived from Landsat Thematic Mapper images in Owens Valley, *in* Hall, C.A., Jr., and Doyle-Jones, V. (eds.), Plant Biology of Eastern California, Mary DeDecker Symposium: Bishop, University of California White Mountain Research Station, April 30-May 3, 1987, p. 293-302.

CHAPTER G.--EVALUATING EVAPOTRANSPIRATION FROM RANGELAND VEGETATION BY USE OF AIRBORNE RADIOMETRY AND GROUND-BASED METEOROLOGICAL DATA USING THE PENMAN EQUATION

By M. Susan Moran, Ray D. Jackson, *and* Robert J. Reginato

(U.S. Water Conservation Laboratory, Phoenix, Arizona)

INTRODUCTION

A technique has been developed that uses remotely sensed data in conjunction with ground-based meteorological data to estimate the spatial distribution of evapotranspiration (*ET*) (Jackson, 1985; Reginato and others, 1985). This technique has been shown to yield values of evapotranspiration measured as latent-heat flux (λE) in satisfactory agreement with ground-based latent-heat flux estimates by the Bowen-ratio method (λE_{br}) data for agricultural fields. It has not been tested under conditions of unevenly vegetated surfaces, such as rangeland, where exposed soil temperatures may greatly exceed vegetation temperatures.

Airborne radiometers can be used to collect data rapidly over large areas, encompassing a number of sites that may have very different *ET* rates. *ET* rates calculated from these data are virtually instantaneous values. Ground-based methods for measuring *ET*, such as the Bowen ratio (Gay and Fritschen, 1979; Spittlehouse and Black, 1980; Gay and Greenberg, 1985), record data continuously, but the values apply only to an area surrounding the instruments where evaporation is taking place at the same rate. This makes a comparison of the methods difficult because, during a particular measurement sequence, only one value from each method is coincident in both space and time.

This chapter presents the results of an experiment in which airborne and ground-based radiometers were used to obtain reflected radiation and surface temperatures over three sites (designated C, F, and L, fig. 1) in Owens Valley. These data, combined with ground-based measurements of incoming solar radiation, air temperature, vapor pressure, and horizontal windspeed, provided a means of estimating the spatial distribution of evapotranspiration over the three sites in the valley.

REMOTE METHOD

Calculation of evapotranspiration with remote inputs depends upon the evaluation of net radiation (Q), soil-heat flux (G), and sensible-heat flux (H), as related by the energy balance for a surface,

$$Q+G+H+\lambda E = 0, \tag{G1}$$

where

Q is the net radiation, in watts per square meter;
G is the soil-heat flux, in watts per square meter;
H is the sensible-heat flux, in watts per square meter; and
λE is the latent-heat flux, in watts per square meter.

NET RADIATION

Net radiation is the sum of incoming and outgoing radiant fluxes,

$$Q = R_S\downarrow - R_S\uparrow + R_L\downarrow - R_L\uparrow, \tag{G2}$$

where

R is the radiant flux, in watts per square meter;
S is the subscript signifying solar shortwave radiation (0.15 to 4 μm), in watts per square meter;
L is the subscript signifying solar longwave radiation (>4 μm), in watts per square meter;
$\downarrow$ indicates the flux direction is incoming; and
$\uparrow$ indicates the flux direction is outgoing.

Jackson and others (1985) suggested that the incoming shortwave radiation ($R_S\downarrow$) and longwave radiation ($R_L\downarrow$) could be measured with traditional ground-based instruments and the data extrapolated radially for some distance from the point of measurement, and that the outgoing shortwave radiation ($R_S\uparrow$) and longwave radiation ($R_L\uparrow$) could be obtained from multispectral data. They proposed that $R_S\downarrow$ be measured with a calibrated pyranometer sensitive to radiation for most of the solar spectrum. The area over which a point measurement of $R_S\downarrow$ could be extrapolated would be governed largely by the areal uniformity of the scattering and absorbing properties of the atmosphere.

Only part of the reflected solar shortwave term, $R_S\uparrow$, is measured with a multispectral radiometer. Because each radiometer measures a different fraction of the total reflected radiation, the total must be estimated from the partial. Jackson (1984) used a radiative transfer model to calculate the irradiance at the Earth's surface for a number of atmospheric scattering and absorption conditions. Measured spectral reflectance distributions for 14 different surface conditions (bare soil to full green canopy) were used along with the calculated irradiance data to determine the ratio of the radiation measured by a multispectral radiometer to the total reflected solar radiation (partial/total ratio).

The incoming longwave radiation, $R_L\downarrow$, can be estimated from ground-based measurements of air temperature and vapor pressure using the relation (Brutsaert, 1975):

$$R_L\downarrow = \varepsilon_a \sigma T^4, \tag{G3}$$

and

$$\varepsilon_a = 1.24(e/T)^{1/7}, \tag{G4}$$

where

ε_a is longwave emissivity of the atmosphere, dimensionless;
σ is the Stefan-Boltzmann constant, equal to 5.67×10^{-8} watts per square meter per kelvin (to the 4th power);
T is air temperature, in kelvin; and
e is vapor pressure, in millibars.

Inputs needed to calculate this term are from ground-based measurements.

The outgoing longwave radiation, $R_L\uparrow$, is obtained from the remotely measured surface temperature:

$$R_L\uparrow = \varepsilon_s \sigma T_s^4, \tag{G5}$$

where

ε_s is longwave emissivity of the surface, dimensionless; and
T_s is soil surface temperature, in kelvin.

The small contribution to $R_L\uparrow$ by reflected sky radiation is not considered. At this point, it is not necessary to evaluate ε_s. If the thermal radiometer is calibrated with reference to a blackbody whose emissivity is near unity, the surface emissivities would be implicit in the apparent surface temperatures and would cancel when the emitted longwave energy is calculated (Jackson and others, 1985).

SOIL-HEAT FLUX

Soil-heat flux (G) traditionally is measured with sensors buried just beneath the soil surface. This flux is dependent on whether the surface is wet or dry; bare or vegetated. Therefore, a ground-based measurement should not be extrapolated areally. A remote measurement of G is not possible, but several relations between G and Q have been proposed (Clothier and others, 1986; Jackson and others, 1987). Several studies have shown that G is attenuated by vegetation and can be as high as 0.5 Q for dry bare soil and as low as 0.1 Q for full vegetative cover.

Vegetative cover can be assessed remotely by using spectral data in the red and near-infrared (*IR*) wavebands. The normalized difference (*ND*) is a combination of these bands. This is, $ND = (IR - red)/(IR + red)$. This spectral-vegetation index is more sensitive to low-density vegetation than other indices such as the simple ratio, *IR/red*. The relation between *ND* and *G/Q* was developed on the basis of data collected at sites C and L on June 5, 1986. This relation is

$$G/Q = -0.1009\ ND + 0.1748, \tag{G6}$$

where *ND* is the normalized difference, dimensionless.

G was measured at each site with soil-heat flux sensors buried 1 cm below the surface. Each symbol in figure G1 represents the output from three sensors. *Q* was calculated using remote spectral measurements and ground-based meteorological measurements. *ND* was obtained from spectral-reflectance measurements collected with both ground-based and airborne radiometers. The data were collected over a 6-hour period.

Equation G6 was tested by using a second set of data collected June 3, 1986, at sites C and L (fig. G2). This correlation coefficient was 0.9, indicating that the relation provides an adequate estimate of *G/Q* from spectral data.

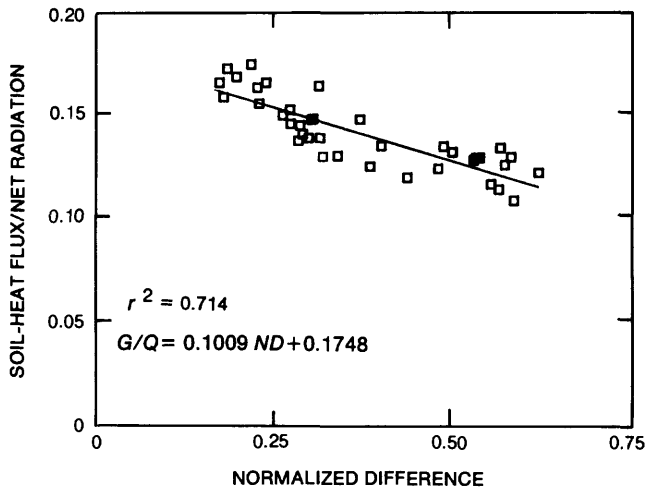

Figure G1. Relation between soil-heat flux, net radiation, and the normalized difference vegetation index. Vegetation index data are for site C and L over a 6-hour period, June 5, 1986. Soil-heat flux (*G*) was measured with heat-flux sensors; each symbol represents output from three sensors. Net radiation (*Q*) was calculated using the remote method.

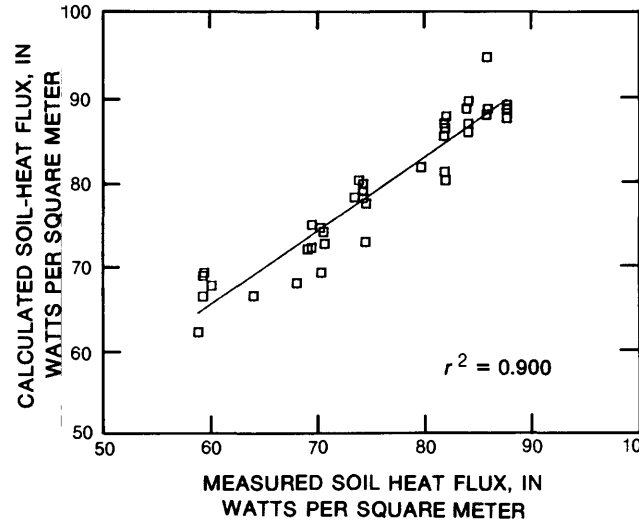

Figure G2. Comparison of calculated and measured soil-heat flux for sites C and L, June 3, 1986.

SENSIBLE-HEAT FLUX

The final term to be evaluated is the sensible-heat flux (H), which can be expressed as

$$H = \rho C_p (T_s - T)/r_a, \quad \text{(G7)}$$

where ρC_p is the volumetric heat capacity of air, in joules per cubic meter per degree Celsius; and
r_a is a stability corrected aerodynamic resistance, in seconds per meter.

Up to this point the equations apply to a uniformly vegetated surface (with the exception of the soil-heat flux), a condition not found in Owens Valley. The vegetation at site C is not uniformly distributed. The treatment of this partial canopy condition has received some theoretical attention by considering that the aerodynamic resistance in equation G7 is composed of momentum resistance and an additional resistance to transfer of heat and water vapor. However, use of the temperature difference (T_s-T) in equation G7 also assumes that the surface is at a uniform temperature (T_s) and that evapotranspiration is spatially uniform. With a surface consisting of a partial canopy, the vegetation may be at one temperature, the soil at another, with the composite temperature measured and entered into equation G7. This problem has not been successfully approached theoretically.

Two approaches are used in this chapter. Evapotranspiration will be calculated using (1) recent theoretical developments concerning the inclusion of resistance for heat transfer, and (2) an empirical adjustment to (T_s-T) in an attempt to approximate the temperature differences that drive evapotranspiration from vegetative surfaces under conditions of partial canopy.

THEORETICAL APPROACH

For unstable conditions, Kustas and Brutsaert (1986) have shown that r_a can be expressed by the relation

$$r_a = [B^{-1} + k^{-1} \ln(Z-d)/Z_o]/U_*, \quad \text{(G8)}$$

where B^{-1} is essentially an additional resistance to the transfer of heat above that for momentum (Garratt, 1978), in seconds per meter;
k is Von Karman's constant equal to 0.4, dimensionless;
Z is the height above the surface at which the horizontal windspeed and air temperatures are measured, in meters;
d is the displacement height, in meters;
Z_o is the roughness length for momentum, in meters; and
U_* is the friction velocity, solved by iteration, in meters per second.

For unstable conditions, $[(T_s-T)]>0$ (Choudhury and others, 1986).

$$U_* = (kU)/\{\ln[Z-d)/Z_o] - \varphi\}, \quad \text{(G9)}$$

where U is the horizontal windspeed, in meters per second; and
φ is a complex expression that includes U_* and the temperature difference, thus the necessity for an iterative solution. It is discussed by Choudhury and others (1986).

Values for B^{-1} are dependent on the roughness of the surface and the permeability of the roughness obstacles. For this experiment, B^{-1} was estimated using equations developed from empirical data (summarized by Brutsaert, 1982). For site L, B^{-1} was estimated to be 7.5, corresponding to results over grassland. For site F, B^{-1} was 10, corresponding to a "permeable rough" condition. Site F was particularly complex because it consisted of large roughness obstacles scattered sparingly across bare soil. In such conditions, B^{-1} is dependent upon temperature and cannot be approximated by a constant. From data collected at site C on June 3 and 5 the following relation was developed with a correlation coefficient (r^2) of 0.84:

$$B^{-1} = -1.9397\times10^{-7}(Z_o+)^2 + 4.5191\times10^{-3}(Z_o+) - 7.3914, \quad \text{(G10)}$$

where Z_o+ is equal to $(U_* Z_o)/\upsilon$, where υ is the kinematic viscosity of air, in square meters per second.

EMPIRICAL APPROACH

The empirical approach requires an expression for the aerodynamic resistance that does not require iteration. The following equation is from Mahrt and Ek (1984) for the unstable case:

$$r_a = \{\ln[(Z-d+Z_o)/Z_o]/k\}^2\{1-15Ri/[1+C(-Ri)^{1/2}]\}^{-1}/U, \quad \text{(G11)}$$

where

Ri is the Richardson number, equal to $g(T-T_s)(Z-d)/TU^2$, dimensionless;

g is acceleration due to gravity, in meters per second squared; and

C is equal to $75k^2[(Z-d+Z_o)/Z_o]^{1/2}/\{\ln[(Z-d+Z_o)/Z_o]\}^2$.

For uniformly vegetated areas, Z_o and d can be estimated from the vegetation height. For agricultural fields, values of $Z_o=0.05h$ and $d=0.63h$ (h is the plant height, in meters) have been used (Monteith, 1973). When the vegetation is nonuniform, these values are not appropriate. The apparent displacement height d, would be less for the nonuniform case than for uniform areas. The relation $d=0.63hC_b$ was used, where C_b is the fraction of vegetative cover. Thus, at complete cover and at zero cover, the relation reduces to the form for uniform cover.

The roughness length, Z_o, also must be adjusted for a nonuniform, partial cover. The relation $Z_o= 0.05h[1-C_b(C_b-1)]$ is used, which reduces to the uniform case at $C_b = 1$ and $C_b = 0$, but is a maximum at $C_b = 0.5$.

In equation G7, the sensible-heat flux (H) is directly proportional to the temperature difference ($T_s - T$). This relation does not hold for the partial canopy case. Consider an area in which a number of shrubs having a deep root system cover only part of the surface. The composite temperature as measured from an aircraft would be dominated by the hot bare soil, though the leaf surface at which the transpiration takes place may be at a much lower temperature. The temperature difference to be used in equation G7 may be much less than the measured composite temperature. This condition was approximated by raising ($T_s - T$) to a power less than one, but dependent on the amount of vegetative cover, reducing to 1 at full cover and at zero cover. The relation $\alpha = 1 - 3.2ND(1 - ND)$ is used, and replaces the temperature difference in equation G7 by $(T_s - T)^{\alpha}$. An exact treatment of this condition is beyond the scope of this report.

ESTIMATION OF DAILY TOTALS OF EVAPOTRANSPIRATION FROM INSTANTANEOUS VALUES

Jackson and others (1983) assumed that the daily course of *ET* measured as λE would generally follow the trend of solar radiation throughout the daylight period. They showed that for cloudless skies, the ratio of total daily solar radiation to an instantaneous value could be approximated by the relation

$$K\downarrow_d / K\downarrow_i = 2N/[\pi sin(\pi t/N)], \quad \text{(G12)}$$

where

$K\downarrow$ is solar radiation, in watts per square meter;
d is a subscript representing daily average;
i is a subscript representing instantaneous data;
N is the daylength, in hours; and
t is time starting at sunrise, in hours.

With the assumption that $\lambda E_d / \lambda E_i = K\downarrow_d / K\downarrow_i$, equation G12 allows a factor to be calculated to convert to daily totals from instantaneous values of λE from the time of day that the instantaneous measurement was made. An additional assumption was that environmental factors such as windspeed were relatively constant over the daily period.

PROCEDURE

Sites C, F, and L represented areas of varying vegetative cover and evapotranspiration rates. Site C was characterized by tall, scattered bushes covering about 30 percent of the area. In general, little grass or annual vegetation cover was present at this site. Site F was similar to site C although the bushes tended to be shorter and vegetation cover was more sparse (about 20 percent cover). Site L was a grassland of about 75 percent vegetative cover consisting of perennial and annual grasses with scattered, small bushes. The area surrounding the grass area was similar to site F, which had scattered bushes.

Ground-based radiometric data were collected in a 60- by 60-m study area chosen to represent the vegetative type at each site. Reflectance measurements were recorded along 12 transects in east-west and north-south directions within the study area. Meteorological data were collected throughout the day at a location immediately adjacent to the target area. Bowen-ratio and eddy-correlation instruments were located near the target area, within the same vegetative type. Ground-based radiometric and meteorological data were not collected at site F during the first 2 days of the experiment.

Airborne radiometer data were collected over the three sites three times during each day. The flights were at 1030 hours, 1230 hours, and 1500 hours at site L. Ground-based reflectance measurements and meteorological data were collected at the time of the aircraft flyover at each site.

The aircraft covered two 1.6-km-long flightpaths at each site. The two paths were perpendicular to each other, crossing at the study site. The remote-sensing equipment aboard the aircraft consisted of a four-band multispectral radiometer, a single-band thermal infrared thermometer, and a video camera. In flight, the instruments scanned normal to the surface with a nominal 15° field of view. At an altitude of about 150 m, a circle of approximately 40 m diameter was observed on the ground. On the approach to a flightpath over a site, a data logger was triggered to record the output from the five channels and

the time (to 0.0001 hour) at 2-second intervals. A character generator on the video system recorded the elapsed time on each frame. The video time and data-logger time were used to identify the video frame corresponding to a particular sample. The video provided ground location for each sample and information on the composition of the surface.

The four-band radiometer data were converted to radiance values by use of calibration factors provided by the manufacturer. The radiances of the four bands were summed and divided by the partial/total ratio (0.32), determined using a method described by Jackson (1984), to yield values of $R_S\uparrow$ (eq. G2). The surface temperatures measured with the infrared radiometer were used to calculate $R_L\uparrow$, and corrected for emissivity (ε = 0.985 for site L, 0.975 for site C, and 0.970 for site F) to obtain the temperature difference (T_s - T). Soil-heat flux was estimated from Q by using the spectral data to calculate the fraction G/Q (eq. G6).

Portable micrometeorological stations, located at sites C and L, recorded incoming solar radiation, wet and dry bulb air temperature, and windspeed at 6-second intervals. Fluctuations of the 6-second windspeed values were reduced by smoothing the data with a 30-point (3 minute) running average. These measurements provided data for the calculation of $R_S\downarrow$, $R_L\downarrow$, and r_a, of equations G2, G7, G8, and G11. The instantaneous evapotranspiration, λE_i, was calculated using equation G1.

RESULTS AND DISCUSSION

Net radiation calculated from the remote measurements correlated well with values measured with ground-based net radiometers. Soil-heat-flux values estimated with the remote method were in substantial agreement with the values obtained using soil-heat-flux plates.

Daily *ET* rates of native vegetation in Owens Valley were estimated on four consecutive days using both the theoretical and the empirical approaches. Measurements on the third day (June 4) were hampered by heavy cirrus and cumulus cloud cover. Because estimates of daily λE from instantaneous values are based on the assumption that the daily course of radiation can be described by a sine function, the daily estimates are unreliable on cloudy days. Thus, results from only 3 of 4 days are reported here (table G1).

Table G1. Daily evapotranspiration, in millimeters, estimated using the remote method with both theoretical and empirical approaches, June 2, 3, and 5, 1986

Date	Theoretical		Empirical	
	Ground	Air	Ground	Air
	Site C			
June 2	-3.2	-3.3	-4.5	-3.9
June 3	-3.4	-1.9	-4.0	-2.2
June 5	-2.5	-1.1	-4.3	-2.2
	Site F			
June 5	-2.1	-1.6	-2.1	-1.1
	Site L			
June 2	-5.2	-6.3	-6.3	-6.8
June 3	-5.5	-5.4	-6.4	-6.6
June 5	-5.4	-4.1	-6.4	-6.8

On June 2, the theoretical and empirical approaches yielded similar values of λE_d. On this day, surface soil temperatures were relatively low because of recent rains. On subsequent days the surface soil became increasingly warmer than the air, and the theoretical values of λE_d decreased. This decrease in λE_d is attributed to the fact that the temperature difference is not adequately accounted for in the theoretical approach. Because the vegetation, for the most part, had roots reaching the water table, the *ET* rate would not be expected to decrease with time at the rate shown by the theoretical calculations. The empirical approach yielded values of λE_d that were relatively constant for the 4 days of measurements, a result also found by using the Bowen-ratio and eddy-correlation methods. Subsequent discussion will be confined to results from the empirical approach.

Remote estimates of daily *ET* at site L were significantly higher than at sites C and F. This result was expected because the water table at site L was estimated to be 1 m below the surface, compared to 3.4 m and 3 m at sites C and F. Furthermore, the vegetative cover at site L was more lush and more extensive than at either site C or F. Evapotranspiration at site C was slightly higher than at site F, though insufficient data were collected at site F to make a definitive conclusion.

Estimates of λE_d within a 1.6-km^2 area varied significantly depending on vegetative cover and density. A good example of this variation was seen along the east-west transect at site C. On June 5, the λE_d estimates along a single transect ranged from 0 to 7.2 (fig. G3*A*). The extreme low values of λE_d corresponded to a region of dry, scrub vegetation; the high values reflect an area of standing water covered by tall trees and sedges. Values of λE_d based on Bowen-ratio and eddy-correlation measurements at the study site are represented in figure G3*A* by the asterisk and open circle, respectively.

At site L, the east-west transect followed the length of a moist creekbed, deviating slightly from the creek at the east end. The north-south flight line started and ended over dry rangeland vegetation, crossing the creek and grassland at the midpoint of the flight line. The variation in λE_d over these flight lines, and results from Bowen-ratio and eddy-correlation methods are shown in figure G3*B*.

When comparing the Bowen-ratio and eddy-correlation data with the remote values, it should be kept in mind that the flight lines did not consistently pass directly over the ground-based instruments. This is particularly important to remember at sites C and L, where the vegetation at the site where the ground measurements were made was considerably different than the vegetation surrounding the site. Therefore, the remote data may have been more influenced by the surrounding area than were the ground-based measurements, thus leading to different values of λE_d.

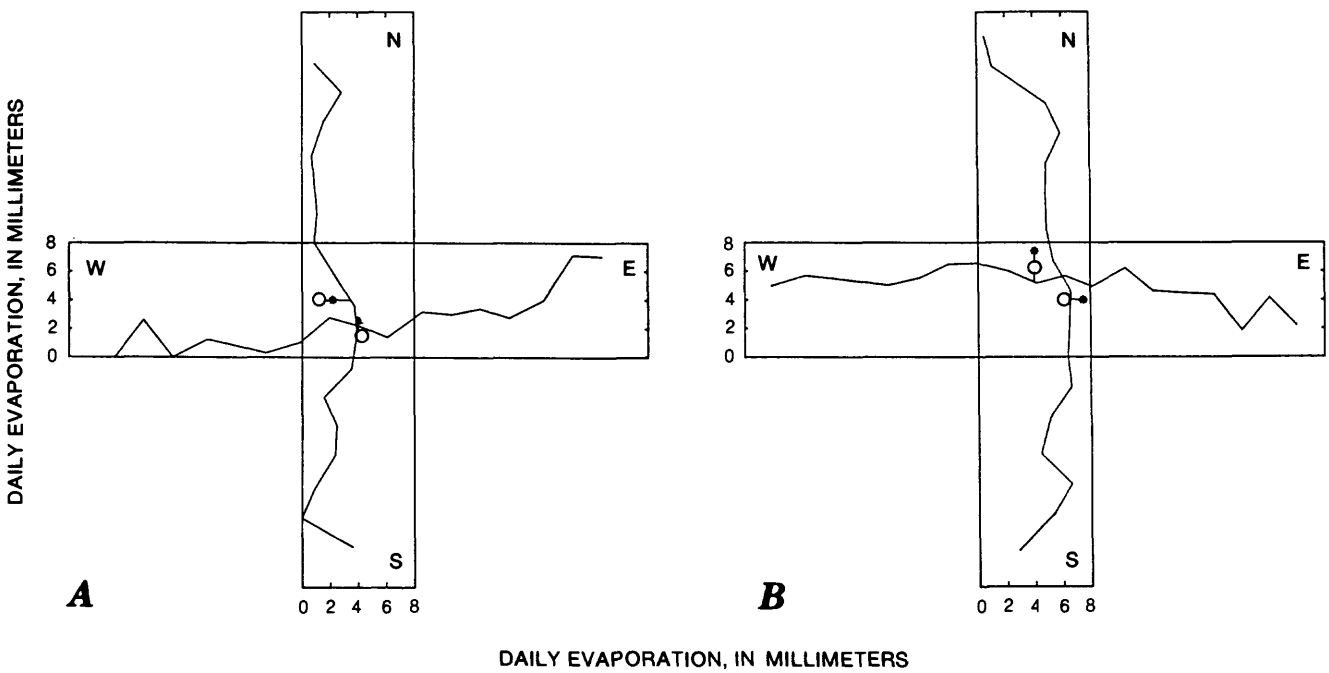

Figure G3. Estimated values of daily evaporation using the remote method along two 1.6-kilometer flight lines over sites C and L, June 5, 1986. The symbols * and o are corresponding values of daily evaporation measured using the Bowen-ratio and eddy-correlation methods, respectively. *A*, Site C. *B*, Site L.

CONCLUSIONS

The results reported here indicate that an airborne remote-sensing technique will yield satisfactory values of evaporation from arid rangeland. The remote method developed for use over uniform agricultural fields produced close estimates of net radiation and soil-heat flux when applied to a heterogeneous landscape in Owens Valley. Sensible-heat flux, on the basis of theoretical models, was overestimated at all sites because of measurement of high surface temperatures that were dominated by the hot soil surface rather than the transpiring vegetation. An empirical approach was developed to adjust the surface-air temperature difference (T_s - T) in proportion to the amount of vegetation present at the site. This approach produced values of evaporation that were in agreement with values obtained with Bowen-ratio and eddy-correlation techniques. These results indicate that a thorough examination of the sensible-heat-flux theory is needed before adequate λE_d estimates can be expected for landscapes where vegetation is sparse and soil temperatures often exceed 50 °C.

An advantage of the airborne remote-sensing method over conventional methods is that the spatial distribution of evaporation can be estimated over entire fields. The areal limitation of the method is determined by the distance that the ground-based micrometeorological measurements can be extrapolated. With clear skies, the areal extrapolation of incoming solar radiation could extend many kilometers with little error. Under these conditions, the spatial variations in windspeed and air temperature would probably be the limiting factors.

REFERENCES

Brutsaert, W.H., 1975, On a derivable formula for long-wave radiation from clear skies: Water Resources Research, v. 11, p. 742-744.

-----1982, Evaporation into the atmosphere: Dordrecht, D. Reidel Publishing, p. 299.

Choudhury, B.J., Reginato, R.J., and Idso, S.B., 1986, An analysis of infrared temperature observations over wheat and calculation of latent heat flux: Agricultural and Forest Meteorology, v. 37, p. 75-88.

Clothier, B.E., Clawson, K.L., Pinter, P.J., Jr., Moran, M.S., Reginato, R.J., and Jackson, R.D., 1986, Estimation of soil heat flux from *ET* radiation during the growth of alfalfa: Agricultural and Forest Meteorology, v. 37, p. 319-329.

Garratt, J.R., 1978, Transfer characteristics for a heterogeneous surface of large aerodynamic roughness: Quarterly Journal of Royal Meteorology Society, v. 104, p. 491-502.

Gay, L.W., and Fritschen, L.J., 1979, An exchange system for precise measurements of temperature and humidity gradients in the air near the ground: Hydrology and Water Resources in Arizona and the Southwest, v. 9, p. 37-42.

Gay, L.W., and Greenberg, R.J., 1985, The AZET battery-powered Bowen ratio system: American Meteorology Society, Conference on Agriculture and Forest Meteorology, 17th, Scottsdale, Arizona, Proceedings, p. 181-182.

Jackson, R.D., 1984, Total reflected solar radiation calculated from multi-band sensor data: Agricultural and Forest Meteorology, v. 33, p. 163-175.

-----1985, Evaluating evapotranspiration at local and regional scales: Institute of Electrical and Electronics Engineers, v. 73, Proceedings, p. 1086-1096.

Jackson, R.D., Hatfield, J.L., Reginato, R.J., Idso, S.B., and Pinter, P.J., Jr., 1983, Estimation of daily evapotranspiration from one time-of-day measurements: Agriculture Water Management, v. 7, p. 352-362.

Jackson, R.D., Moran, M.S., Gay, L.W., and Raymond, L.H., 1987, Evaluating evaporation from field crops using airborne radiometery and ground-based meteorological data: Irrigation Science, v. 8, p. 81-90.

Jackson, R.D., Pinter, P.J., Jr., and Reginato, R.J., 1985, Net radiation calculated from remote multispectral and ground station meteorological data: Agricultural and Forest Meteorology, v. 35, p. 153-164.

Kustas, W.P., and Brutsaert, W.H., 1986, Wind profile constants in a neutral atmospheric boundary layer over complex terrain: Boundary Layer Meteorology, v. 34, p. 35-54.

Mahrt, L., and Ek, M., 1984, The influence of atmospheric stability on potential evaporation: Journal of Climate and Applied Meteorology, v. 23, p. 222-234.

Monteith, J.L., 1973, Principles of Environmental Physics: London, Edward Arnold, p. 241.

Reginato, R.J., Jackson, R.D., and Pinter, P.J., Jr., 1985, Evapotranspiration calculated from remote multispectral and ground station meteorological data: Remote Sensing Environment, v. 18, p. 75-89.

Spittlehouse, D.L., and Black, T.A., 1980, Evaluation of the Bowen ratio/energy balance method for determining forest evapotranspiration: Atmosphere and Oceans, v. 18, p. 98-116.

CHAPTER H.--COMPARISON OF EVAPOTRANSPIRATION MEASUREMENTS

By Robert J. Reginato and Ray D. Jackson

(U.S. Water Conservation Laboratory, Phoenix, Arizona)

The purpose of the experiment was to evaluate the spatial and temporal variation of evapotranspiration (*ET*) by use of methods on the ground and in the air, and to compare these values with separate ground-based observations by use of Bowen-ratio and eddy-correlation methods.

Daily values of *ET*, in millimeters, for each site were measured by the methods given in table H1. For each site, the agency responsible for the measurements and the type of instruments used is specified. Although the California Irrigation Management Information System (CIMIS) weather station was located on the southern edge of Bishop, California, in a well-watered pasture, information on the calculated values of potential and measured values of *ET* from a hydraulic lysimeter and of evaporation from a pan are included in each of the tables for comparison.

The remotely sensed observations made by the U.S. Water Conservation Laboratory were ground-based and airborne aircraft-based, using both theoretical and empirical methods. Instantaneous values of latent-heat flux (λE) from both levels of observation were used to derive daily totals of *ET*. The airborne data covered two 1.6-km-long transects at each site, but the information given in table H1 is from data collected, as closely as we could determine, where the ground-based radiometer was located. Because the method of calculation is identical for both types of observations, the differences are attributed to the radiometers not scanning at the exact area at the study sites.

Where there are differences between the methods at any one site, it would be necessary to examine the individual components of the energy balance in order to determine the causes of the differences. For example, for the ground-based methods, sensors, such as net radiometers and soil-heat-flux plates, need to be placed in areas that are representative of the larger area. Consideration must be given as to how much vegetation or soil is being monitored by the net radiometer, and whether the soil-heat-flux plates are in shaded or sunlit exposures. Systems for measuring *ET* that are meters apart may vary significantly because of different sensor placement.

The daily *ET* data at the three sites during the 4 days of measurement are summarized in table H1.

Generally, all the methods used gave approximate values at the three sites. In nearly all instances, the Bowen-ratio method gave slightly larger values of *ET* than did the eddy-correlation method. Ground-based remote sensing of *ET* gave larger values than the airborne-derived values at sites C and F, but virtually identical values at site L. At each site, *ET* was quite uniform during the 4-day period because the weather conditions were similar. There are no data for June 4 for the remote-sensing techniques because of moderate to heavy cirrus clouds. Under these conditions, the ground-based *ET* systems performed quite well; they were not hampered by clouds. On any day, at any site, the daily *ET* from all methods was similar, indicating that each system can adequately describe the water loss from that site.

Table H1. Daily evapotranspiration, in millimeters, June 2-5, 1986

Method used	Site C					Site F					Site L				
	June 2	June 3	June 4	June 5	Average	June 2	June 3	June 4	June 5	Average	June 2	June 3	June 4	June 5	Average
U.S. Water Conservation Laboratory															
Ground based															
Theoretical	-3.2	-3.4	--	-2.5	-3.0	--	--	--	-2.1	-2.1	-5.2	-5.5	--	-5.4	-5.4
Empirical	-4.5	-4.0	--	-4.3	-4.3	--	--	--	-2.1	-2.1	-6.3	-6.4	--	-6.4	-6.4
Airborne															
Theoretical	-3.3	-1.9	--	-1.1	-2.1	--	--	--	-1.6	-1.6	-6.3	-5.4	--	-4.1	-5.3
Empirical	-3.9	-2.2	--	-2.2	-2.8	--	--	--	-1.1	-1.1	-6.8	-6.6	--	-6.8	-6.7
University of Arizona															
Bowen ratio	-2.4	-2.3	-2.3	-2.3	-2.3	--	--	--	--	--	-7.9	-8.3	-8.0	-7.4	-7.9
U.S. Geological Survey															
Bowen ratio	-1.8	--	--	--	-1.8	--	--	-1.3	-1.4	-1.3	--	--	--	--	--
Eddy correlation, direct	-1.4	-1.3	-1.6	-1.6	-1.5	--	--	--	-1.4	-1.4	--	--	--	--	--
Eddy correlation, residual	-1.6	-1.7	-1.8	-1.6	-1.7	--	-1.3	-1.4	-1.2	-1.3	--	--	--	--	--
Eddy correlation, direct 1	--	--	--	--	--	--	--	--	--	--	--	--	--	--	--
Eddy correlation, direct 2	--	--	--	--	--	--	--	--	--	--	--	-6.4	-6.4	-6.1	-6.3
Eddy correlation, residual 1	--	--	--	--	--	--	--	--	--	--	-7.0	-7.2	-6.9	-6.3	-6.9
Eddy correlation, residual 2	--	--	--	--	--	--	--	--	--	--	-5.8	-6.8	-6.6	-6.2	-6.4
Inyo County Water Department and City of Los Angeles															
Porometer measurements	--	-1.9	-1.5	--	-1.7	--	--	--	--	--	--	--	--	-7.3	-7.3
Transpiration model	-1.3	-1.3	-1.4	-1.4	-1.4	-0.8	-0.8	-0.9	-0.9	-0.8	-6.2	-6.4	-6.7	-6.9	-6.7
University of California															
CIMIS, potential *ET*	-7.1	-6.9	-7.2	-6.7	-7.0	-7.1	-6.9	-7.2	-6.7	-7.0	-7.1	-6.9	-7.2	-6.7	-7.0
Lysimeter	--	-7.4	-8.9	-7.4	-7.9	--	-7.4	-8.9	-7.4	-7.9	--	-7.4	-8.9	-7.4	-7.9
Class A pan	-6.4	-8.4	-6.1	-8.9	-7.5	-6.4	-8.4	-6.1	-8.9	-7.5	-6.4	-8.4	-6.1	-8.9	-7.5
Average of all techniques except University of California					-2.3 (±0.9)					-1.5 (±0.5)					-6.5 (±0.8)

The airborne remote-sensing technique offers the possibility of estimating *ET* over a large area, because data are collected rapidly over great distances. This method allows an assessment of the spatial variability of *ET* in the valley on any day, and with periodic flights, the temporal variability of *ET* during the course of a year. Both the airborne remote-sensing and ground-based techniques give values of actual *ET*, and are sensitive to climatic and soil conditions occurring at the time of measurement. Some plant models are not affected by climatic factors, nor are they sensitive to changes in water-table depth. But, in some areas, where the climate is the same year to year and water-table depths do not fluctuate appreciably, the models are satisfactory.

Where pumping-well tests are being conducted, the remote assessment of *ET* can be quite useful. Not only can the change in *ET* with time be measured at a pump site, but the areal extent of the drawdown also can be evaluated.

By knowing the estimated *ET* over the entire valley, a more accurate assessment of the hydrologic balance can be made. With this information, water-management strategies can be developed using sound, physically based information.

☆U.S. GOVERNMENT PRINTING OFFICE: 1992-687-199/79149